DESIGN STUDIES FOR DIRECT CONTACT CONDENSERS WITH AND WITHOUT THE PRESENCE OF NONCONDENSIBLE GAS

by

Ranga Nadig

A dissertation submitted to the faculty of
The University of Utah
in partial fulfillment of the requirements for the degree of

Doctor of Philosophy

in

Mechanical Engineering

Department of Mechanical and Industrial Engineering

University of Utah

December 1984

THE UNIVERSITY OF UTAH GRADUATE SCHOOL

SUPERVISORY COMMITTEE APPROVAL

of a dissertation submitted by

Ranga Nadig

This dissertation has been read by each member of the following supervisory committee and by majority vote has been found to be satisfactory.

17 Aug 84 — Chairman: Harold R. Jacobs

Aug 29, 1984 — Robert F. Boehm

Sept. 21, 1984 — Lavar K. Issacson

21 Sept 84 — Gary M. Sandquist

Aug. 20. 1984 — Kuan Chen

THE UNIVERSITY OF UTAH GRADUATE SCHOOL

FINAL READING APPROVAL

To the Graduate Council of The University of Utah:

I have read the dissertation of Ranga Nadig in its final form and have found that (1) its format, citations, and bibliographic style are consistent and acceptable; (2) its illustrative materials including figures, tables, and charts are in place; and (3) the final manuscript is satisfactory to the Supervisory Committee and is ready for submission to the Graduate School.

20 Sept 1984
Date

Harold R. Jacobs
Chairperson, Supervisory Committee

Approved for the Major Department

Gary M. Sandquist
Chairman / Dean

Approved for the Graduate Council

James L. Clayton
Dean of The Graduate School

ABSTRACT

Analytical models are presented to predict the condensation in film type direct contact condensation and related processes. The related processes include condensation on a thin film flowing over an isothermal vertical surface and condensation on tube bundles. In addition the effects of noncondensible gases on the above processes are examined.

The analysis is based on conservation laws alone and does not use any empirical data. The theoretical models developed are applicable for condensation of a vapor on a thin film which is the same or different from the condensate. However, the cases studied are those of steam condensing on a thin film of water. Valuable design criteria and heat transfer behaviour are presented which provide better insight in designing and understanding the performance of direct contact condensers.

TABLE OF CONTENTS

		Page
ABSTRACT		iv
NOMENCLATURE		vii
ACKNOWLEDGEMENTS		x
Chapter		
1	INTRODUCTION	1
2	CONDENSATION ON COOLANT JETS AND SHEETS	11
	2.1 Introduction	11
	2.2 General Assumptions	13
	2.3 Physical Model and Mathematical Formulation	15
	2.4 Results and Discussion	25
3	CONDENSATION ON COOLANT JETS AND SHEETS IN THE PRESENCE OF A NONCONDENSIBLE GAS	35
	3.1 Introduction	35
	3.2 General Assumptions	37
	3.3 Physical Model and Mathematical Formulation	37
	3.4 Results and Discussion	49
4	CONDENSATION ON A THIN FILM FLOWING OVER AN ISOTHERMAL VERTICAL SURFACE	61
	4.1 Introduction	61
	4.2 Physical Model and Mathematical Formulation	62
	4.3 Results and Discussion	78
5	CONDENSATION ON A THIN FILM FLOWING OVER AN ISOTHERMAL VERTICAL SURFACE IN THE PRESENCE OF A NONCONDENSIBLE GAS	95
	5.1 Introduction	95
	5.2 Physical Model and Mathematical Formulation	96
	5.3 Results and Discussion	118
6	CONDENSATION ON A FILM FLOWING OVER SINGLE AND MULTIPLE ISOTHERMAL HORIZONTAL TUBES	158

6.1 Introduction 158
6.2 Physical Model and Mathematical Formulation 160
6.3 Results and Discussion 172

REFERENCES 180

NOMENCLATURE

C_p	Specific heat
D	Diffusion coefficient
D	Diameter
D_H	Hydraulic diameter
g	Acceleration due to gravity
Gz	Grzetz number
h_{fg}	Heat of varporiztion
h	Heat transfer coefficient
Ja	Jakob number $Cp\Delta T/h_{fg}$
k	Thermal conductivity
L	Thickness
M	Molecular weight
$\dot{m}$	Mass flow rate per unit width
Nu	Nusselt number
Pr	Prandtl number
P	Pressure
q	Heat flux per unit area
R	Gas constant
R	Radius
Re	Reynolds number $\dot{m}/\mu$
Re_{D_H}	Reynolds number based on hydraulic diameter UDH/ν
Sc	Schmidt number
T	Temperature

u Velocity in the x direction

v Velocity in the y direction

w Mass fraction of noncondensible gas

x Direction along the surface

y Direction perpendicular to the surface

Greek Letters

β Temperature gradient $\frac{\partial T}{\partial y}$

δ Boundary layer thickness

θ Nondimensional temperature

μ Absolute viscosity

ν Dynamic viscosity

ρ Density

ϕ Angle from upper stagnation point

Subscripts

c Condensate

D At the end of Region I

f Film

g Noncondensible gas

i Interface between film and condensate liquid

l Liquid

m Velocity layer in gas-vapor mixture

s Species layer in gas vapor mixture

v Vapor

w Wall

$*$ Interface between condensate and gas vapor mixture

∞ In gas vapor mixture remote from interface

Superscript

$\bar{}$ Nondimensional quantity

ACKNOWLEDGEMENTS

I wish to express my sincere appreciation to my committee chairman, Dr. H.R. Jacobs, for his suggestions, guidance and encouragement during the period this work was undertaken. A special thanks is extended to Dr. R.F. Boehm, Dr. L.K. Isaacson, Dr. K. Chen and Dr. G.M. Sandquist for serving on my graduate committee.

I would like to thank the Department of Electrical Engineering, University of Utah, for permitting me to carry out the numerical computations on their HP 3000 computer. Deep gratitude is expressed to Walt Howard, Manager, HP 3000 computer, for the help extended in use of the computer.

In this dissertation, Chapters 2 and 3 have been published by ASME as paper numbers 84-HT-29 and 84-HT-28, respectively. They were both presented at the National Heat Transfer Conference in August 1984, Niagara Falls, N.Y.

Chapter 6 has also been published by ASME as paper number 8T-3A, under the title "Fundamentals of Two Phase Flow: Boiling Consensation." This paper was presented at the National Heat Transfer Conference in December 1984, New Orleans, Louisiana.

CHAPTER 1

INTRODUCTION

Direct contact condensation process have been commercially used in steam power plants and many chemical processes since the early 18th century [1]. In these condensers a saturated or slightly superheated vapor is brought into direct contact with the cooling fluid to condense all or part of the vapor. Typically these condensers find application in vacuum pumping of vapor, condensation of steam, pyrolysis gas quenching, in petroleum industries, open feed water heaters, and the Heller Power cycle [2]. More recently direct contact condensers have been suggested for use in desalination systems and in alternate energy application such as solar and geothermal power systems [3].

Direct contact condensers offer numerous advantages over the conventional shell and tube heat exchangers. These advantages include simplicity of design, lower capital and maintenance costs, high specific transfer areas and higher transfer rates. In addition, due to the intimate mixing of the two fluids, the direct contact condensers work effectively under low temperature driving forces. In a Direct Contact Condenser (DCC) the cooling fluid may be the same or different (say, a hydrocarbon condensing on water) than the condensate. In the former case it is desirable that the cooling fluid be as pure as possible to ensure trouble free operation of subsequent equipment. However, if the cooling fluid and the condensate are different it is desirable that the two

fluids be immiscible with sufficient difference in density to facilitate separation without sizeable losses in the hot well. In addition, low solubility, no affinity to form stable emulsions, chemical inertness and stability are necessary for economical and trouble free operation.

Although direct contact condensers have been designed and built in numerous ways, they can be classified into three distinct categories. In a 1977 literature survey published by Jacobs and Fannir [4], the three categories were named; the bubble type, the drop type, and the film type.

The bubble type of condensers includes all those systems where the condensing vapor is injected into a continuous pool or stream of cold liquid. This type of device has been of interest in the design of open feed water heaters and in vapor suppression systems for nuclear reactors [5].

The drop type DCC includes all those condensers where the vapor in the continuous media and condensation takes place on either drops or jets. Typical of this type of condenser is the standard barometric condenser. Figure 1.1.1 shows a drop type direct contact condenser where the vapor condenses on the spray or drops of coolant. Here the condensation is dominated by the transient conduction in the growing drops. Figures 1.1.2 and 1.1.3 illustrate the design of curtain types of DCC. Here the coolant flows under the action of gravity in the form of sheets or jets on which the vapor condenses.

The film type of DCC bears a sizeable resemblance to the curtain type DCC. In the film type of condenser the coolant is sprayed on a packing material. The coolant flows down the packing in the form of a thin film on which the vapor condenses as illustrated in Figure 1.1.4

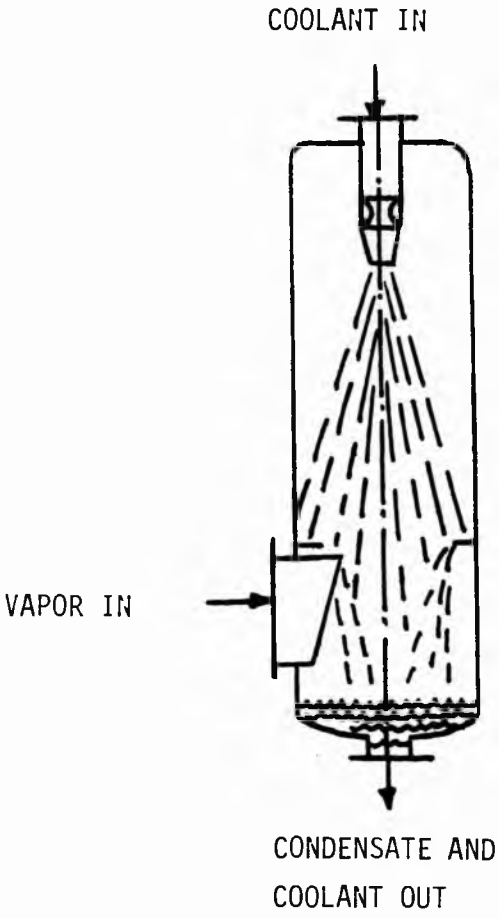

Figure 1.1.1. Counterflow condenser.

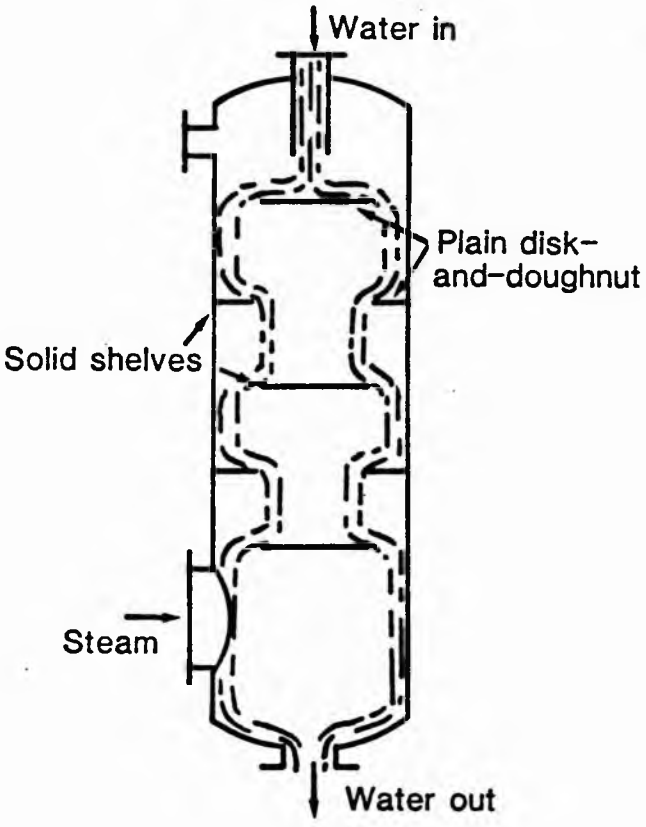

Figure 1.1.2. Cascade "solid curtain" condenser.

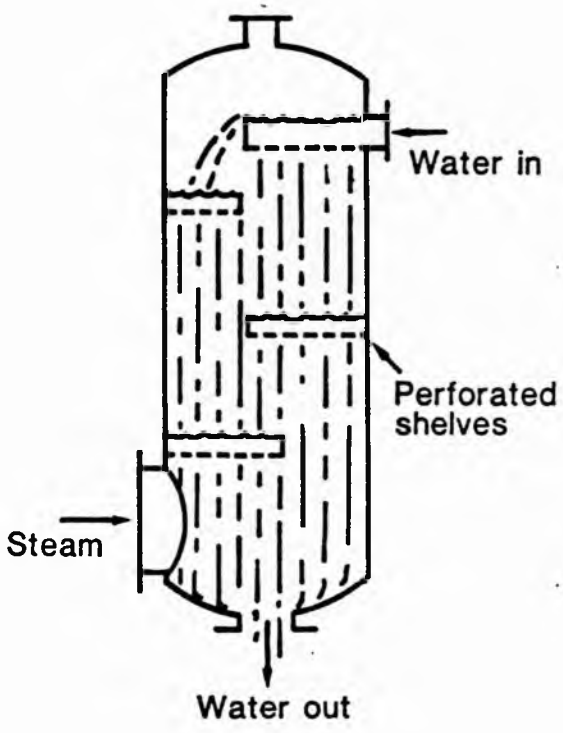

Figure 1.1.3. Cascade (sheet) type condenser.

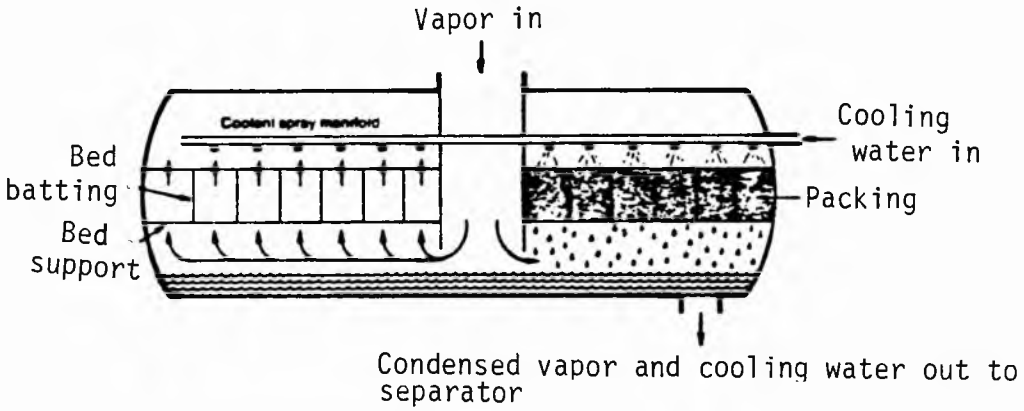

Figure 1.1.4. Packed bed condenser.

An alternate design is the tray type of condenser where the coolant flows over an inclined tray and at the end forms a short curtain as it moves down to the next tray. Here the coolant can be the same or different from the condensate as noted earlier.

Occurrences of film type direct contact condensers are numerous. The primary example is the condensation in a shell and tube heat exchanger. In a shell and tube heat exchanger, the vapor condenses on a vertical or staggard row of tubes. It is observed that for the topmost tube, the vapor condenses on the bare tube surface. Subsequently the condensate drips off the tube in the form of a thin sheet. As the condensate travels the distance between the tubes additional condensation occurs on the condensate sheet. The condensation process occurring between the tubes is similar to that in a drop type DCC. The process continues as the condensate sheet impinges on the second tube and flows around it in the form of a thin film. The vapor condenses on the thin film. Subsequently the condensate and the film drip off the second tube in the form of a thin sheet and thus the condensation process repeats over the remaining tubes in the row. The thickness of the film or sheet increases as the condensation proceeds down the tube bank. It is observed that for the second tube onward the vapor no longer condenses on the bare tube surface; instead it condenses on a thin film of condensate flowing over the tube leading to direct contact condensation. The direct contact condensation process occurring on the second or subsequent tube in a tube bank is similar to that occurring in a film type DCC. The primary difference is the condition at the wall. In the former case, the cooling fluid flows through the tubes makes the tube wall isothermal at any given cross section whereas in the

later case the packing material renders the wall adiabatic.

In dealing with direct condensation processes so far it was assumed that the condensing vapor was free of noncondensible gas. Usually the condensing vapor is mixed with varying amount of noncondensible gases such as air, nitrogen or inert gases. This is primarily due to microscopic leaks in the process equipment and the inability to totally strip the noncondensible gases from the condensing vapor. The presence of these noncondensible gases can drastically reduce the condensation heat transfer. For example, in condensation of steam it has been reported that the presence of air equal to one half percent by mass can reduce the condensation heat transfer by over 50% [6].

A review of the literature reveals that although direct contact condensers have been designed and built for over 80 years, very little work of analytical or experimental nature has been reported. Thus, it was decided to develop analytical models to predict the heat transfer performance and design criterion for direct contact condensers. As the treatment of the entire family of direct contact condensers is well beyond the scope of this dissertation, it was decided to restrict the studies to film type direct contact condensation and related processes. Due to the significant influence of noncondensible gases on condensation process, it was decided to establish analytical models to examine the effects of noncondensible gas.

The film type direct contact condensation process was treated by Jacobs and Bogart [7] in 1980. They defined the problem as condensation on an immiscible film flowing over an adiabatic surface. Utilizing an integral approach they determined the local and the average Nusselt as a function of the thermal driving force, falling film Reynolds

number, and the ratios of the two liquids thermal conductivities, viscosities and Prandtl numbers. Their solution is applicable to those immiscible fluid combinations where the surface tension allows the condensate to form a continuous layer wetting the film.

The effect of noncondensible gases on film type direct contact condensation was treated by the author in 1983 [8,9]. An integral approach was used to analyze the condensation of a saturated vapor in the presence of a noncondensible gas, on a thin laminar film of the same or a different liquid flowing down an adiabatic plate. Expressions were presented for the average Nusselt number and for the length of plate necessary for complete utilization of the cooling capacity of the film as functions of important nondimensional parameters governing the problem. Thus the basic analytical models were established to predict the condensation and design criterion for the standard film type DCC.

As noted earier the condensation processes occurring on the second or subsequent tube in a shell and tube heat exchanger, in a curtain and jet tube condenser are similar to that in the film type DCC. Thus, it was decided to establish analytical models to predict the condensation with and without the presence of nondensible gas for each of the processes related to film type direct contact condensation process. The condensation in curtain and jet type condensers was modeled as condensation on coolant jets and sheets. Condensation on second or subsequent tube in a shell and tube heat exchanger was first treated as condensation on a thin film flowing over an isothermal surface and subsequently the analysis was applied to tube bundles.

In this disseratation, Chapter 2 deals with condensation on coolant

sheets and jets. Condensation on coolant sheets in the presence of a noncondensible is treated in Chapter 3. Condensation on a thin film flowing over an isothermal vertical surface is dealt with in Chapter 4. The influence of noncondensible gases on condensation on a thin film flowing over an isothermal vertical surface is examined in Chapter 5. Chapter 6 deals with condensation on a vertical row of isothermal tubes. General conclusions related to the family of problems treated in these previous chapters are presented in Chapter 7.

CHAPTER 2

CONDENSATION ON COOLANT JETS AND SHEETS

2.1 Introduction

Direct contact condensers have been built and used industrially for well over 80 years. Hausbrand's book [10], Evaporation, Condensing and Cooling Apparatus, appeared in its first German edition in 1900 and was later translated into English, appearing in five English language editions through 1933. Despite this early start the development of theory for the heat transfer lagged greatly behind that for surface condensers. This point is emphasized by the fact that How's (11) article, "How to Design Barometric Condensers," published in 1956 was simply a description of rules of thumb for designing equipment.

The article by How describes a wide range of equipment including curtain and jet condensers such as those shown in Figures 1.1.2 and 1.1.3. As can be seen these condensers have the coolant injected as a series of jets or solid sheets which fall down through a relatively quiescent vapor. Typically the vapor flows upward so that a counter flow exists. However, the vapor velocity is maintained sufficiently low that no coolant is stripped from the jets or sheets.

Jet and curtain type direct contact condensers have received considerable attention in the USSR and England (12). They are being used to replace feedwater heaters and in the Heller power cycles. In

1976 Oliker (12) noted that there was a significant lack of technical data of even an experimental nature dealing with their design. He states that "the evaluation of this apparatus usually consists of determination of a heat balance and the necessary flow rates of condensed steam. A calculation of the heat and mass transfer in those heat exchangers is not made." He then points out that precise evaluation of direct contact condenser design is desirable.

The earliest theoretical treatment of curtain and jet condensers is that due to Kutateladze (13). In his work and the subsequent work of Hasson et al. (14,15) in 1964, it was assumed that the surface of the jet, which entered the vapor chamber at a temperature T_o, was suddenly changed to the saturation temperature of the vapor. The vapor induced negligible shear on the liquid; thus the velocity in the jet was essentially constant. These assumptions for a laminar jet allowed for an analytical solution in terms of the Graetz number. As the resistance of the condensate was assumed negligible, the solutions were applicable only if the Jakob number, defined as

$$C_{p_\ell} (T_{sat} - T_o)/h_{fg},$$

was infinitesimally small. This can occur if either $(T_{sat} - T_o) \to 0$ or if $h_{fg} \to \infty$. If $(T_{sat} - T_o)$ equals zero then no condensation takes place and the Graetz number

$$(Re_{D_{H\ell}} Pr_\ell D_H/x)$$

required for complete condensation is infinite. If h_{fg} is infinite with $(T_{sat} - T_o)$ finite, the Graetz number for complete utilization of the coolant tends to zero. It is thus clear that the theory of

Kutateladze and Hasson et al. cannot be applied unless a more accurate solution is first obtained which would define where their solutions provide approximate results.

Recently Jacobs and co-workers (7,16,8) at the University of Utah carried out analyses applicable to the design of packed bed flat plate (7) and a sphere (16), and for flow over a vertical flat plate with a noncondensible gas present (8). The first paper differs from the present problem for condensation on a sheet in that the velocity was not uniform. The analytical methods should thus be easily adapted to the case on condensation on a laminar sheet and also to a jet. Thus in this paper we develop a set of integral energy equations for the coolant stream and the condensate film in order to calculate the length of sheet or jet necessary to utilize various fractions of the coolant's capacity to absorb heat.

2.2. General Assumptions

1. The velocity profiles in the jet or sheet of coolant will be assumed uniform. The basis for this assumption, used previously by Kutateladze (13) and Hasson et al. (14,15), is that the shear induced by a low pressure vapor on a moving liquid will be small. This assumption is one of the classical assumptions of Nusselt for laminar film condensation on a vertical plate.

2. The other assumptions inherent in the Nusselt analysis hold, i.e.,

(a) the temperature at the interface between the vapor and condensate is T_{sat} (no interfacial resistance),

(b) the flow is laminar with no surface waves,

(c) the properties of the liquid are constant.

3. A further assumption will be made that the Jakob number is small. The Jakob number for this paper is defined as

$$Ja = C_{p_\ell}(T_{sat} - T_o)/h_{fg}.$$

The reason for this assumption is as follows: if we assume an energy balance from where the coolant enters the saturated vapor chamber to where its average temperature is T_{sat} and set it equal to the energy released by the condensed vapor, then

for a jet

$$\rho_\ell \, C_{p_\ell} \, U(T_{sat} - T_o) \, \pi R^2 = \rho_\ell \, U h_{fg} \, 2\pi R \delta_{x\to\infty} \qquad 2.1.1$$

and for a sheet

$$\rho_\ell \, C_{p_\ell} \, U(T_{sat} - T_o) \, L = \rho_\ell \, U h_{fg} \, \delta_{x\to\infty} \quad . \qquad 2.2.2$$

Thus for a jet

$$\frac{\delta_{x\to\infty}}{R} = \frac{C_{p_\ell}(T_{sat} - T_o)}{2h_{fg}} = \frac{Ja}{2} \qquad 2.2.3$$

and for a sheet

$$\frac{\delta_{x\to\infty}}{L} = \frac{C_{p_\ell}(T_{sat} - T_o)}{h_{fg}} = Ja \quad . \qquad 2.2.4$$

It is clear that if $Ja \to 0$, $\delta_{x\to\infty}/R$ and $\delta_{x\to\infty}/L$ go to zero. Therefore an assumption of a small Jakob number means a thin condensate layer.

For a fluid condensing on its own liquid this generally means that $T_{sat} - T_o$ is of moderate size and therefore the Nusselt assumption of constant properties should be reasonable. Further, the assumption of small mass addition supports the prior assumption of uniform jet velocity, axially as well as laterally. If the mass addition were large it would affect the inertia of the sheet or jet. A small Jakob number, for low pressure systems, provides for negligible dynamic influences.

2.3. Mathematical Formulation and Physical Models

Condensation on a Sheet

Consider the sheet of coolant shown in Figure 2.3.1. The cold liquid temperature T_o, has a thickness 2L and a uniform velocity, U. It entered a chamber filled with a quiescent saturated pure vapor at temperature T_{sat}. The coolant starts to heat up as condensation occurs. The problem as shown can be divided into two regions. Region I defines a region where a thermal boundary layer develops in the sheet, penetrating from the condensate layer-sheet interface towards the wall. This region, which extends along the length of the sheet until $\delta_t = L$, can be defined as a thermal entrance region. As the condensate layer is thin and vapor shear is small the velocity in the condensate layer will approximately equal that in the sheet. Beyond Region I lies Region II where the entire sheet is heated. The condensate layer will grow until $T_{cL} = T_{sat}$. As this increase will be exponential, calculations will cease when $(T_{sat} - T_{cL})/T_{sat} - T_o)$ is 0.001.

In Region I an energy balance for the coolant sheet yields

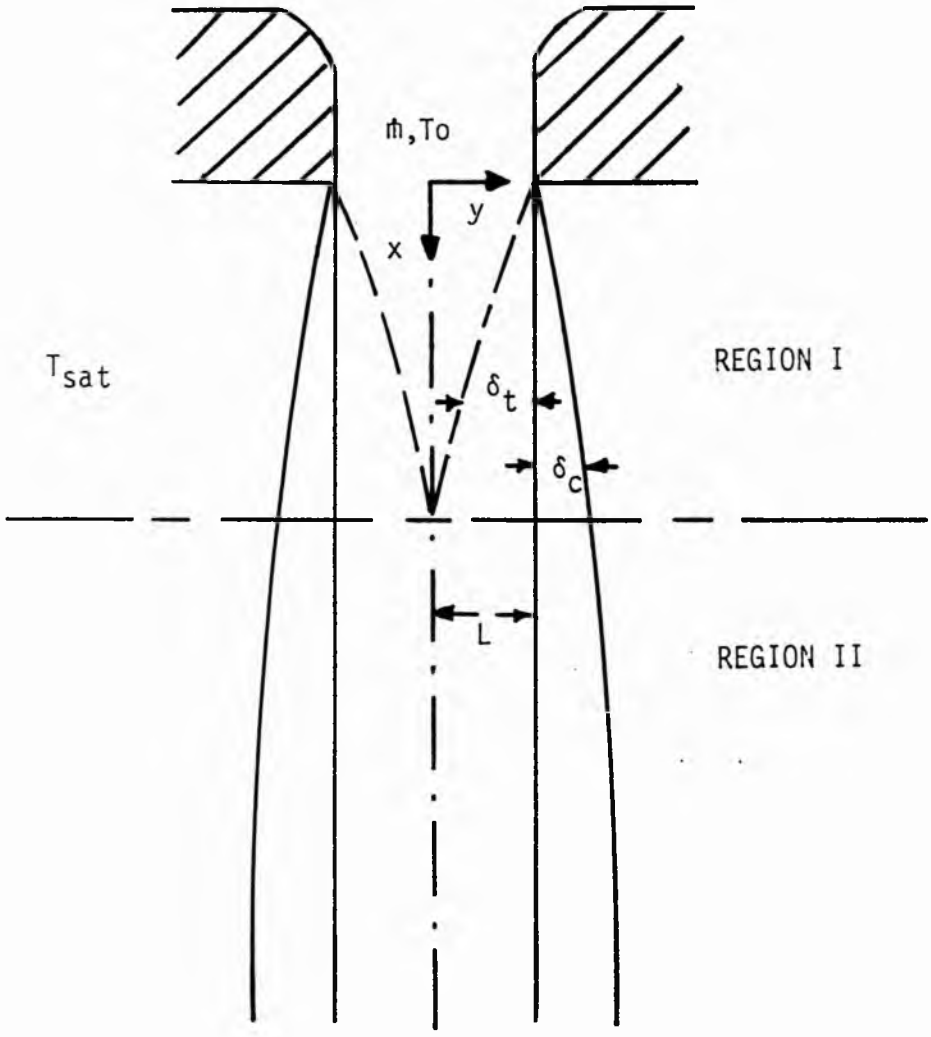

Figure 2.3.1. Schematic for condensation on a sheet.

$$\frac{d}{dx}\int_{L-\delta_t}^{L} \rho_\ell C_{p_\ell} U(T_\ell - T_o)dy = k_\ell \left.\frac{\partial T_\ell}{\partial y}\right|_{y=L} . \qquad 2.3.1$$

For the condensate layer the energy equation is

$$\frac{d}{dx}\int_{L}^{L+\delta_c} \rho_\ell C_{p_\ell} U(T_{sat} - T_c)\, dy +$$

$$h_{fg}\frac{d}{dx}\int_{L}^{L+\delta_c} \rho_\ell U dy = k_\ell \left.\frac{\partial T_c}{\partial y}\right|_{y=L} . \qquad 2.3.2$$

As the condensate layer is thin and Jakob number is small, the first term on the left side of Equation 2.3.2 can be assumed negligible. Thus Equation 2.3.2 reduces to

$$h_{fg}\frac{d}{dx}\int_{L}^{L+\delta_c} \rho_\ell U dy = k \left.\frac{\partial T_c}{\partial y}\right|_{y=L} . \qquad 2.3.3$$

The assumption of negligible thermal capacitance of the condensate layer implies a linear temperature profile across it. Thus,

$$T_c = T_i + (y - L)\frac{(T_{sat} - T_i)}{\delta_c} . \qquad 2.3.4$$

The thermal capacitance of the sheet is the only heat sink to induce the condensation; therefore for it a more general profile is necessary. The boundary conditions are

$$T_\ell = T_o \text{ and } \frac{\partial T_\ell}{\partial y} = 0 \quad \text{at} \quad y = L - \delta_t \qquad 2.3.5$$

and $T = T_i$ at $y = L$. These conditions lead to

$$T_\ell = T_i + \frac{T_i - T_o}{\delta_t^2}\left[L^2 - 2L\,\delta_t + 2y\,(-L + \delta_t) + y^2\right] . \qquad 2.3.6$$

The compatability condition of the heat fluxes at the interface between the sheet and condensate film

$$\left.\frac{\partial T_c}{\partial y}\right|_{y=L} = \left.\frac{\partial T_\ell}{\partial y}\right|_{y=L} \qquad 2.3.7$$

leads to the following expression for the interfacial temperature

$$T_i = \frac{T_o + \frac{1}{2}\,\frac{\delta_t}{\delta_c}\,T_{sat}}{1 + \frac{1}{2}\,\frac{\delta_t}{\delta_c}} . \qquad 2.3.8$$

Defining a dimensionless temperature

$$\theta = \frac{T - T_o}{T_{sat} - T_o} , \qquad 2.3.9$$

nondimensionalizing all lengths with respect to the hydraulic diameter of the sheet $D_H = 4L$, and substituting the temperature profiles and expression for T_i into Equations 2.3.1 and 2.3.3 yields

$$\frac{d\bar{\delta}_t^2}{d\bar{x}} = \frac{\frac{12}{Re_{D_H}\,Pr}\left(1 + \frac{1}{2}\,\frac{\bar{\delta}_t}{\bar{\delta}_c}\right) + 2\left(\frac{\bar{\delta}_t}{\bar{\delta}_c}\right)^2 \frac{Ja}{Re_{D_H}\,Pr}\left(\frac{1}{1 + \frac{1}{2}\,\frac{\bar{\delta}_t}{\bar{\delta}_c}}\right)}{2 + \frac{1}{2}\,\frac{\bar{\delta}_t}{\bar{\delta}_c}} \qquad 2.3.10$$

and

$$\frac{d\bar{\delta}_c^2}{d\bar{x}} = \frac{2Ja}{Pr\,Re_{D_H}}\,\frac{1}{1 + \frac{1}{2}\,\frac{\bar{\delta}_t}{\bar{\delta}_c}} . \qquad 2.3.11$$

Equations 2.3.10 and 2.3.11 make up a set of two coupled nonlinear first order differential equations. The necessary boundary conditions, as can be seen from Figure 2.3.1, are $\delta_t(x = 0) = 0$ and $\delta_c(x = 0) = 0$. The equations may be solved numerically after establishing the values of the first derivatives at $x = 0$. Conversely they can be solved assuming a series solution. It may be shown that the solutions are satisfied by the expressions

$$\bar{\delta}_c = a_o \bar{x}^{1/2} + \ldots \qquad 2.3.12$$

and

$$\bar{\delta}_t = b_o \bar{x}^{1/2} + \ldots \quad . \qquad 2.3.13$$

Region II begins when $\delta_t = L$. From this point the entire sheet heats up. Thus the integral energy equation for the sheet becomes

$$\frac{d}{dx}\int_0^L \rho_\ell C_{p_\ell} U(T_\ell - T_o)dy = k_\ell \left.\frac{\partial T_\ell}{\partial y}\right|_{y=L} \quad . \qquad 2.3.14$$

The energy equation for the condensate layer remains as given in Equation 2.3.3. The expressions for the interfacial temperature and temperature profile in the sheet change, however. For the sheet the entire fluid heats up but the thickness to the center L is a constant. The boundary conditions governing the temperature profile include

$$y = 0, \quad \frac{\partial T_\ell}{\partial y} = 0, \quad T_\ell = T_{cL}$$
$$y = L \qquad T_\ell = T_i \qquad 2.3.15$$

resulting in

$$T_\ell = T_{cL} + \frac{T_i - T_{cL}}{L^2} y^2 \quad . \qquad 2.3.16$$

Utilizing this profile the following expression is obtained relating the nondimensional sheet centerline temperature, condensate and sheet thicknesses.

$$\theta_{cL} = \theta_i - \frac{(1 - \theta_i)}{8\bar{\delta}_c} \quad . \qquad 2.3.17$$

Note that at the end of Region I $\theta_{cL} = 0$ and $\theta_i = 1/(1 + 8\ \bar{\delta}_c)$. Thus if $\bar{\delta}_c \to 0$, θ_i at the end of Region I goes to one. Utilizing Equations 2.3.14, 2.3.16 and 2.3.17 there results

$$\frac{d\theta_i}{d\bar{x}} = \frac{(1 - \theta_i)\left[3 - \dfrac{(1 - \theta_i)\ Ja}{16\ \bar{\delta}_c^{\,2}}\right]}{Re_{D_H}\ Pr\ (1 + 12\ \bar{\delta}_c)} \quad . \qquad 2.3.18$$

The condensate energy equation is

$$\frac{d\bar{\delta}_c^{\,2}}{d\bar{x}} = \frac{2Ja}{Re_{D_H}\ Pr}(1 - \theta_i) \quad . \qquad 2.3.19$$

Equations 2.3.17, 2.3.18 and 2.3.19 define the necessary parameters to describe the condensation in Region II. The boundary conditions for θ_i and $\bar{\delta}_c$ are defined by their values at the end of Region I.

If we define the heat transfer in terms of the temperature difference $(T_{sat} - T_o)$, the local Nusselt number in Region I can be shown to be given by

$$Nu_{D_H}(\bar{x}) = \frac{1}{\bar{\delta}_c + \bar{\delta}_t/2} \qquad 2.3.20$$

and in Region II by

$$Nu_{D_H}(\bar{x}) = \frac{1 - \theta_i}{\bar{\delta}_c} \quad . \qquad 2.3.21$$

The fraction of coolant capacity utilized can be obtained by evaluating 100% x (θ_{avg}).

Condensation on a Jet

The schematic for condensation on a jet is shown in Figure 2.3.2. As can be seen the basic model is the same as for a sheet. There is a thermal development region, Region I, and a region where the entire jet heats up, Region II. The primary difference in the formulation is in the fact that one must consider an axisymmetric geometry. The choice of coordinate system is y in the jet and y' in the condensate film.

The energy equation for the jet in Region I is

$$\frac{d}{dx}\int_0^{\delta_t} (1 - \frac{y}{R})\,(T_\ell - T_o)dy = -\frac{\alpha_\ell}{U}\frac{\partial T_\ell}{\partial y}\,(y = 0) \qquad 2.3.22$$

and for the condensate layer, assuming $\delta_c/R << 1$

$$\frac{d}{dx}\int_0^{\delta_c} \rho_c\, U\, h_{fg}\, dy' = k_\ell \left.\frac{\partial T_c}{\partial y'}\right|_{y'=0} \quad . \qquad 2.3.23$$

As for the case of the sheet one can assume a linear temperature profile in the condensate layer

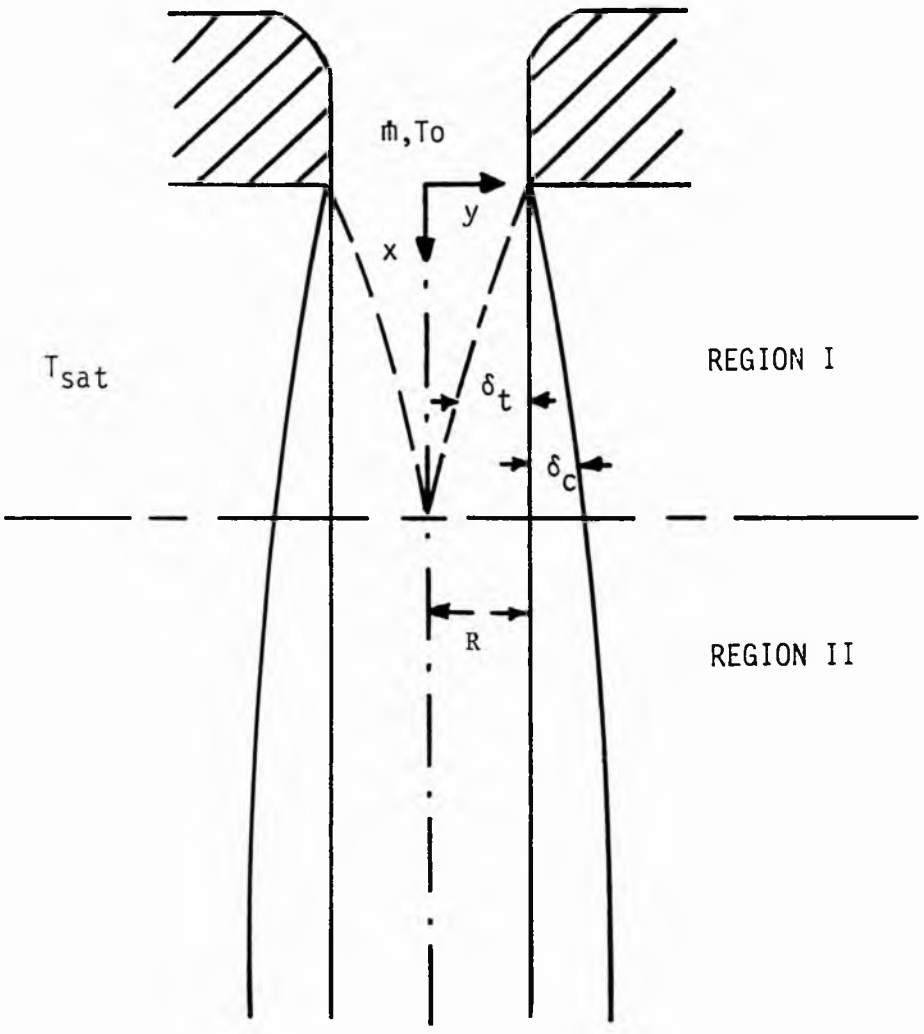

Figure 2.3.2. Schematic for condensation on a jet.

$$T_c = T_i + \frac{T_{sat} - T_i}{\delta_c} y' \qquad 2.3.24$$

and for the jet

$$T_\ell = T_o + (T_i - T_o)\ (1 - \frac{y}{\delta_t})^2 \quad . \qquad 2.3.25$$

The compatability of heat fluxes yields

$$\theta_i = \frac{1}{1 + 2\ \bar{\delta}_c/\bar{\delta}_t} \qquad 2.3.26$$

where $\theta_i = T_i - T_o/T_{sat} - T_o$ and the lengths are nondimensionalized with respect to the jet diameter. Substitution of Equations 2.3.24 and 2.3.25 into Equations 2.3.22 and 2.3.23 yields

$$\frac{d}{d\bar{x}}[\theta_i(\frac{\bar{\delta}_t}{3} - \frac{\bar{\delta}_t^2}{6})] = \frac{2}{Re_{D_H} Pr}\frac{\theta_i}{\bar{\delta}_t} \qquad 2.3.27$$

and

$$\frac{d\bar{\delta}_c^2}{d\bar{x}} = \frac{2Ja}{Pr\ Re_{D_H}}(1 - \theta_i) \quad . \qquad 2.3.28$$

The boundary conditions at $x = 0$ as with the sheet are $\bar{\delta}_t(0) = 0$ and $\bar{\delta}_c(0) = 0$. The growth of these layers are, at $x = 0$, of the form

$$\underset{x\to 0}{\bar{\delta}_t}(x) = a\bar{x}^{1/2} \quad \text{and} \quad \underset{x\to 0}{\bar{\delta}_c}(x) = b\bar{x}^{1/2} \quad . \qquad 2.3.29$$

Thus $\theta_i(\bar{x} = 0)$ is a constant.

When the thermal boundary layer has penetrated to $\delta_t = R$, i.e., the

the centerline of the jet, the entire jet starts to heat up. Here the energy equation in the jet is

$$\frac{d}{dx}\int_0^R (T_\ell - T_o)\ (1 - \frac{y}{R})dy = -\frac{\alpha_\ell}{U}\frac{\partial T_\ell}{\partial y}\ (y = 0) \qquad 2.3.30$$

with a temperature profile of

$$T_\ell - T_{cL} = T_i - T_{cL}(1 - \frac{y}{R})^2 \quad . \qquad 2.3.31$$

Substituting Equation 2.3.13, into Equation 2.3.30 and nondimensionalizing yields

$$\frac{d}{dx}[\theta_{cL} + \theta_i] = \frac{32}{Re_{D_H}Pr}\ (\theta_i - \theta_{cL}) \quad . \qquad 2.3.32$$

The compatability of heat fluxes at the condensate jet interface yields

$$\theta_{cL} - \theta_i = \frac{(1 - \theta_i)}{4\bar{\delta}_c} \qquad 2.3.33$$

and the condensate film energy equation remains

$$\frac{d\bar{\delta}_c^{\,2}}{d\bar{x}} = \frac{2Ja}{Re_{D_H}Pr}\ (1 - \theta_i) \quad . \qquad 2.3.34$$

The boundary conditions at the start of Region II are those at the end of Region I. For θ_{cL} the value is zero. Thus at the start of Region II, $\theta_i = 1/(1 + 8\delta_c)$. If δ_c is very small then $\theta_i \sim 1$. It is thus clear that as $Ja \to 0$ the temperature at the surface of the jet approaches that used by Kutateladze (13), and Hasson et al. (14, 15).

The expressions for the local Nusselt numbers for the jet in Regions I and II are the same as given for the sheet in terms of θ_i, δ_c and δ_t. In addition the percent coolant utilization is calculated in the same manner. The primary difference is that for the average coolant temperature, θ_{avg} in Region II,

$$\theta_{avg_{jet}} = (\theta_{cL} + \theta_i)/2 \qquad 2.3.35$$

and for the sheet

$$\theta_{avg_{sheet}} = 2/3\ \theta_{cL} + 1/3\ \theta_i\ . \qquad 2.3.36$$

2.4. Results and Discussion

Condensation on a Sheet

Examination of the governing differential equations for the condensation on a sheet indicates that the heat transfer is dependent on the product of Re_{DH} and Pr, and Ja and x/D_H. For very small values of x/D_H a similarity solution exists, and δ_c and δ_t can be expressed as

$$\bar{\delta}_c = a_o \bar{x}^{1/2}$$

and $$2.4.1$$

$$\bar{\delta}_t = b_o \bar{x}^{1/2}$$

respectively as indicated by equations 2.3.12 and 2.3.14. Thus for small values of x it can be shown that

$$Nu_{D_H}(x) = \frac{(Re_{D_H} \; Pr \; D_H/x)^{1/2}}{(3/4 + 2Ja)^{1/2} + (3/4)^{1/2}} \quad . \qquad 2.4.2$$

For the limiting case of Ja → 0 and small x

$$Nu_D \; (x) = \frac{1}{\sqrt{3}} (Re_D \;\; Pr \; D_H/x)^{1/2} \qquad 2.4.3$$

which is nearly equal to the results of Kutateladze (13) and Hasson et al. (14) for large Graetz number. The analytical Graetz problem they solve differs only in the coefficient being $1/\sqrt{\pi}$ instead of $1/\sqrt{3}$. The difference would indicate that for large Graetz number the present solution gives a slightly faster heating of the sheet than the Graetz solution. The two solutions yield results within 3% of each other for Jakob number less than 0.05.

Although it is usual to present correlations of Nusselt number for heat transfer problems, for direct contact condensation it is more valuable to present curves showing the percent of coolant utilization as a function of the height of heat exchanger. For our problem of condensation on a sheet, percent sheet coolant utilization is shown in Figure 2.4.1 versus Graetz number for a range of Jakob number of interest. Also shown on the figure are the results for the sheet with its surface held at T_{sat}. The curve shown for the latter is Percent Coolant Utilized =

$$100\% \left\{ 1 - \sum_{n=0}^{\infty} \frac{8}{(2n + 1)^2 \; \pi^2} \exp\left[\frac{(-(4n + 2) \; \pi)^2}{Gz} \right] \right\} . \qquad 2.4.4$$

The curve given by Equation 2.4.4 appears to correspond closely to

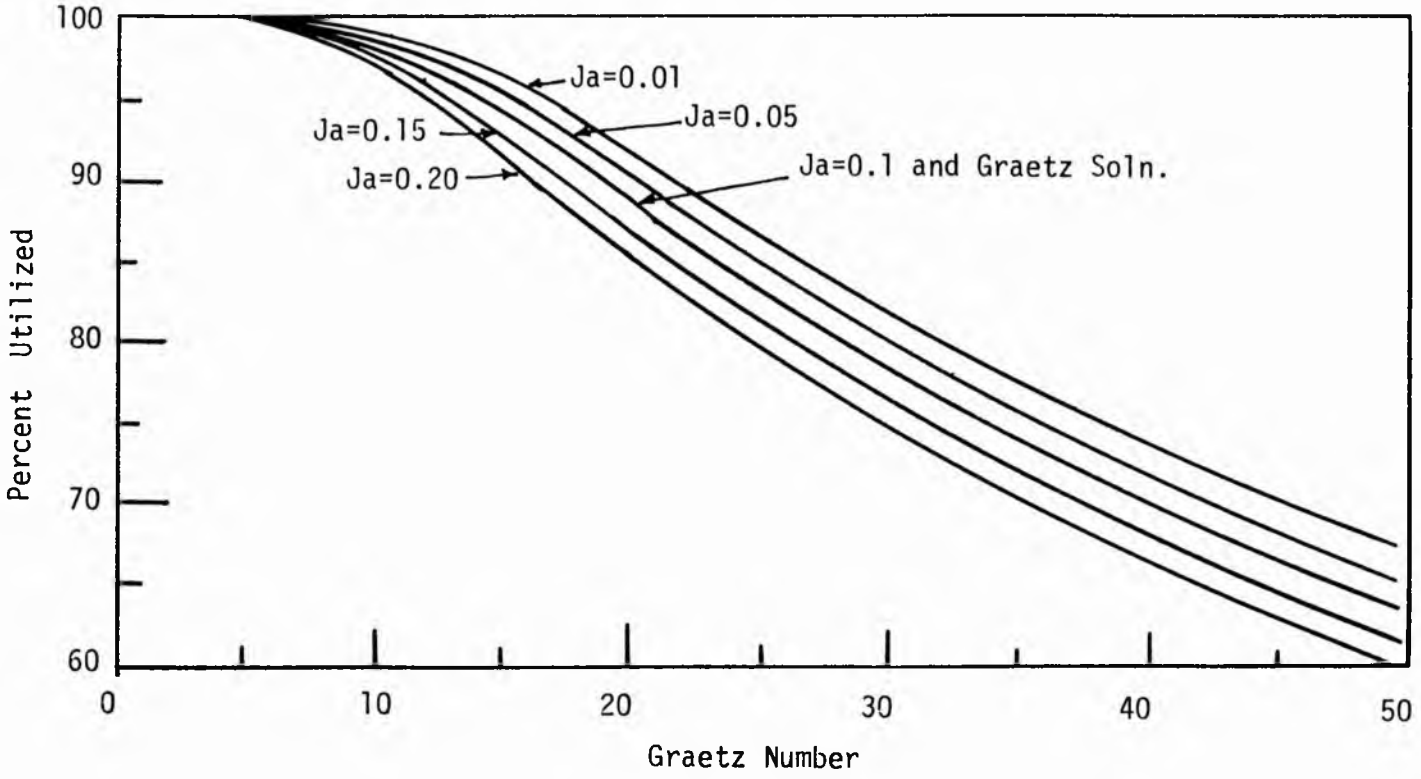

Figure 2.4.1. Percent coolant capacity utilized as a function of Graetz number for condensation on a sheet.

the curve for Ja = 0.10 over the range of Graetz number from 5 to 70. Between Graetz numbers of 70 and 130 the agreement is close to Ja = 0.05. This follows from the Nusselt number expansion accuracy shown by comparison of Equations 2.4.2 and 2.4.3. As can be seen from Figure 2.4.1 for a given degree of utilization an increase in Jakob number requires an increase in coolant sheet length or a decrease in Graetz number. For example the figure shows that for 80% utilization for a Jakob number increase from 0.01 to 0.2 the Graetz number decreases from 32.3 to 24.2. This corresponds to a 33% increase in jet length.

At high degrees of thermal utilization of the coolant it appears from the figure that the curves converge; however, this is not true. A better understanding is obtained from looking at tabulated data. Table 2.4.1 presents percent of coolant utilization for the Jakob numbers shown in Figure 2.4.1 as well as from the Graetz solution, as a function of the Graetz number.

Condensation on a Cylindrical Jet

For condensation on a cylindrical jet as x goes to zero ($Gz \to \infty$) the heat transfer yields the same form of solution as for the sheet. In other words the behaviour of the local Nusselt number is given by Equation 2.4.2 for arbitrary Jakob number and by Equation 2.4.3 for Jakob number → 0. Kutateladze (13) and Hasson (14) again show that

$$\underset{Gz\to\infty}{Nu(x)} = \frac{\sqrt{Gz/\pi}}{1 - 8/\sqrt{\pi Gz}} \sim \sqrt{\frac{Gz}{\pi}} \qquad 2.4.5$$

which is in excellent agreement with our solution.

The percentage of utilization of the coolant for a cylindrical

TABLE 2.4.1

Percent Coolant Capacity Utilized for Condensation on a Sheet

	Percent Coolant Capacity Utilized					
Gz	Gz Sol.	Ja-0.01	Ja=0.05	Ja=0.10	Ja=0.15	Ja=0.20
78.9	50.8	53.1	51.7	50.2	48.8	47.5
56.6	59.7	62.9	61.3	59.5	57.8	56.3
49.6	63.5	67.0	65.3	63.4	61.6	60.0
44.1	66.9	70.7	68.9	66.9	65.0	63.4
39.7	70.0	73.9	72.1	70.0	68.1	66.4
36.1	72.9	76.9	74.9	72.8	70.9	69.2
33.1	75.4	79.4	77.5	75.4	73.4	71.7
30.6	77.7	81.7	79.8	77.7	75.7	73.9
28.4	79.8	83.7	81.9	79.7	77.8	75.9
26.5	81.7	85.5	83.7	81.6	79.7	77.9
24.9	83.4	87.1	85.3	83.3	81.4	79.6
24.4	84.9	88.5	86.8	84.8	82.9	81.2
22.1	86.4	89.8	88.1	86.2	84.4	82.7
20.9	87.7	90.9	89.3	87.4	85.7	83.9
19.9	88.8	91.9	90.4	88.6	86.8	85.2
18.1	90.8	93.6	92.2	90.5	88.9	87.4
17.3	91.7	94.3	93.0	91.4	89.8	88.3
15.9	93.2	95.5	94.3	92.9	91.4	90.0
13.8	95.4	97.1	96.3	95.1	93.9	92.7
12.1	96.9	98.2	97.6	96.6	95.6	94.6
10.5	98.1	99.0	98.5	97.9	97.1	96.3
8.9	99.1	99.6	99.3	98.9	98.4	97.8
7.9	99.4	99.8	99.6	99.3	98.9	98.5
7.4	99.6	99.8	99.7	99.5	99.2	98.9
6.9	99.7	99.9	99.8	99.7	99.6	99.2
6.4	99.8		99.9	99.8	99.6	99.4
6.2	99.9		99.9	99.8	99.7	99.5
5.9	99.9			99.9	99.7	99.6
5.6	99.9			99.9	99.8	99.7
5.3	99.9				99.9	99.8
5.1	99.9				99.9	99.8
4.8	99.9					99.9
4.7	99.9					99.9

jet from the cylindrical Graetz problem is

Percent Coolant Utilized =

$$100\% \left[1 - \sum_{n=1}^{\infty} \frac{4}{\lambda_n^2} \exp\left(-4\lambda_n^2/Gz\right) \right] \qquad 2.4.6$$

where λ_n = the roots of $J_0(\lambda_n) = 0$.

Comparison of the cylindrical Graetz problem results with those of the present solution are shown in Figure 2.4.2 and Table 2.4.2. As can be seen the cylindrical Graetz solution is in approximate agreement with Ja = 0.15 at a Graetz number of 41 and with Ja = .20 at Graetz number less than 10.

Comparison Between Condensation on a Sheet and a Jet

Comparison between condensation on a jet and a sheet can be made by comparing values of coolant utilization shown in Tables 2.4.1 and 2.4.2 and by looking at Figure 2.4.3 which shows the utilization for Ja = 0.05. For $Gz \to \infty$ the heat transfer is the same as already noted; however, as can be seen from Figure 2.4.3 and the tables a considerable divergence of percent coolant utilized is noted for $Gz < 50$. For a percent coolant utilization of 99.5% the jet requires a 41% longer coolant stream than the sheet.

Our results further show that for the range of Jakob number between 0.01 and 0.20 that the heat transfer of the entire range of Region I is well satisfied by Equation 2.4.2. For the jet θ_i varies by about 5% over Region I for Jakob number of 0.20 but less than 1% for Jakob number of 0.01. Thus, even for the jet the solution given in

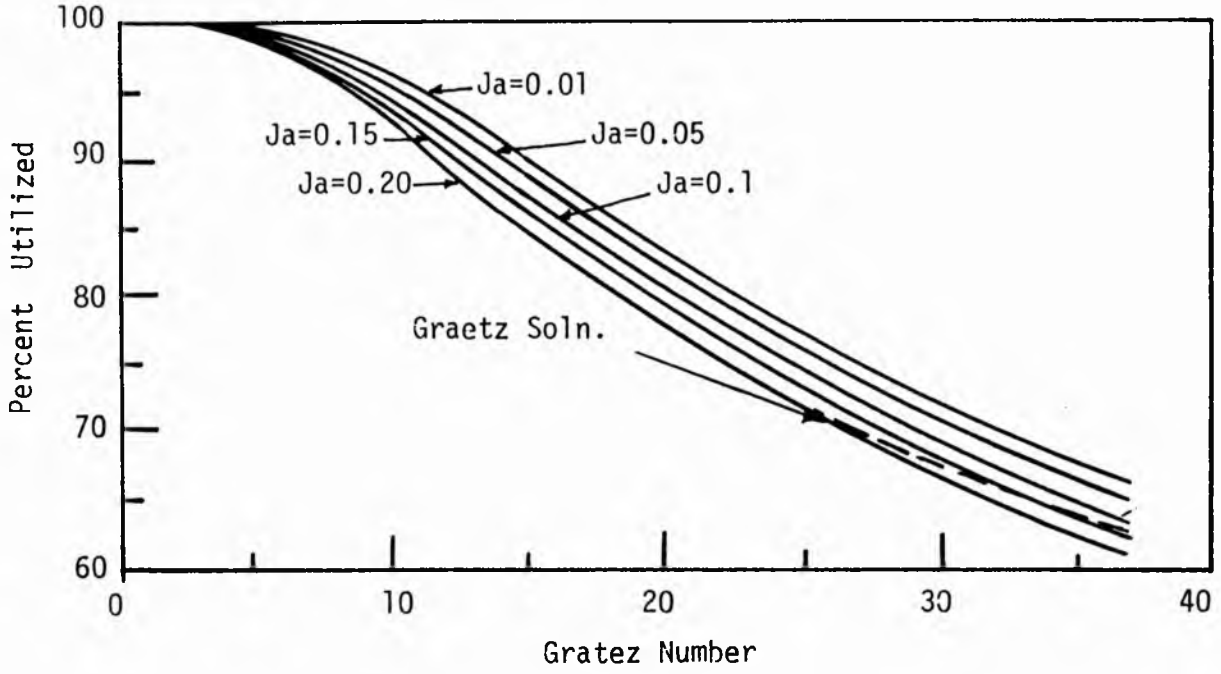

Figure 2.4.2. Percent utilized as a function of Graetz number for condensation on a cylindrical jet.

TABLE 2.4.2

Percent Coolant Capacity Utilized for Condensation on a Jet

	Percent Coolant Capacity Utilized					
Gz	Gz Sol.	Ja=0.01	Ja=0.05	Ja=0.10	Ja=0.15	Ja=0.20
58.8	51.7	53.6	52.6	51.4	50.3	49.3
45.5	57.5	60.4	59.2	57.9	56.7	55.6
37.0	62.5	66.2	64.9	63.5	62.2	61.0
31.3	66.7	71.1	69.8	68.3	66.9	65.7
27.0	70.5	75.3	73.9	72.5	71.0	69.7
23.8	73.7	78.9	77.6	76.0	74.6	73.3
21.3	76.6	81.9	80.7	79.1	77.7	76.4
19.2	79.2	84.6	83.3	81.8	80.4	79.1
17.5	81.5	86.7	85.6	84.2	82.8	81.5
16.1	83.5	88.8	87.6	86.2	84.8	83.6
14.9	85.3	90.4	89.3	87.9	86.7	85.4
13.9	86.9	91.8	90.7	89.5	88.2	87.1
12.9	88.3	92.9	92.0	90.8	89.6	88.5
12.2	89.6	94.0	93.1	91.9	90.9	89.8
11.5	90.8	94.9	94.0	92.9	91.9	90.9
10.9	91.8	95.6	94.8	93.9	92.9	91.9
10.1	93.1	96.5	95.9	94.9	94.1	93.2
9.3	94.2	97.3	96.7	95.9	95.1	94.3
8.7	95.1	97.8	97.3	96.7	95.9	95.2
8.2	95.9	98.3	97.9	97.3	96.6	95.9
7.4	96.9	98.8	98.5	98.0	97.5	96.9
6.8	97.7	99.2	98.9	98.6	98.2	97.7
6.3	98.3	99.5	99.3	98.9	98.7	98.3
5.8	98.7	99.6	99.5	99.3	99.0	98.7
5.4	99.0	99.8	99.7	99.5	99.3	99.0
5.1	99.3	99.8	99.8	99.6	99.5	99.3
4.7	99.5	99.9	99.9	99.8	99.7	99.5
4.4	99.6		99.9	99.8	99.8	99.7
4.3	99.7			99.9	99.8	99.7
4.1	99.8				99.9	99.8
3.9	99.8					99.9

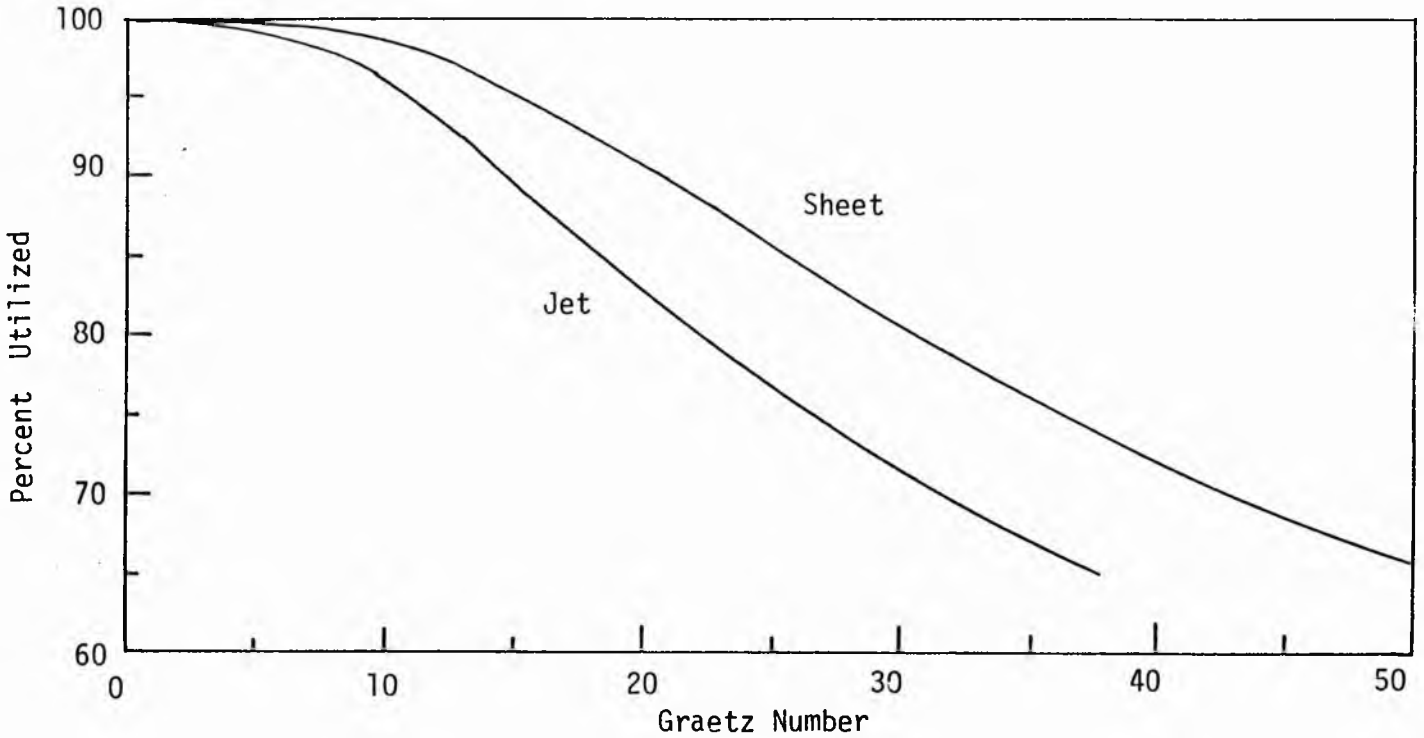

Figure 2.4.3. Comparison of coolant capacity utilized for condensation on a jet and a sheet for Ja=0.05.

Equation 2.4.2 should hold. However, to design a jet condenser or a sheet condenser, the entire solution must be obtained.

CHAPTER 3

CONDENSATION ON COOLANT JETS AND SHEETS IN THE PRESENCE OF A NONCONDENSIBLE GAS

3.1. Introduction

When a small amount of noncondensible gas is present in a vapor the rate of condensation can be appreciably reduced. This observation has been made for both surface type condensers and direct contact condensers. Hasson et al. (15) in experiments where steam was condensing on a fan jet have shown that the average heat transfer coefficient could be reduced by as much as 50 % for a concentration of one percent air in steam and could be reduced to approximately 21% of the pure vapor value for a concentration of three percent air in the bulk steam. This type of drastic reduction has been shown by Minkowycz and Sparrow (6) to be due to a buildup of the noncondensible gas at the liquid-vapor interface. Further it has been shown that an interfacial resistance is negligible.

Sparrow (17) was the first to formulate a theory to evaluate the effect of noncondensibles. His study and others (6,18,19) were concerned with condensation on a solid surface. Taitel and Tamir (20) were the first to theoretically consider the effects of noncondensibles for direct contact condensation on a sheet of coolant. Their study neglected the added resistance due to the condensate forming on the sheet. More recently Jacobs and Nadig (8,9) evaluated the effects

of noncondensibles on the condensation of a vapor on an immiscible liquid flowing over an adiabatic surface. In the present analyses condensation of vapor on a laminar sheet and on a cylindrical jet of the same fluid in the presence of a noncondensible gas are treated.

Theoretical analyses of the condensation of a pure vapor on jets or sheets of coolant were first carried out by Kutateladze (13). His analyses assumed that the coolant flowed at a uniform velocity. The energy equation was solved for the coolant assuming that it entered at a fixed temperature below the saturation temperature of the vapor. The effect of the added mass due to condensation was ignored. This latter assumption reduced the problem to one similar to the so-called Graetz problem. The difference between the Graetz problem and his analyses was that the velocity was uniform. Kutateladze's solution is strictly applicable only when the heat of vaporization, h_{fg}, becomes infinite. In Chapter 2 it has been shown the error in computing the length of coolant stream if Kutateladze's solution is used, was presented. For example, for a Jakob number less than 0.20 the error can exceed 30% when Kutateladze's results are used. The error is caused by neglecting the effect of the added mass due to condensation even at these low values of Jakob number.

Since it is necessary to consider the thermal resistance of the condensate for condensation of a pure vapor, it should also be important when noncondensibles are present in the vapor. Thus, the present work was initiated.

3.2. General Assumption

1. The velocities in the coolant stream and the condensate film are constant. The basis for this assumption is that the shear induced by a low pressure vapor on a moving liquid is small.
2. The velocity in the gas-vapor phase is not influenced by gravity due to the fact that the velocity in the coolant stream is relatively high.
3. The liquid-vapor interface is impermeable to the noncondensible gas.
4. Interfacial resistance is negligible. Thus, the temperature at the interface between the condensate and the vapor-gas mixture is that of the local saturation temperature of the vapor.
5. Axial conduction is negligible in the coolant stream.
6. The Jakob number is small; thus the condensate film is thin compared to the thickness of the coolant stream (6,8,9). Further, the properties of the fluid can be assumed constant since a small Jakob number implies small temperature difference between the coolant and the vapor-gas mixture (6,8,9).

3.3. Mathematical Formulation and Physical Models

The basic models for condensation on a sheet or jet in the presence of a noncondensible gas are shown in Figures 3.3.1 and 3.3.2. As can be seen the sheet or jet is divided into two regions. Region I defines a region in which a thermal boundary layer forms at the condensate layer-coolant interface and grows toward the centerline. Region II starts when the thermal boundary layer has reached the coolant centerline and continues until the condensation ceases. Outside the con-

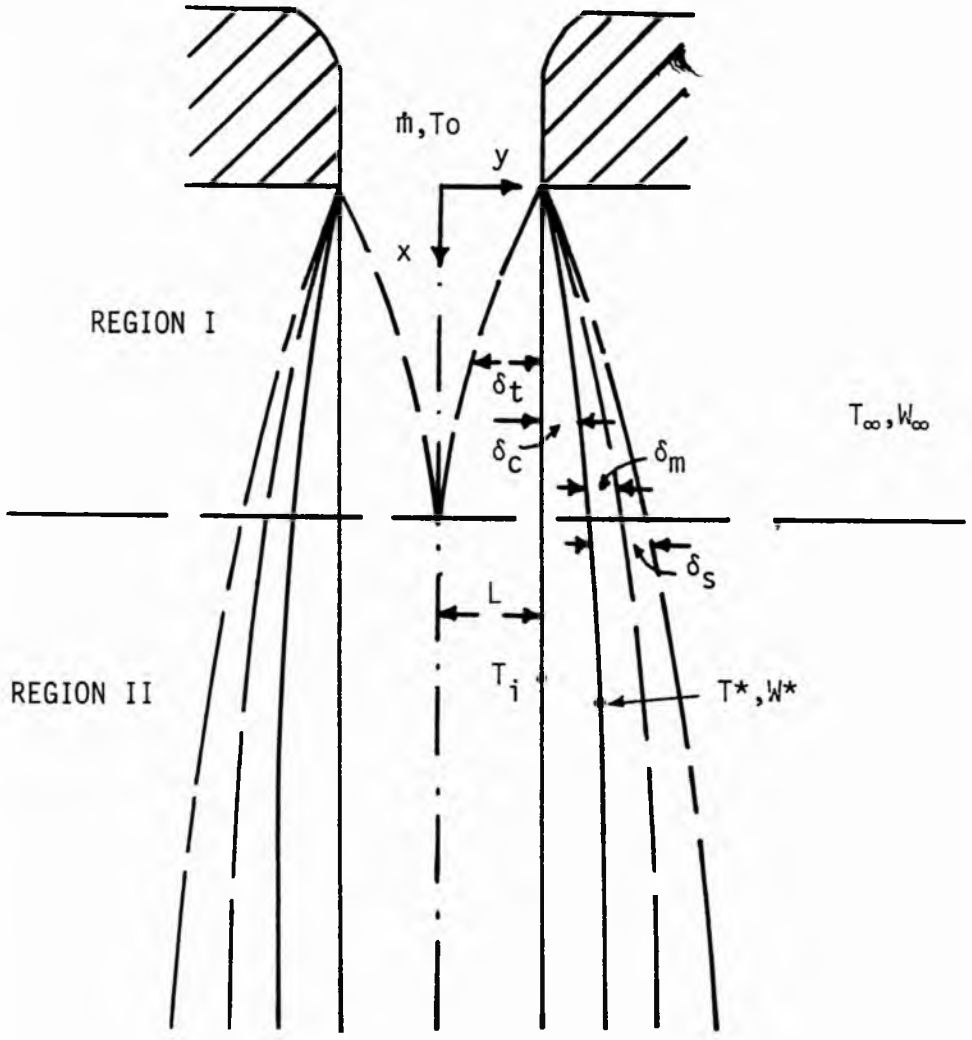

Figure 3.3.1. Schematic of model for condensation on a sheet in the presence of a noncondensible gas.

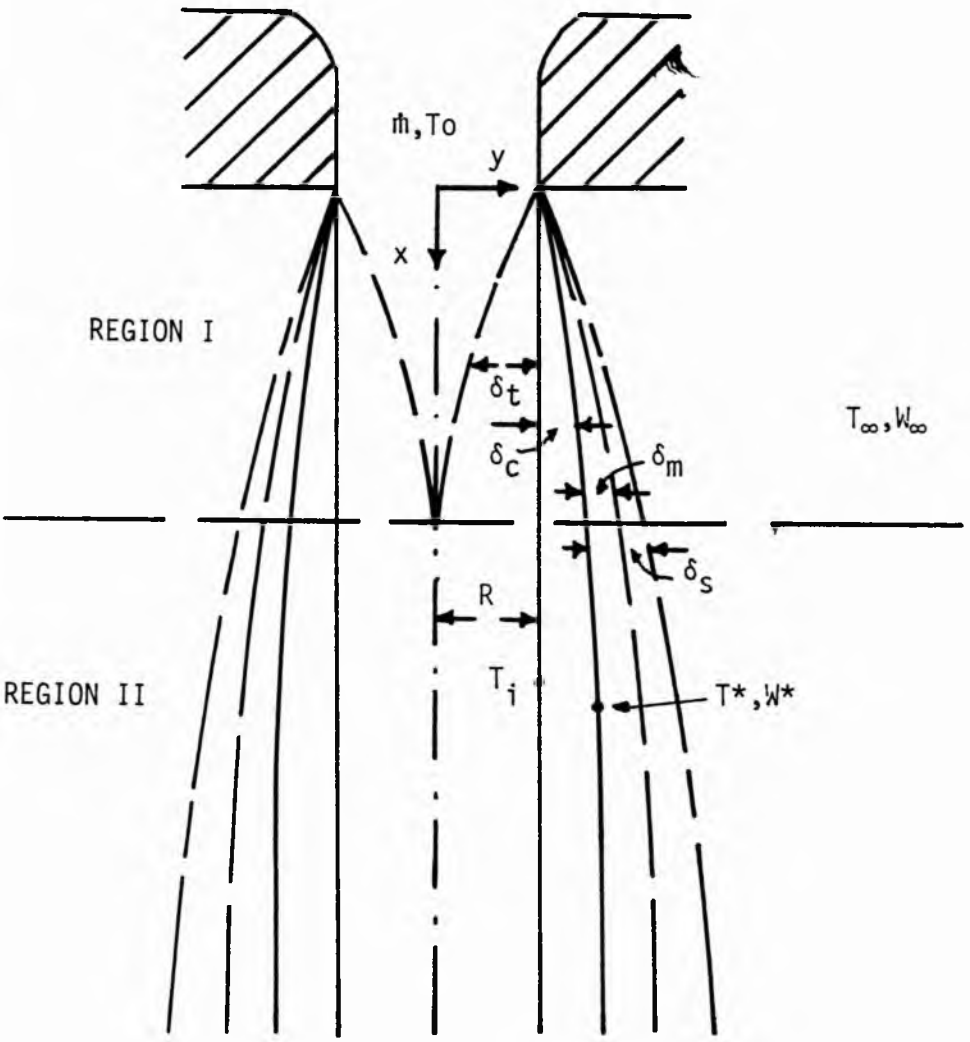

Figure 3.3.2. Schematic of model for condensation on a cylindrical jet in the presence of a noncondensible gas.

densate layer of thickness δ_c, the vapor-gas mixture forms a thin boundary layer, δ_M, induced by the flow of liquid. Within the mixture is also a species boundary layer in which the noncondensible gas concentration varies from W* at the liquid-mixture interface to the free stream value of W_∞. At the vapor-gas condensate interface the temperature is T*. At the interface between the liquid coolant and the condensate layer the temperature is T_i.

Region I Equations

In Region I the energy equation for the coolant is

$$\frac{d}{dx}\int_{L-\delta_t}^{L} \rho_\ell C_{p\ell} U(T_\ell - T_o)\, y^n\, dy = k_\ell \left(y^n \frac{\partial T_\ell}{\partial y}\right)\Big|_{y=L} . \qquad 3.3.1$$

For the sheet n is equal to zero and for the cylindrical jet it is equal to one. Further, for the jet L = R which is the coolant jet radius while for the sheet L = L, the half thickness of the sheet as shown in Figures 3.3.1 and 3.3.2.

In the condensate layer the assumption of a small Jakob number insures that the sensible heat capacity of the condensate is small compared to the heat of vaporization and that the condensate layer is thin. These assumptions further make the effects of curvature small in the condensate layer for the cylindrical jet (8,9), thus the energy balance across the condensate yields

for both the sheet and jet

$$h_{fg} \frac{d}{dx}\int_{L}^{L+\delta_c} \rho_\ell U dy = k_\ell \frac{\partial T_c}{\partial y}\Big|_{y=L} . \qquad 3.3.2$$

In the coolant stream Jacobs and Nadig (8,9) have shown that for Region I an assumption of a quadratic temperature profile which satisfies the conditions

$$\left.\begin{aligned} T_\ell(L - \delta_t) &= T_o \\ \frac{\partial T_\ell}{\partial y}(L - \delta_t) &= 0 \\ T_\ell(L) &= T_i \end{aligned}\right\} \qquad 3.3.3$$

provides an excellent agreement with the analytical results for $h_{fg} \to \infty$. If we define a new variable $\xi = L - y$, the temperature profile in the coolant can be represented as

$$T_\ell - T_o = (T_i - T_o)\left(1 - \frac{\xi}{\delta_t}\right)^2. \qquad 3.3.4$$

In the condensate layer, the assumptions utilized in developing the energy equation imply a linear temperature profile

$$T_c - T_i = (T^* - T_i)\left(\frac{y - L}{\delta_c}\right). \qquad 3.3.5$$

Utilizing the compatability of heat fluxes between the condensation and the coolant

$$\left.\frac{\partial T_L}{\partial y}\right|_L = \left.\frac{\partial T_c}{\partial y}\right|_L \qquad 3.3.6$$

one can solve for the temperature T_i

$$T_i = \frac{T_o + \frac{1}{2}\frac{\delta_t}{\delta_c} T^*}{1 + \frac{1}{2}\frac{\delta_t}{\delta_c}} \quad . \qquad 3.3.7$$

Substituting Equations 3.3.4, 3.3.5 and 3.3.7 into Equations 3.3.1 and 3.3.2 for the case of a sheet results in

$$\frac{d\bar{\delta}_t^2}{d\bar{x}} = \frac{\left(\frac{12}{Pr\ Re_{D_H}} - \frac{2\,\bar{\delta}_t^2 \frac{d\theta^*}{d\bar{x}}}{\theta^*}\right)\left(1 + \frac{1}{2}\frac{\bar{\delta}_t}{\bar{\delta}_c}\right) + \frac{\bar{\delta}_t^2}{\bar{\delta}_c^2}\frac{d\bar{\delta}_c^2}{dx}}{2 + \frac{1}{2}\frac{\bar{\delta}_t}{\bar{\delta}_c}} \qquad 3.3.8$$

and

$$\frac{d\delta_c 2}{dx} = \frac{2Ja}{Pr\ Re_{D_H}} \frac{\theta^*}{1 + \frac{\bar{\delta}_t}{\bar{\delta}_c}} \qquad 3.3.9$$

where lengths have been nondimensionalized with respect to the hydraulic diameter and

$$\theta = \frac{T - T_o}{T_\infty - T_o} \quad . \qquad 3.3.10$$

For a cylindrical jet the governing equations for δ_t and δ_c are

$$\frac{d\bar{\delta}_t^2}{d\bar{x}} = \left\{\left[\frac{12}{Re_{D_H} Pr} - \frac{2\bar{\delta}_t^2}{\theta^*}\left(1 - \frac{\bar{\delta}_t}{2}\right)\frac{d\theta^*}{d\bar{x}}\right]\left(1 + \frac{1}{2}\frac{\bar{\delta}_t}{\bar{\delta}_c}\right) + \right. \qquad 3.3.11$$

$$\left. 1 - \left(\frac{\bar{\delta}_t}{2}\right)\frac{\bar{\delta}_t^2}{\bar{\delta}_c^2}\frac{d\bar{\delta}_c^2}{d\bar{x}}\right\} \div$$

$$\left\{(1 - \bar{\delta}_t)\left(1 + \frac{1}{2}\frac{\bar{\delta}_t}{\bar{\delta}_c}\right) + \left(1 + \frac{\bar{\delta}_t}{2}\right)\right\}$$

and

$$\frac{d\bar{\delta}_c^2}{d\bar{x}} = \frac{2Ja}{Re_{D_H} Pr} \quad \frac{\theta^*}{1 + \frac{1}{2}\frac{\bar{\delta}_t}{\bar{\delta}_c}\ (1 + 2\delta_c)} \ . \qquad 3.3.12$$

In order to solve the equations given above it is first necessary to determine the value of θ^*, the nondimensional saturation temperature at the condensate vapor-gas mixture interface. This of course requires solving for the concentration of the vapor at the interface, which in turn requires the solution of the vapor-gas momentum and species equations. The assumption of a small value of Jakob number and small variation in h_{fg} allows for integration of the Clausius Clapeyron equation (8,9) to yield

$$\theta^* = \frac{\theta_{sat_\infty} - \frac{T_o - T_{sat_\infty} R}{h_{fg}(T_\infty - T_o)} \ln \frac{P_{v\infty}}{P_v^*}}{1 + \frac{T_{sat_\infty} R}{h_{fg}} \ln \frac{P_{v\infty}}{P_v^*}} \ . \qquad 3.3.13$$

The ratio of partial pressure of the vapor to total pressure

$$\frac{P_v}{P} = \frac{1 - W}{1 - W\left(1 - \frac{M_v}{M_g}\right)} \qquad 3.3.14$$

then allows for relating the mass concentration of gas to the value of θ^*.

The integral forms for the momentum and species equations in the gas-vapor mixture, assuming that the condensate vapor-gas interface is impenetrable to the gas, reduce to (8,9)

$$\frac{d}{dx}\int_{L+\delta_c}^{L+\delta_c+\delta_M} u^2\, y^n\, dy + U^2(L+\delta_c)^n \frac{\rho_\ell}{\rho_m^*}\frac{d\delta_c}{dx} = -\nu\left(y^n \frac{\partial u}{\partial y}\right)\Big|_{L+\delta_c} \qquad 3.3.15$$

and

$$\frac{d}{dx}\int_{L+\delta}^{L+\delta_c+\delta_s} (W - W_\infty)\, u y^n\, dy = D\frac{W_\infty}{W^*}\left(y^n \frac{\partial W}{\partial y}\right)\Big|_{L+\delta} . \qquad 3.3.16$$

As with the energy equations for the coolant and condensate, for the cylindrical jet n = 1 and L = R while for the sheet n = 0 and L = L.

The conditions of no slip at the condensate vaporgas mixture interface, zero velocity in the mixture as $y \to \infty$ and the condition of $\partial u/\partial y = 0$ as $y \to \infty$ suggest that in the mixture

$$u = U\left[1 - \frac{y - (L+\delta_c)}{\delta_m}\right]^2 . \qquad 3.3.17$$

For the species equation,

$$\begin{aligned} y &= L + \delta_c & W &= W^* \\ y &= L + \delta_c + \delta_s & W &= W_\infty \text{ and } \frac{\partial w}{\partial y} = 0 \end{aligned} \qquad 3.3.18$$

results in

$$W - W_\infty = (W^* - W_\infty)\left(1 - \frac{y - (L+\delta_c)}{\delta_s}^2\right) . \qquad 3.3.19$$

Substitution of Equations 3.3.17 and 3.3.19 into Equations 3.3.15 and 3.3.16 and nondimensionalizing results in

$$\frac{d\bar{\delta}_m^2}{d\bar{x}} = \frac{20}{Re_{D_H}\frac{\nu_\ell}{\nu_m}} - 5\,\frac{\rho_\ell}{\rho_m}\,\frac{\bar{\delta}_m}{\bar{\delta}_c}\,\frac{d\bar{\delta}_c^2}{d\bar{x}} \qquad 3.3.20$$

and

$$\frac{d\bar{\delta}_s^2}{d\bar{x}} = \left\{\left[\frac{12}{Re_{D_H}\,Sc} - \frac{2\bar{\delta}_s^2}{W^* - W_\infty}\left(1 + \frac{1}{2}\,\frac{\bar{\delta}_s}{\bar{\delta}_m} + \frac{1}{10}\,\frac{\bar{\delta}_s^2}{\bar{\delta}_m^2}\right)\cdot\right.\right.$$

$$\left.\left.\frac{d(W^* - W_\infty)}{d\bar{x}} - \left(\frac{1}{2}\,\frac{\bar{\delta}_s^3}{\bar{\delta}_m^3} - \frac{1}{5}\,\frac{\bar{\delta}_s^4}{\bar{\delta}_m^4}\right)\frac{d\bar{\delta}_m^2}{d\bar{x}} - 3\,\frac{\rho_\ell}{\rho_m}\,\frac{\bar{\delta}_s}{\bar{\delta}_c}\,\frac{d\bar{\delta}_c^2}{d\bar{x}}\right]\right\} \div$$

$$\left(1 - \frac{\bar{\delta}_s}{\bar{\delta}_m} + \frac{3}{10}\,\frac{\bar{\delta}_s^2}{\bar{\delta}_m^2}\right) \qquad 3.3.21$$

for the sheet. For the jet the following equations are obtained

$$\frac{d\bar{\delta}_m^2}{d\bar{x}} = \frac{\dfrac{12}{Re_{D_H}\frac{\nu_\ell}{\nu_m}} - 3\,\dfrac{\rho_\ell}{\rho_m}\,\dfrac{\bar{\delta}_m}{\bar{\delta}_c}\,\dfrac{d\bar{\delta}_c^2}{d\bar{x}}}{1 + \bar{\delta}_m} \qquad 3.3.22$$

and

$$\frac{d}{d\bar{x}}\left[(W^* - W_\infty)\left\{\left(\frac{1}{2} + \bar{\delta}_c\right)\bar{\delta}_s\left(1 - \frac{1}{2}\,\frac{\bar{\delta}_s}{\bar{\delta}_m} + \frac{1}{10}\,\frac{\bar{\delta}_s^2}{\bar{\delta}_m^2}\right) + \right.\right.$$

$$\left.\left.\bar{\delta}_s^2\left(\frac{1}{4} - \frac{1}{5}\,\frac{\bar{\delta}_s}{\bar{\delta}_m} + \frac{1}{10}\,\frac{\bar{\delta}_2^2}{\bar{\delta}_m^2}\right)\right\}\right]$$

$$= \frac{6}{Re_{D_H}\,Sc\,\frac{\nu_\ell}{\nu_m}}\left(\frac{1}{2} + \bar{\delta}_c\right)\frac{W_\infty}{W^*}\left(\frac{W^* - W_\infty}{\bar{\delta}_s}\right). \qquad 3.3.23$$

For both the sheet and the jet the condition of impermeability of the condensate vapor-gas mixture interface leads to

$$W^* = \frac{W_\infty}{1 - \frac{1}{4} Re_{D_H} Sc \frac{\mu_\ell}{\mu_m} \frac{\bar{\delta}_s}{\bar{\delta}_c} \frac{d\bar{\delta}_c^2}{d\bar{x}}} \qquad 3.3.24$$

Thus, for Region I, Equations 3.3.8, 3.3.9, 3.3.13, 3.3.14, 3.3.20, 3.3.21, and 3.3.24 completely define the condensation on a sheet in the presence of a noncondensible gas. For a cylindrical at the governing equations are Equations 3.3.11, 3.3.12, 3.3.13, 3.3.16, 3.3.22, 3.3.23 and 3.3.24.

Region II Equations

Region II begins when $\delta_t = L$. From this point the entire coolant stream heats up such that the centerline temperature will be continuously increasing. The energy equation for the coolant stream in Region II is

$$\frac{d}{dx} \int_0^L \rho_\ell \, UC_p \, T_\ell \, y^n \, dy = k_\ell \left(y^n \frac{\partial T_\ell}{\partial y} \right) \Big|_{y=L} . \qquad 3.3.25$$

The temperature profile in the coolant must satisfy the boundary conditions

$$y = 0 \quad \frac{\partial T_\ell}{\partial y} = 0 \quad , \quad T_\ell = T_c$$
$$y = L \quad T = T_i \ . \qquad 3.3.26$$

These conditions are satisfied by the expression

$$T_\ell - T_{cL} = (T_i - T_{cL}) \left(\frac{y}{L}\right)^2 \quad . \qquad 3.3.27$$

The governing equation and the temperature profile for the condensate layer are the same as those in Region I. Using the compatability of heat fluxes at the interface between the original coolant stream and the condensate layer yields

$$\theta_i - \theta_{cL} = \frac{1}{8} \frac{(\theta^* - \theta_i)2^n}{\delta_c} . \qquad 3.3.28$$

Substituting Equation 3.3.27 into Equation 3.3.25, nondimensionalizing the resulting equations and utilizing Equation 3.3.28 produces the following equations for the sheet and jet, respectively

for the sheet
$$\frac{d\theta_i}{d\bar{x}} = \frac{\dfrac{48(\theta^* - \theta_i)}{Re_{D_H} Pr} - \dfrac{1}{2} \dfrac{\theta^* - \theta_i}{\bar{\delta}_c^2} \dfrac{d\bar{\delta}_c^2}{d\bar{x}} + \dfrac{d\theta^*}{d\bar{x}}}{12\,\bar{\delta}_c + 1} \qquad 3.3.29$$

for the jet
$$\frac{d\theta_i}{d\bar{x}} = \frac{\dfrac{32(\theta^* - \theta_i)}{Re_{D_H} Pr} - \dfrac{1}{2} \dfrac{\theta^* - \theta_i}{\bar{\delta}_c^2} \dfrac{d\bar{\delta}_c^2}{d\bar{x}} + \dfrac{d\theta^*}{d\bar{x}}}{8\,\bar{\delta}_c + 1} \quad . \qquad 3.3.30$$

The energy equations for the condensate films in the sheet and jet are expressed in Region II as

for the sheet
$$\frac{d\bar{\delta}_c^2}{d\bar{x}} = \frac{2Ja}{Re_{D_H} Pr} (\theta^* - \theta_i) \qquad 3.3.31$$

and for the jet
$$\frac{d\bar{\delta}_c^2}{d\bar{x}} = \frac{2Ja}{Re_{D_H} Pr} \frac{(\theta^* - \theta_i)}{(1 + 2\bar{\delta}_c)} \quad . \qquad 3.3.32$$

The expressions for $\bar{\delta}_m^2$, W^*, $\bar{\delta}_s^2$ remain as given in Region I. The initial conditions for the variables θ_i, $\bar{\delta}_c^2$, θ^*, W^*, $\bar{\delta}_m^2$ and $\bar{\delta}_s^2$ for Region II are the conditions obtained at the end of Region I.

Calculation of Percent Coolant Utilized

The mean temperature of the coolant is calculated from the equation

$$T_m \int_0^L \rho_\ell C_{p_\ell} u y^n \, dy = \int_0^L \rho_\ell C_{p_\ell} u T_\ell y^n \, dy \quad . \qquad 3.3.33$$

For Region I for a sheet

$$\theta_m = \frac{4}{3} \theta_i \bar{\delta}_t \qquad 3.3.34$$

and for a jet

$$\theta_m = \frac{8}{3} \theta_i \delta_t (1 - \bar{\delta}_t) \quad . \qquad 3.3.35$$

In Region II for a sheet

$$\theta_m = \frac{2}{3} \theta_{cL} + \frac{1}{3} \theta_i \qquad 3.3.36$$

and for a jet

$$\theta_m = \frac{\theta_{cL} + \theta_i}{2} \quad . \qquad 3.3.37$$

Note that the definition of θ is

$$\theta = \frac{T - T_o}{T_\infty - T_o} \quad ; \qquad 3.3.10$$

thus, the value of θ_m gives the fraction of the coolants capacity to absorb the heat given up by the condensation process. For direct contact condensation, it is this quantity that is important to the designer rather than the heat transfer coefficient or local value of Nusselt number. The heat transfer coefficient or Nusselt number are only reported for comparison with the results of prior studies.

3.4. Results and Discussion

The governing differential equations derived herein indicate that the problem of condensation of a vapor on a coolant stream of its own liquid can be defined in terms of the $^{Re}D_H$, Pr, x/D_H, Ja, M_v/M_g, ρ_ℓ/ρ m, ν_ℓ/ν_m, and W_∞ when a noncondensible gas is present in the vapor. Due to the large number of variables, we have restricted the results to be presented in this chapter to parameters which typify the problem for a steam-air system. In this way we are able to more easily compare our results with those of other investigators (15).

As noted, the problem is divided into two regions. For Region I, which defines the zone where a thermal wave penetrates the coolant and moves to its centerline, a similarity solution is available for very small values of $\bar{x}$. In fact, for the problem of the sheet the similarity solution is applicable; for small values of the Jakob number the entire region applies. For the cylindrical jet a small error exists if the similarity solution is used to describe the entire region. The similarity solution is satisfied by $\delta_t = ax^{1/2}$, $\delta_c = bx^{1/2}$, $\delta_m = cx^{1/2}$, and $\delta_s = dx^{1/2}$. These solutions indicate that W^*, θ^*, and θ_i are of constant value in Region I. Similar results were found by Taitel and Tamir (20), for condensation in the presence of a

noncondensible gas. The extent of Region I, as one would guess for $\theta_i - \theta^*$ equal to constants, is a function only of the hydraulic diameter of the jet and the value of the Peclet number. For a sheet the extent of Region I is given by

$$\bar{x}_{D_{sheet}} = 0.083 \, Re_{D_H} \, Pr \, . \qquad 3.4.1$$

This is in agreement with the value obtained by Taitel and Tamir who neglected the influence of the condensate layer.

The governing equations for the cylindrical jet are highly nonlinear and do not yield a similarity solution unless $\bar{x} \to 0$. Thus, the extent of Region I is dependent upon other parameters. However, for Ja < 0.05, an approximate value of $x_{D_{jet}}$ can be obtained as the changes in θ_i, W^* and θ^* are small. The approximate value is given by

$$\bar{x}_{D_{jet}} = 0.146 \, Re_{D_H} \, Pr \, . \qquad 3.4.2$$

Equations 2.2.34 and 2.3.35 give the value of the mean temperature for Region I. As Ja $\to$ 0, and $W_\infty \to 0$, θ_i goes to 1. Thus for a sheet the mean temperature, θ_m, goes to 1/3 at $\delta_t = L$ and for a jet the mean temperature, θ_m, goes to 2/3 at $\delta_t = R$. The effect of the presence of a noncondensible is to lower the values of θ^* and θ_i, even for very small Jakob number. Since the value of θ_m is the fraction of coolant utilized, it is clear that an increase in the value of W_∞ will decrease the fraction of coolant utilized. Thus, it is necessary, under all conditions where one wishes to utilize a major portion of the coolant capacity, to carry out the analyses for Region

II.

Typical behavior for θ_i, θ^* and θ_M, and W^* are shown in Figures 3.4.1 through 3.4.4 as a function of x. Figures 3.4.1 and 3.4.2 are shown for a vapor-gas mixture pressure of 2.86 psia and Figures 3.4.3, 3.4.5 and 3.4.6 for 14.7 psia. It is clear that the effects of the noncondensible gas are more pronounced at the lower pressure. This fact was previously noted by Taitel and Tamir (20) for condensation on a sheet and by Minkowycz and Sparrow (6) for the case of condensation on a cooled plate. An examination of the governing equations developed in Chapter 2 would indicate that this is due to the change in the parameter ρ_ℓ/ρ_m with pressure. As pressure decreases the value of ρ_ℓ/ρ_m increases thus increasing the interfacial concentration of noncondensible gas. This in turn leads to a lower value of heat transfer and extends the length of the coolant stream necessary to achieve a given coolant utilization.

In Region II the entire coolant stream heats up. Thus, the rate of condensation decreases. The decrease in condensation rate brings less noncondensibles to the condensate-vapor gas interface which allows θ^* and θ_i to increase. Eventually W^* decreases to the free stream value W_∞. The decrease in W^* leads to a "recovery of the heat transfer coefficient" above that for a pure vapor at large values of x in Region II. However, the length of coolant stream necessary to achieve a given degree of coolant utilization for condensation is generally larger than that for a pure vapor even though W_∞ might might become extremely large. Jacobs and Nadig (8) have indicated that for condensation on an immiscible thin film that it is possible for a maximum value of coolant stream length to occur. Further increase in the

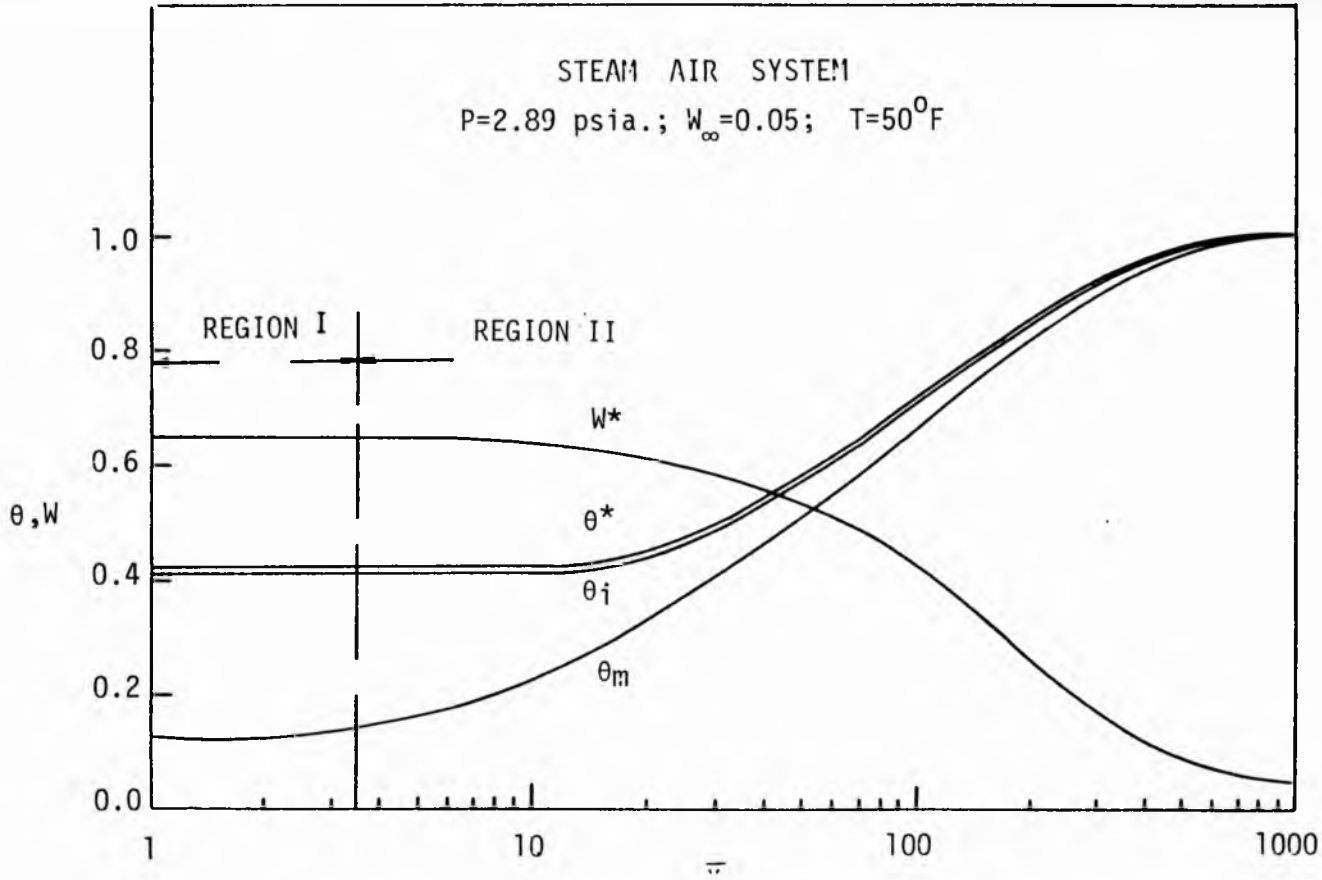

Figure 3.4.1. Condensation of a sheet. θ*,θi,θm,W* as a function of X̄, P = 2.89 psia.

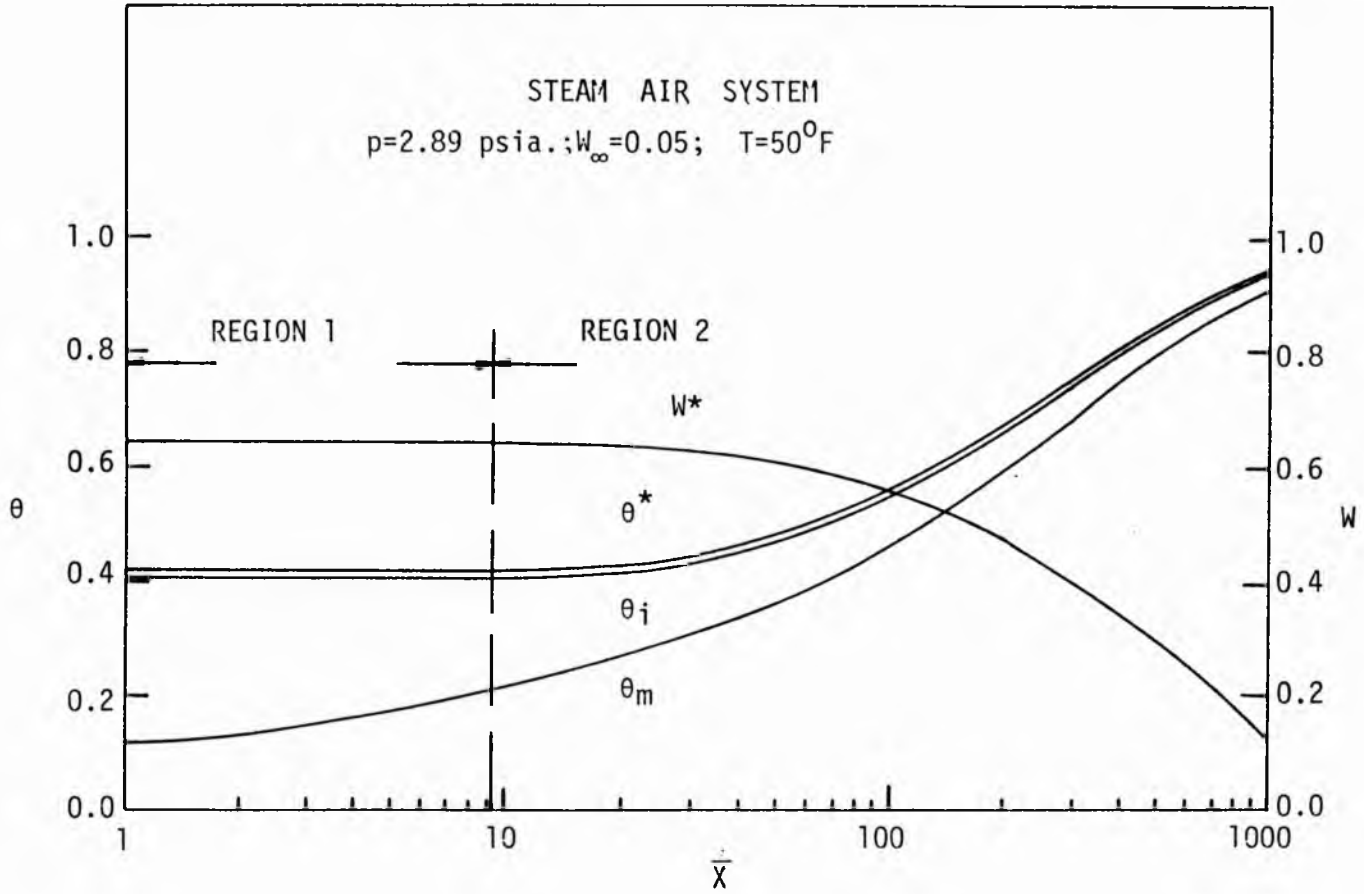

Figure 3.4.2. Condensation on a jet. θ*,θi,θm,W* as function of $\bar{X}$, p = 2.89 psia.

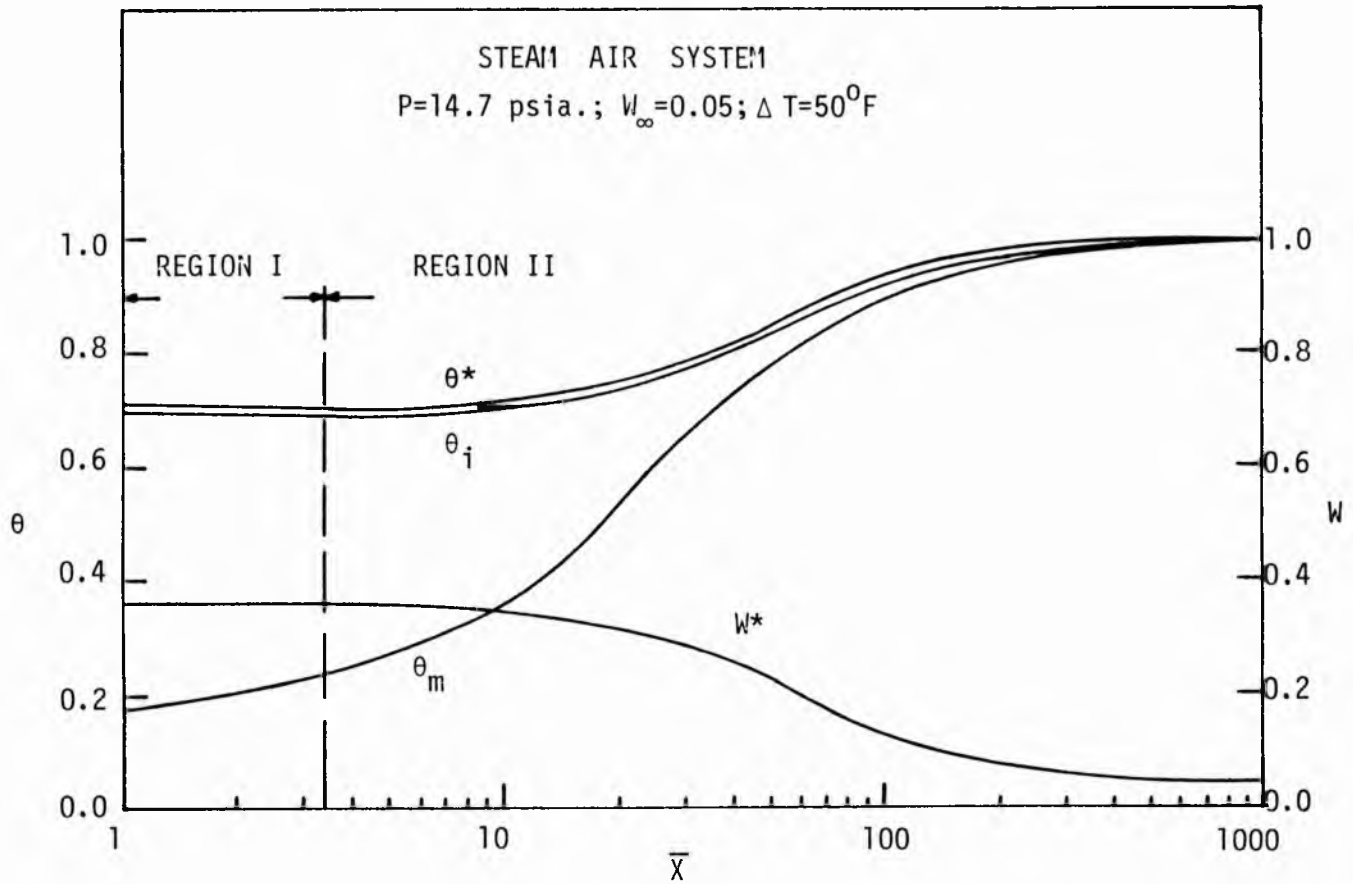

Figure 3.4.3. Condensation on a sheet. $\theta^*, \theta_i, \theta_m, W^*$ as a function of $\overline{X}$, P = 14.7 psia.

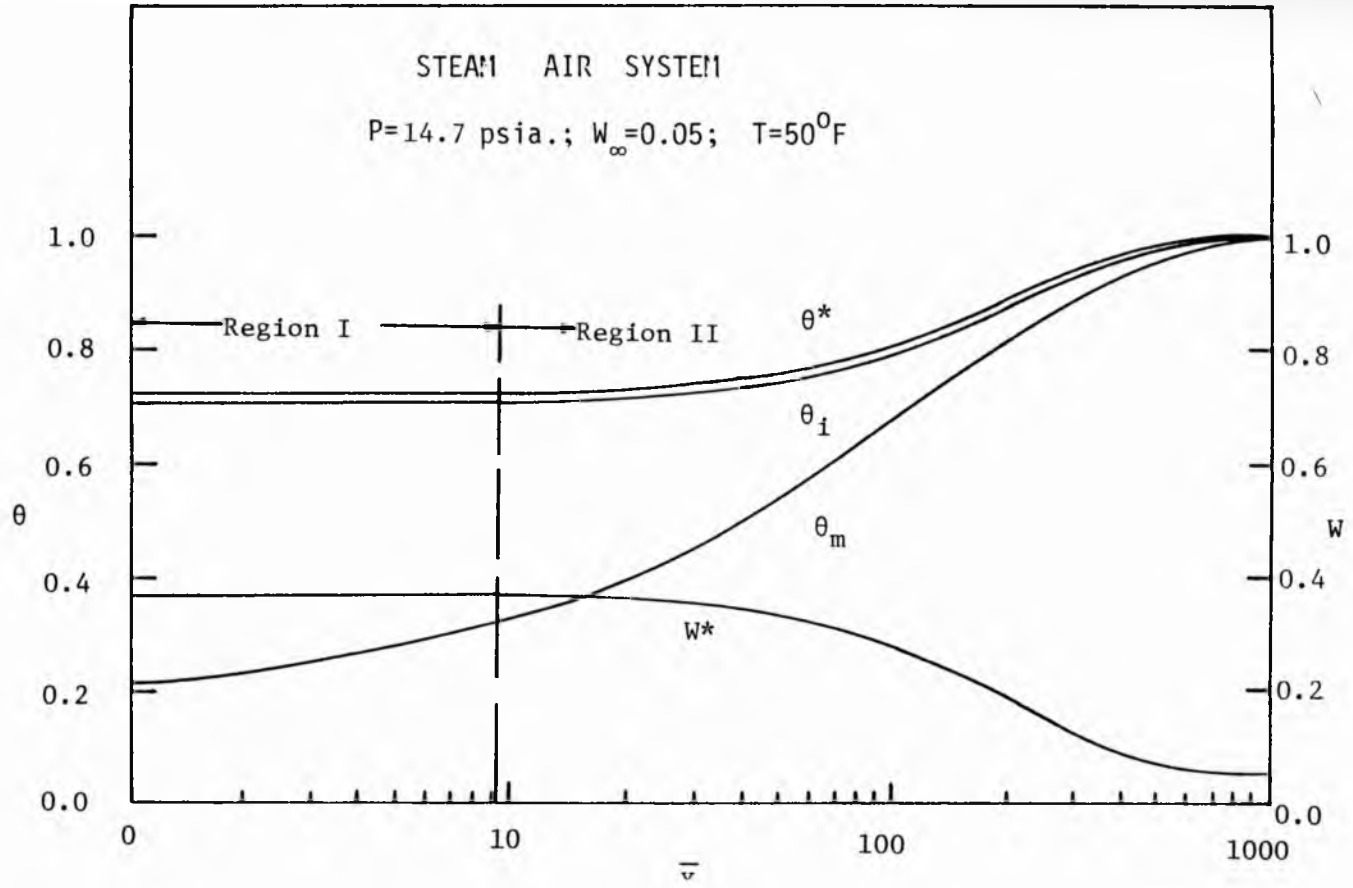

Figure 3.4.4. Condensation on a jet. $\theta^*, \theta_i, \theta_m, W^*$ as a function of $\bar{X}$, P = 14.7 psia.

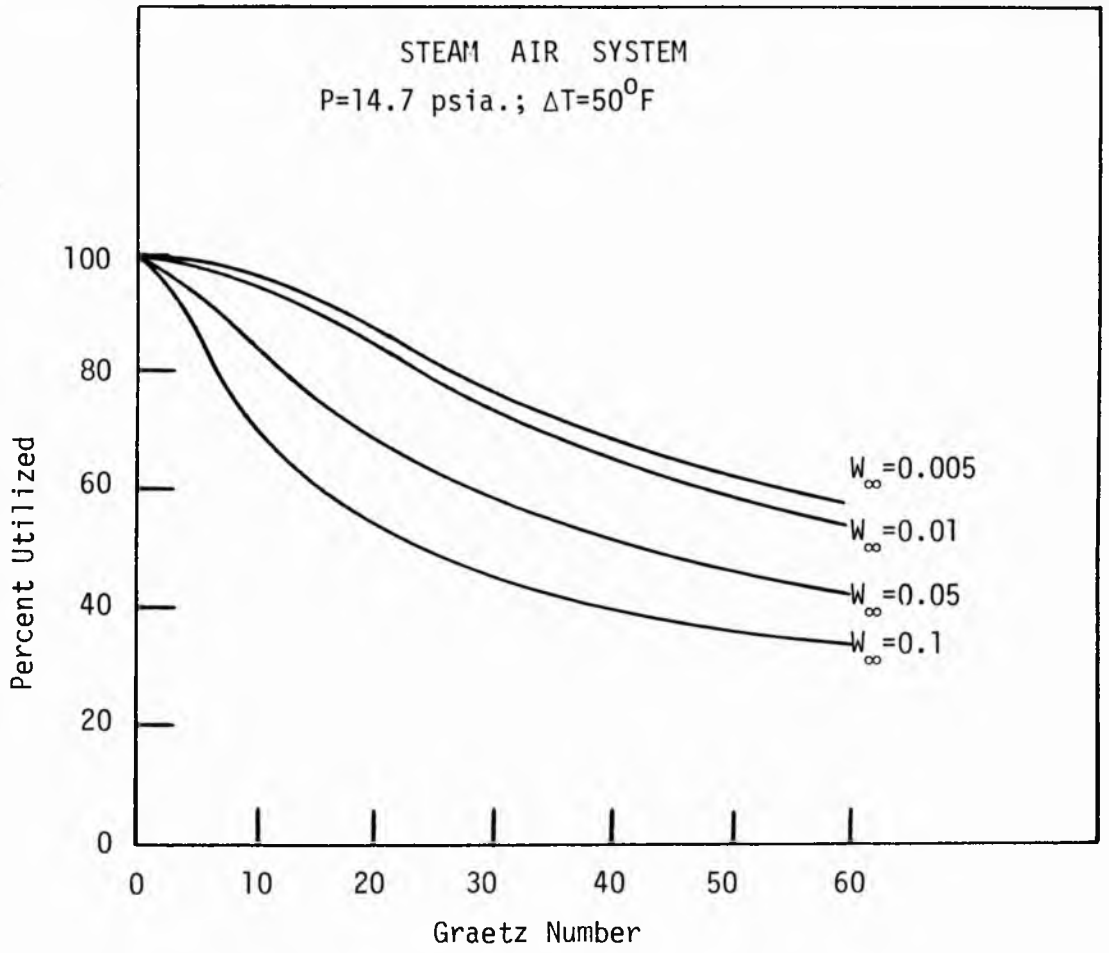

Figure 3.4.5. Condensation on a sheet. Percent utilized as a function of Graetz number.

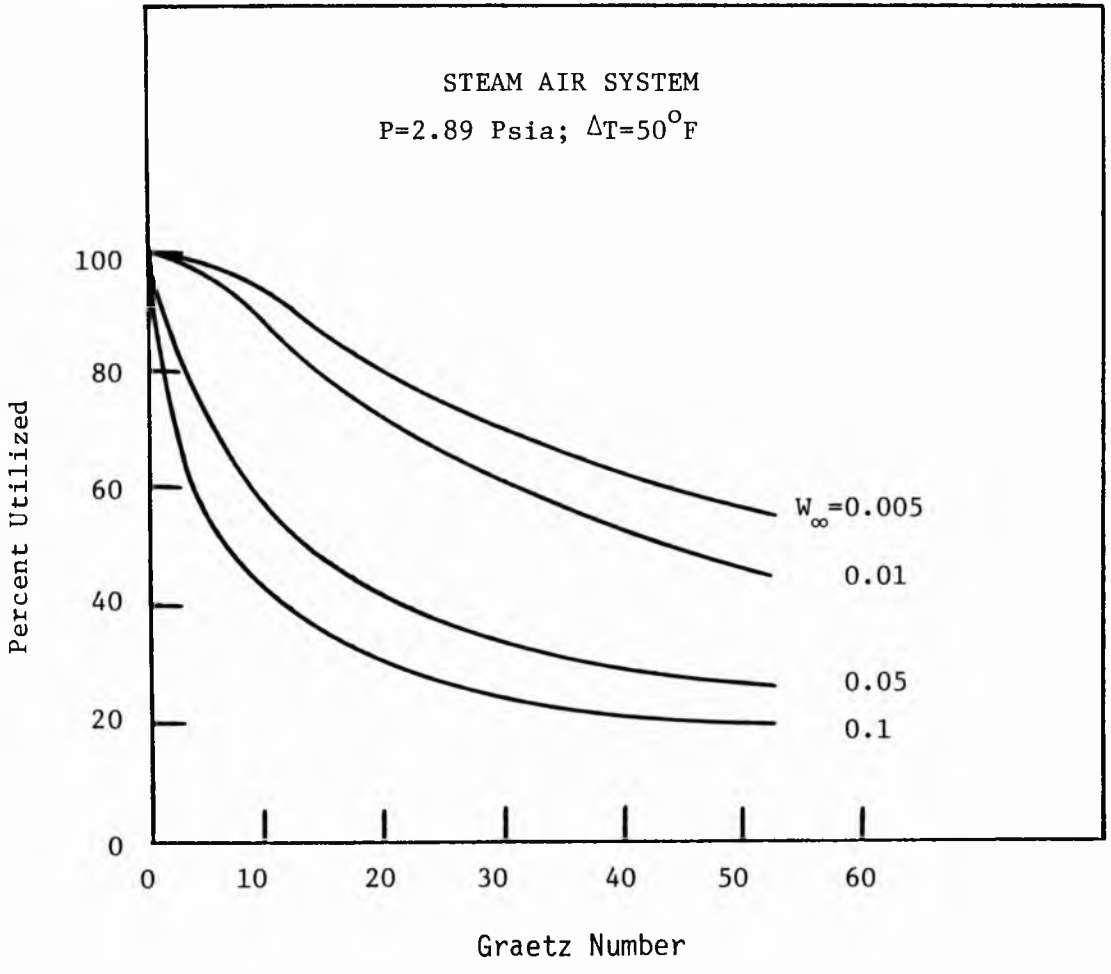

Figure 3.4.6. Condensation on a jet. Percent utilized as a function of Graetz number.

value of W_∞ would lead to a decrease in the length required for a given degree of utilization. Although for the present problem we did not observe this behavior, examination of the governing equations would indicate the possibility as P_v/P tends to zero.

For the case of steam-air, Tables 3.4.1 and 3.4.2 indicate the ratio of Graetz number without noncondensibles to that with noncondensibles present as a function of W_∞ and Jakob number for the two pressures illustrated in Figures 3.4.1 through 3.4.4. These results are also shown in Figures 3.4.5 and 3.4.6. The experimental data of Hasson et al. (15) for condensation on a sheet were carried out at the two pressures shown in Table 3.4.1. He claims accuracy of ± 35%. For W_∞ = 0.01 his experiments would indicate a ratio of Graetz number of 1.8 for effectively complete condensation. Table 3.4.1 indicates a value of 1.826 for 90% utilization at p = 2.89 psia and ΔT = 75°F. At the higher pressure his ΔT would be approximately 142°F. Extrapolation of the data in Table 3.4.1 would yield at ratio of Graetz number of 1.65. These values are well within his experimental spread and indicate good agreement.

TABLE 3.4.1.

Condensation on a Sheet

% Util.	Pressure Psia	W_∞	Ratio of Graetz Number $\Delta T=25°F$	$\Delta T=50°F$	$\Delta T=75°F$	$\Delta T=100°F$
60	14.7	0.005	1.047	1.089	1.107	1.168
70	14.7	0.005	1.050	1.091	1.139	1.177
80	14.7	0.005	1.060	1.103	1.153	1.198
90	14.7	0.005	1.080	1.129	1.173	1.220
60	14.7	0.01	1.117	1.179	1.235	1.356
70	14.7	0.01	1.121	1.191	1.293	1.384
80	14.7	0.01	1.131	1.217	1.316	1.428
90	14.7	0.01	1.168	1.266	1.368	1.473
60	14.7	0.05	1.632	2.117	2.797	3.702
70	14.7	0.05	1.720	2.259	3.008	3.863
80	14.7	0.05	1.848	2.470	3.223	4.102
90	14.7	0.05	2.042	2.708	3.479	4.334
60	14.7	0.1	2.567	3.860	5.556	7.764
70	14.7	0.1	2.824	4.235	6.079	8.203
80	14.7	0.1	3.185	4.479	6.624	8.781
90	14.7	0.1	3.749	5.380	7.249	9.316
60	2.98	0.005	1.185	1.383	1.622	1.956
70	2.89	0.005	1.213	1.413	1.686	2.021
80	2.98	0.005	1.244	1.472	1.747	2.090
90	2.98	0.005	1.291	1.542	1.826	2.150
60	2.89	0.01	1.397	1.865	2.448	3.274
70	2.89	0.01	1.446	1.921	2.573	3.395
80	2.89	0.01	1.516	2.035	2.693	3.513
90	2.89	0.01	1.615	2.180	2.842	3.597
60	2.89	0.05	3.596	6.698	10.840	16.309
70	2.89	0.05	3.962	7.263	11.672	16.838
80	2.89	0.05	4.439	7.997	12.357	17.460
90	2.89	0.05	5.088	8.818	13.108	17.885
60	2.89	0.1	7.573	14.944	24.508	36.916
70	2.89	0.1	8.582	16.426	26.606	38.387
80	2.89	0.1	9.884	18.322	28.444	40.164
90	2.89	0.1	11.798	20.507	30.420	41.398

TABLE 3.4.2.

Condensation on a Jet

% Util.	Pressure Psia	W_∞	Ratio of Graetz Number ΔT=25°F	ΔT=50°F	ΔT=75°F	ΔT=100°F
60	14.7	0.005	2.000	1.698	1.444	1.268
70	14.7	0.005	2.042	1.822	1.480	1.282
80	14.7	0.005	2.000	1.924	1.713	1.554
90	14.7	0.005	1.872	1.883	2.148	2.261
60	14.7	0.01	2.451	1.981	1.667	1.536
70	14.7	0.01	2.620	2.219	1.840	1.744
80	14.7	0.01	2.634	2.505	2.324	2.384
90	14.7	0.01	2.481	2.620	3.059	3.392
60	14.7	0.05	5.333	5.226	6.019	7.339
70	14.7	0.05	6.282	6.603	7.653	8.974
80	14.7	0.05	6.911	7.724	9.074	10.357
90	14.7	0.05	6.955	8.074	9.728	11.063
60	14.7	0.1	10.549	11.849	13.704	15.232
70	14.7	0.1	12.211	13.877	15.653	16.987
80	14.7	0.1	13.178	14.848	16.750	18.080
90	14.7	0.1	13.205	14.632	16.550	17.926
60	2.89	0.005	2.393	1.638	1.940	4.657
70	2.89	0.005	2.707	1.858	2.892	6.862
80	2.89	0.005	3.238	2.583	4.029	8.387
90	2.89	0.005	3.613	3.943	5.093	8.387
60	2.89	0.01	3.120	2.556	4.429	9.989
70	2.89	0.01	3.748	3.440	6.034	12.215
80	2.89	0.01	4.722	4.757	7.346	13.308
90	2.89	0.01	5.510	6.477	8.410	3.156
60	2.89	0.05	12.784	14.208	17.870	23.589
70	2.89	0.05	15.070	16.534	19.720	25.090
80	2.89	0.05	16.743	18.314	20.917	25.536
90	2.89	0.05	17.032	19.577	21.692	24.994
60	2.89	0.1	26.765	27.057	29.648	34.143
70	2.89	0.1	29.014	29.589	31.613	35.590
80	2.89	0.1	30.158	30.981	32.685	36.018
90	2.89	0.1	29.609	31.319	32.899	35.278

CHAPTER 4

CONDENSATION OF A PURE VAPOR ON AN ISOTHERMAL VERTICAL PLATE

4.1 Introduction

Laminar film condensation finds applications in trickling type cooling towers, packed and wetted wall towers for rectification and gas absorption and in various types of coolers and evaporators. Nusselt [22] was the first to analyze the problem of laminar film condensation in 1916. He assumed a linear temperature profile in the condensate film, neglected the vapor shear and the interfacial resistance. Over the years numerous investigators have dealt with the same problem examining each of the assumptions made by Nusselt. Roshnow [23] treated the problem in 1956 including the sensible heat of condensation. Sparrow and Greg [24] used a similarity transformation to solve the boundary layer equations. Chen [25] considered the effect of drag due to an initially stagnant vapor.

Although sizeable work has been done on laminar film condensation, very little work has been reported on direct contact condensation on thin film. Thus, it was decided to analyze the problem of condensation of a pure vapor on a thin film flowing over an isothermal vertical surface.

A survey of literature reveals that there are two prior works reported which bear slight resemblence to the present problem. Murty and

Sastry [26] dealt with the problem of condensation on a thin film flowing over an inclined isothermal plate. They assume that the incoming film is at the same temperature as the plate. However, in the present problem, the incoming film temperature is assumed to lie between the plate temperature and the saturation temperature of the vapor. Another situation of importance is when the incoming film temperature is the same as the saturation temperature of the vapor. The assumption that the incoming film temperature is not the same as the plate temperature leads to an entirely different analysis than that of Reference 26.

Jacobs and Bogart [7] treated the problem of condensation on a thin film flowing over an adiabatic vertical plate. Their work is related to the heat transfer behavior in packed bed condensers used in geothermal applications. The present problem is different as the vertical plate is isothermal instead of being adiabatic. In the present problem the isothermal surface acts as the heat sink instead of the cooling capacity of the film leading to an altogether different analysis.

4.2 Physical Model and Mathematical Formulation

Case 1 $T_w < T_o < T_{sat}$

Figure 4.2.1 shows the physical model. The film with a mass flow rate mf and T_o flows down the vertical isothermal plate. The film is subjected to a pure saturated vapor at a temperature T_{sat}. It is assumed that the Jakob number $Cp(T_{sat} - T_w)/hfg$ is small. This condition ensures that the condensate film is thin and does not measurable accelerate the film. As $T_w < T_o$, a thermal boundary layer, δ_1, grows from the wall towards the edge of the film. As $T_o < T_{sat}$ a second

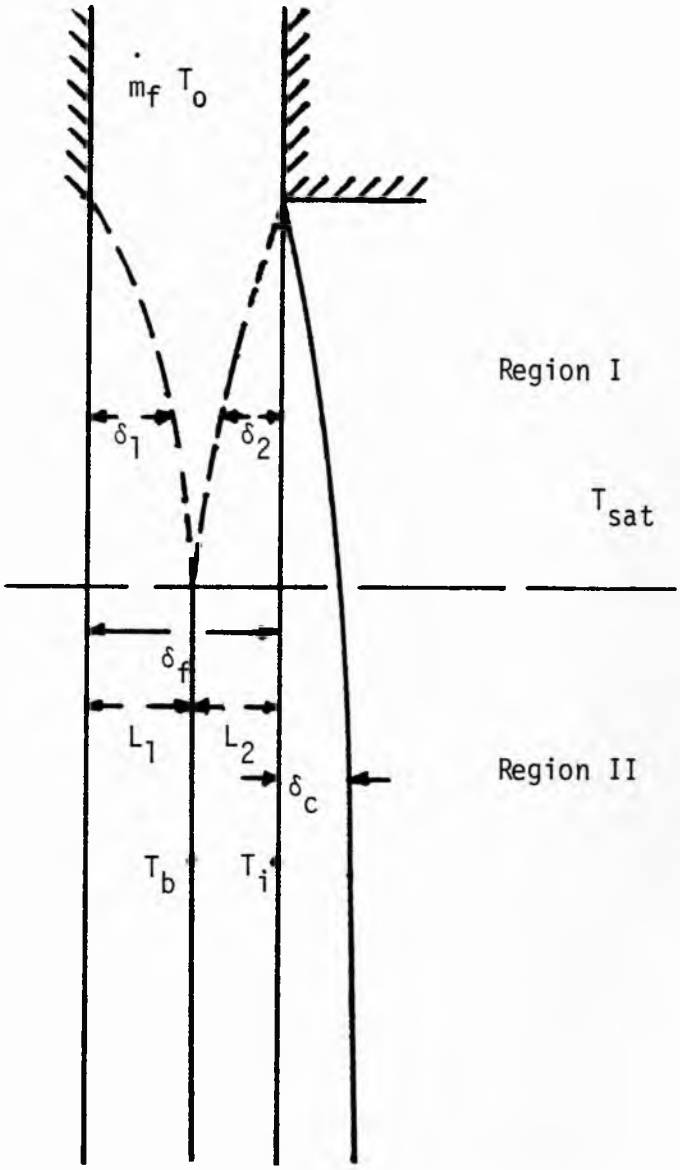

Figure 4.2.1. Physical model for condensation of a pure vapor on an isothermal plate when $T_w<T_o<T_{sat}$.

thermal boundary layer, δ_2, growing from the edge of the film towards the wall. Along the length of the plate at $X = X_D$ the two thermal boundary layers meet such that $\delta_1 + \delta_2 = \delta_f$. The region $0 < X < X_D$ is defined as Region I. Beyond Region I lies Region II. Here the temperature of the film decreases as a whole due to the wall being held at a lower temperature.

Region I

The mass flow rate in the film is

$$m_f = \rho_f \int_0^{\delta_f} u_f \, dy \qquad 4.2.1$$

where

$$u_f = \frac{g}{\nu_f} \left[\delta_f \, y - \frac{y^2}{2} \right] \qquad 4.2.2$$

which leads to

$$\delta_f = \left[\frac{3\dot{m}_f \nu_f}{g\rho_f} \right]^{1/3} . \qquad 4.2.3$$

The integral form of the energy equation for the boundary layer δ_1 is

$$\frac{d}{dx} \int_0^{\delta_f} \rho_f \, Cp_f \, u_f \, (T_1 - T_0) = - k_f \left. \frac{\partial T_1}{\partial y} \right|_{y = \delta_f} . \qquad 4.2.4$$

For the boundary layer δ_2 it is

$$\frac{d}{dx}\int_{\delta_f-\delta_2}^{\delta_f} \rho_f C_{p_f} u_f (T_2 - T_o) = k_f \left.\frac{\partial T_2}{\partial y}\right|_{y = \delta_f} . \qquad 4.2.5$$

For the condensate boundary layer the energy equation is

$$h_{fg} \frac{d}{dx}\int_{\delta_f}^{\delta_{f+}\delta_c} \rho_f u_c \, dy = k_f \left.\frac{\partial T_c}{\partial y}\right|_{y = \delta_f} . \qquad 4.2.6$$

The boundary conditions governing the temperature profile in boundary layer δ_1 are

$$\begin{aligned} &T_1 = T_w \text{ at } y = 0 \\ &T_1 = T_o \text{ at } y = \delta_1 \\ &\frac{\partial T_1}{\partial y} = 0 \text{ at } y = \delta_1 . \end{aligned} \qquad 4.2.7$$

These conditions lead to

$$T_1 - T_o = (T_w - T_o)(1 - \frac{y}{\delta_1})^2 . \qquad 4.2.8$$

The boundary conditions governing the temperature profile T_2 are

$$\begin{aligned} &T_2 = T_i \text{ at } y = \delta_f \\ &T_2 = T_o; \frac{\partial T_2}{\partial y} = 0 \text{ at } y = \delta_f - \delta_2 . \end{aligned} \qquad 4.2.9$$

These conditions lead to

$$T_2 - T_o = (T_i - T_o)\left(1 - \frac{\delta_f - y}{\delta_2}\right)^2 . \qquad 4.2.10$$

The negligible thermal capacitance of the condensate layer indicates a linear temperature profile

$$T_c = T_i + (T_{sat} - T_i)\frac{y - \delta_f}{\delta_c} . \qquad 4.2.11$$

The velocity in the condensate layer is assumed to be constant and equal to the edge velocity of the film.

$$u_c = u_f\Big|_{y = \delta_f} = \frac{g}{2\nu_f}\,\delta_f^2 . \qquad 4.2.12$$

The compatibility of heat fluxes at the interface δ_f

$$k_f \frac{\partial T_2}{\partial y}\Big|_{y = \delta_f} = k_f \frac{\partial T_c}{\partial y}\Big|_{y = \delta_f} \qquad 4.3.13$$

leads to the following expression for the interfacial temperature.

$$T_i = \frac{T_o + \frac{1}{2}\frac{\delta_2}{\delta_c} T_{sat}}{1 + \frac{1}{2}\frac{\delta_2}{\delta_c}} . \qquad 4.2.14$$

Defining a nondimensional temperature

$$\theta = \frac{T - T_o}{T_{sat} - T_o} \qquad 4.1.15$$

the nondimensional interfacial temperature becomes

$$\theta_i = \frac{\frac{1}{2}\frac{\bar{\delta}_2}{\bar{\delta}_c}}{1+\frac{1}{2}\frac{\bar{\delta}_2}{\bar{\delta}_c}} \quad . \qquad 4.2.16$$

Substituting Equations 4.2.2 and 4.2.8 into Equation 4.2.4 and nondimensionalizing the length term by $(\nu_f^2/g)^{1/3}$ leads to

$$\frac{d\bar{\delta}_1^3}{d\bar{x}} = \frac{36}{Pr_f\,(\bar{\delta}_f - (\frac{3}{10})\,\bar{\delta}_1)} . \qquad 4.2.17$$

Substituting Equations 4.2.2 and 4.2.9 into Equation 4.2.5 and nondimensionalizing the length terms by $(\nu f^2/g)^{1/3}$ yields

$$\frac{d\bar{\delta}_2^2}{d\bar{x}} = \frac{\frac{24}{Pr_f} - 2\,\bar{\delta}_2^2\,(\bar{\delta}_f^2 - \frac{1}{10}\,\bar{\delta}_2^2)\,\frac{1}{\theta_i}\,\frac{d\theta i}{d\bar{x}}}{(\bar{\delta}_f^2 - \frac{3}{10}\,\bar{\delta}_2^2)} . \qquad 4.2.18$$

Substituting Equations 4.2.12 and 4.2.11 into Equation 4.2.6 and and nondimensionalizing leads to

$$\frac{d\bar{\delta}_c^2}{d\bar{x}} = \frac{4}{3/^{2/3}}\,\frac{Ja}{Pr_f\,Re_f^{2/3}}\,(1-\theta_i) . \qquad 4.2.19$$

Utilizing the expression for θ_i from Equation 4.2.16, Equations 4.2.19 becomes

$$\frac{d\bar{\delta}_c^2}{d\bar{x}} = \frac{4}{3^{2/3}}\,\frac{Ja}{Pr_f\,Re_f^{2/3}}\,\frac{1}{1+\frac{1\bar{\delta}_2}{2\bar{\delta}_c}} . \qquad 4.2.20$$

Equations 4.2.17, 4.2.18 and 4.2.20 define the condensation in Region I. The boundary conditions as can be seen from the figure are $\delta_1(\bar{x} = 0) = 0$; $\bar{\delta}_2(\bar{x} = 0) = 0$; $\bar{\delta}_c(\bar{x} = 0) = 0$. The differential equations can be solved numerically after establishing the value of the first derivatives at $\bar{x} = 0$. For extremely small values of x it can be shown that

$$\begin{aligned} \bar{\delta}_1 &= a_1 \bar{x}^{1/3} \\ \bar{\delta}_2 &= a_2 \bar{x}^{1/2} \\ \bar{\delta}_c &= a_3 \bar{x}^{1/2} \quad . \end{aligned} \qquad 4.2.21$$

The Region I ends when $\delta_1 + \delta_2 = \delta_f$.

Region II

Region II begins when $\delta_1 + \delta_2 = \delta_f$. From this point onwards the isothermal plate at temperature T_w acts as the heat sinks instead of the cooling capacity of film. As a result the temperature in the film decreases.

At the end of Region I let

$$\bar{\delta}_1 = \bar{L}_1; \quad \bar{\delta}_2 = \bar{L}_2$$

and

$$c_1 = \frac{\bar{L}_1}{\bar{\delta}_f} \quad ; \quad c_2 = \frac{\bar{L}_2}{\bar{\delta}_2} \qquad 4.2.22$$

such that $c_1 + c_2 = 1$.

In the beginning of Region II an inflexion point occurs at $y = \delta_1$ where the slope $\frac{\partial T}{\partial y} = 0$. Therefore it is necessary to analyze the heat transfer in two zones $0 < y < L_1$ and $L_1 < y < \delta_f$.

The energy equation for the film is

$$\frac{d}{dx}\int_0^{L_1} u_f\, T_1\, dy = \frac{k_f}{\rho_f\, C_{p_f}}\left[\left.\frac{\partial T_1}{\partial y}\right|_{y=L_1} - \left.\frac{\partial T_1}{\partial y}\right|_{y=0}\right] \quad \text{for } 0 < y < L_1 \qquad 4.2.23$$

and

$$\frac{d}{dx}\int_{L_1}^{\delta_f} u_f\, T_2\, dy = \frac{k_f}{\rho_f\, C_{p_f}}\left[\left.\frac{\partial T_2}{\partial y}\right|_{y=\delta_f} - \left.\frac{\partial T_2}{\partial y}\right|_{y=L_1}\right]. \qquad 4.2.24$$

$$\text{for } L_1 < y < \delta_f$$

The boundary conditions governing the temperature profile in $0 < y < L_1$ are

$$T_1 = T_w \text{ at } y = 0$$

$$T_1 = Tb;\ \frac{\partial T_1}{\partial y} = -\frac{q}{k} = -\beta\,(x) \text{ at } y = L_1\ . \qquad 4.2.25$$

These conditions lead to

$$T_1 = T_w + 2\left(T_b - T_w + \frac{\beta L_1}{2}\right)\frac{y}{L_1} - \left(T_b - T_w + \beta L_1\right)\frac{y^2}{L_1^2}\ . \qquad 4.2.26$$

The boundary condition governing the temperature profile in $L_1 < y < \delta_f$ are

$$T_2 = T_b\,(x)\ ;\ \frac{\partial T_2}{\partial y} = -\frac{q}{k} = -\beta\,(x) \text{ at } y = L_1 \qquad 4.2.27$$

$$T_2 = T_i \text{ at } y = \delta_f\ .$$

These conditions lead to

$$T_2 = T_b - \beta\,(y - L_1) + \left(T_i - T_b + \beta L_2\right)\left\{\frac{y - L_1}{L_2}\right\}^2\ . \qquad 4.2.28$$

The condensate layer temperature profile remains as

$$T_c = T_i + (T_{sat} - T_i) \frac{y-\delta_f}{\delta_c} \quad . \qquad 4.2.29$$

The compatibility of heat fluxes at the interface δ_f leads to the following expression for the nondimensional interfacial temperature

$$\theta_i = \frac{\bar{L}_2 - \bar{\beta}\,\bar{L}_2\,\bar{\delta}_c + 2\theta_b\,\bar{\delta}_c}{2\,\bar{\delta}_c + \bar{L}_2} \quad . \qquad 4.2.30$$

Substituting Equations 4.2.2 and 4.2.26 into Equation 4.2.23 and nondimensionalizing the length terms by $(\nu_f^2/g)^{1/3}$ leads to

$$\left[\frac{\left(\frac{5}{3} - \frac{3}{5}c_1\right)}{\left(\frac{1}{3} - \frac{c_1}{10}\right)}\right]\frac{d\theta_b}{d\bar{x}} + c_1\,\bar{\delta}_f\,\frac{d\bar{\beta}}{d\bar{x}} = \frac{-8\left[\theta_b - \theta_w + \bar{\beta}c_1\,\bar{\delta}_f\right]}{Pr_f\,c_1^{\,3}\,\bar{\delta}_f^{\,4}\left(\frac{1}{3} - \frac{c_1}{10}\right)} \quad . \qquad 4.3.31$$

Substituting Equations 4.2.28 and 4.2.2 into Equation 4.2.24 and nondimensionalizing leads to

$$M_1\frac{d\theta_b}{d\bar{x}} - M_2\,\delta_f\,\frac{d\bar{\beta}}{d\bar{x}} + M_3\frac{d\theta_i}{dx} = \frac{2}{Pr_f}\frac{\left[\theta_i - \theta_b + \bar{\beta}\,\bar{L}_2\right]}{(1-C_1)\,\bar{\delta}_f^{\,4}} \qquad 4.3.32$$

where

$$M_1 = \frac{2c_1c_2}{3}\left(1 - \frac{c_1}{2}\right) + \frac{c_2^{\,2}}{4}\left(1 - c_1\right) - \frac{c_2^{\,3}}{15}$$

$$M_2 = \frac{c_1c_2^{\,2}}{6}\left(1 - \frac{c_1}{2}\right) + \frac{c_2^{\,3}}{12}\left(1 - c_1\right) - \frac{c_2^{\,4}}{20}$$

$$M_3 = \frac{c_1 c_2}{6} \left(1 - \frac{c_1}{2} + \frac{c_2^2}{4} (1 - c_1) - \frac{c_2^3}{10}\right).$$

The condensate layer energy equation remains the same as Equation 4.2.19.

Equations 4.2.31, 4.2.32, and 4.2.19 describe the condensation in Region II. The initial conditions are $\beta = 0$ and $\theta_b = 0$ at the beginning of Region II. The value of δ_c is that obtained at the end of region I.

Case B $T_w < T_o = T_{sat}$

Figure 4.2.2 shows the physical model for condensation on an isothermal vertical plate when the incoming film temperature is at the saturation temperature. The film with a mass flow rate, mf, enters chamber containing a pure saturated vapor. As the film temperature is greater than the temperature of the plate a thermal boundary layer grows from the wall outwards towards the edge of the film. As $T_o = T_{sat}$, no condensation occurs. The region where the thermal boundary layer grows is called Region I. Region I comes to an end when $\delta_1 = \delta_f$. From this point onwards the film-edge temperature decreases as a result condensation occurs. This region where the film edge temperature decreases is defined as Region II.

Region I

The energy equation and the velocity profile remain the same as Equations 4.2.5 and 4.2.2, respectively. However, the temperature profile changes. The boundary conditions governing the temperature profile in boundary layr δ_1 are

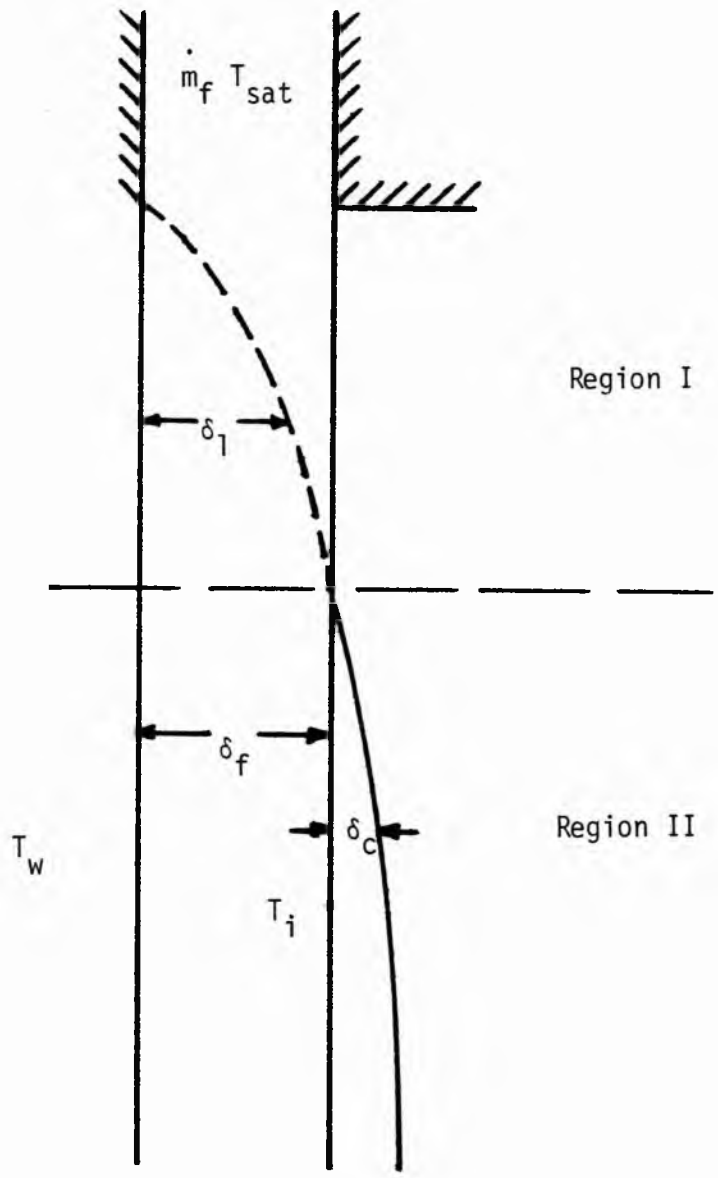

Figure 4.2.2. Physical model for condensation of a pure vapor on an isothermal plate when $T_w<T_o=T_{sat}$.

$$T_1 = T_w \text{ at } y = 0$$

$$T_1 = T_{sat} \quad \frac{\partial T_1}{\partial y} = 0 \quad \text{at } y = \delta_1 \ . \tag{4.2.34}$$

These conditions lead to

$$T_1 - T_{sat} = (T_w - T_{sat}) \left(1 - \frac{y}{\delta_1}\right)^2 \ . \tag{4.2.35}$$

Substituting Equations 4.2.2 and 4.2.34 into Equation 4.2.5 and non-dimensionalizing the length terms by $(\nu_f^2/g)^{1/3}$ leads to

$$\frac{d\bar{\delta}_1^3}{dx} = \frac{36}{Pr_f(\bar{\delta}_f - \frac{3}{10}\bar{\delta}_1)} \ . \tag{4.2.36}$$

Equation 4.2.37 defines the heat transfer in Region I. It can be solved numerically after establishing the value of the first derivative at x = 0. The initial value as can be seen from Figure 4.2.2 is δ_1 (x=0) = 0. For extremely small values of x it can be shown that

$$\bar{\delta}_1 = a_1 \bar{x}^{1/3} \ . \tag{4.2.37}$$

Region I comes to an end when $\delta_1 = \delta_f$.

Region II

Region II begins as the film edge temperature at $y = \delta_f$ drops below the saturation temperature of the vapor. As a result condensation begins and a thin layer, δ_c, develops on the edge of the film.

The boundary conditions governing the temeperature profile in the film are

$$T_f = T_w \text{ at } y = 0$$

$$T_f = T_i \text{ and } \frac{\partial T_f}{\partial y} = -\frac{q}{k} = -\beta \text{ at } y = \delta_f \quad . \qquad 4.2.38$$

The conditions lead to

$$T_f = T_w + \left\{2(T_i - T_w) + \beta\,\delta_f\right\} \frac{y}{\delta_f} - \left\{(T_i - T_w) + \beta\,\delta_f\right\} \frac{y^2}{\delta_f{}^2} . \qquad 4.2.39$$

The temperature profile in the condensate layer remains as Equation 4.2.11. The compatibility of heat fluxes at the interface $y = \delta_f$ leads to the following expression for the interfacial temperature

$$T_i = T_{sat} + \beta\delta_c \quad . \qquad 4.2.40$$

Defining a nondimensional temperature

$$\theta = \frac{T - T_w}{T_{sat} - T_w} \qquad 4.2.41$$

the nondimensional interfacial temperature can be expressed as

$$\theta_i = 1 + \bar{\beta}\,\bar{\delta}_c \qquad 4.2.42$$

where

$$\bar{\beta} = \frac{\beta\,(\nu_f{}^2/g)^{1/3}}{(T_{sat} - T_w)} \quad . \qquad 4.4.43$$

The governing differential equation for the condensate layer remains the same as Equation 4.2.19.

$$\frac{d\bar{\delta}_c}{d\bar{x}} = \frac{2}{3^{2/3}} \frac{Ja}{Pr_f \, Re_f^{2/3}} (1-\theta_i) \quad . \qquad 4.2.44$$

Substituting Equation 4.2.42 into Equation 4.2.44 yields

$$\frac{d\bar{\delta}_c}{d\bar{x}} = -\frac{2}{3^{2/3}} \frac{Ja}{Pr_f \, Re_f^{2/3}} \bar{\beta} \quad . \qquad 4.2.45$$

The energy equation for the film is

$$\frac{d}{dx}\int_0^{\delta_f} u_f \, T_f \, dy = \frac{k_f}{\rho_f \, C_{p_f}} \left[\left.\frac{\partial T_f}{\partial y}\right|_{y=\delta_f} - \left.\frac{\partial T_f}{\partial y}\right|_{y=0} \right] . \qquad 4.2.46$$

Substituting Equations 4.2.1, 4.2.39, 4.4.42 into Equation 4.2.46 and nondimensionalizing yields

$$\frac{d\bar{\beta}}{d\bar{x}} = - \frac{\dfrac{30 \left(1+ \bar{\beta}(\bar{\delta}_c + \bar{\delta}_f)\right)}{Pr_f \, \bar{\delta}_f^{\,4}} + \dfrac{8 \, Ja \, \bar{\beta}^2}{(3Ref)^{2/3} \, Pr_f}}{\left(4 \, \bar{\delta}_c + \dfrac{7}{8}\bar{\delta}_f\right)} \quad . \qquad 4.2.47$$

Equations 4.2.42, 4.2.45 and 4.2.47 describe the condensation in Region II. The initial conditions are $\beta = 0$ and $\delta_c = 0$ at the beginning of Region II.

Heat Transfer Expressions

A heat transfer coefficient can be defined as

$$h(x) = \frac{k \left.\dfrac{\partial T}{\partial y}\right|_{y=0}}{(T_{sat} - T_w)} \qquad 4.2.48$$

from which the local Nusselt number can be defined as

$$Nu(\bar{x}) = \frac{h(x)\ (\nu_f^2/g)^{1/3}}{K} \quad . \qquad 4.2.49$$

Case A $T_w < T_o < T_{sat}$

The heat transfer coefficient for Region I is

$$h(x) = \frac{k \left.\frac{\partial T_1}{\partial y}\right|_{y=0}}{(T_{sat} - T_w)} = \frac{-2(T_w - T_o)k}{(T_{sat} - T_w)\delta_1} \quad . \qquad 4.2.50$$

The local Nusselt number in Region I is

$$Nu_I\ (\bar{x}) = - \frac{2\theta_w}{(1 - \theta_w)\ \bar{\delta}_1} \quad . \qquad 4.2.51$$

Substituting the expression for δ_1 from Equation 4.2.21, Equation 4.2.48 becomes

$$Nu_I\ (\bar{x}) = - \frac{2\theta_w}{(1 - \theta_w) a_1\ \bar{x}^{1/3}} \qquad 4.2.52$$

from which an average Nusselt number in Region I can be evaulated as

$$Nu_I = - \frac{3\theta_w}{(1 - \theta_w) a_1\ \bar{x}^{1/3}} \quad . \qquad 4.2.53$$

Region I comes to an end at $X = X_D$ when $\delta_1 + \delta_2 = \delta_f$. Utilizing the expressions for δ_1 and δ_2 from Equation 4.2.21, the following equation is obtained which defines the extent of Region I.

$$a_1\ \bar{x}_D^{1/3} + a_2\ \bar{x}_D^{1/2} = \bar{\delta}_f \quad . \qquad 4.2.54$$

The local Nusselt number in Region II is given by

$$Nu_{II}(\bar{x}) = \frac{[2\ \theta_b - \theta_w + \bar{\beta}\bar{L}_1]}{\bar{L}_1\ (1 - \theta_w)} . \qquad 4.2.55$$

The average Nusselt in Region II is expressed as

$$Nu_{II} = \frac{\int_{\bar{x}_D}^{\bar{x}} Nu_{II}\ (\bar{x})\ d\bar{x}}{(\bar{x} - \bar{x}_D)} . \qquad 4.2.56$$

The average Nusselt number over Regions I and II is given by

$$\overline{Nu} = \frac{Nu_I\ \bar{x}_D + Nu_{II}\ (\bar{x} - \bar{x}_D)}{\bar{x}} . \qquad 4.2.57$$

Case B $T_w < T_o = T_{sat}$

The local heat transfer coefficient in Region I is given by

$$h(x) = \frac{2k}{\delta_1} . \qquad 4.2.58$$

The local Nusselt number in Region I is expressed as

$$Nu_I\ (\bar{x}) = \frac{2}{\bar{\delta}_1} . \qquad 4.2.59$$

Utilizing the expression for δ_1 from Equation 4.2.37, Equation 4.2.59 becomes

$$Nu_I\ (\bar{x}) = \frac{2}{a_1\ \bar{x}^{1/3}} \qquad 4.2.60$$

from which an average Nusselt number over the length of Region I can be expressed as

$$Nu_I = \frac{3}{a_1 \bar{x}^{1/3}} . \qquad 4.2.61$$

Region I comes to an end when $\delta_1 = \delta_f$. Utilizing the expression for δ_1 from Equation 4.2.37 the following equation is obtained to define, X_D, the extent of Region I:

$$\bar{x}_D = \left(\frac{\bar{\delta}_f}{a_1}\right)^3 . \qquad 4.2.62$$

The local Nusselt number in Region II is given by

$$Nu_{II}\ (\bar{x}) = \frac{2\theta_i + \bar{\beta}\ \bar{\delta}_f}{\bar{\delta}_f} . \qquad 4.2.63$$

The average Nusselt number in Region II can be evaluated as

$$Nu_{II} = \frac{\int_{\bar{x}_D}^{\bar{x}} Nu_{II}\ (\bar{x})\ d\bar{x}}{(\bar{x} - \bar{x}_D)} . \qquad 4.2.64$$

The average Nusselt number in Regions I and II is given by

$$\overline{Nu} = \frac{Nu_I\ \bar{x}_D + Nu_{II}\ (\bar{x} - \bar{x}_D)}{\bar{x}} . \qquad 4.2.65$$

4.3 Results and Discussion

Case A $T_w < T_o < T_{sat}$

Examination of the governing differential equation indicates that the condensation in Region I is dependent on the Reynolds number, the Prandtl number and the Jakob number. In Region I for small values of x simple expressions could be obtained for the coefficients of δ_1,

δ_2 and δ_c indicated in Equation 4.2.21 They are

$$a_1 = \left[\frac{36}{(3Re_f)^{1/3}\ Pr_f}\right]^{1/3}$$

$$a_2 = \left[\frac{24}{(3Re_f)^{2/3}\ Pr_f}\right]^{1/2} \qquad 4.3.1$$

$$a_3 = \frac{1}{2}\left[-\frac{1}{2}\,a_2 + \left\{\frac{1}{4}\,a_2^{\,2} + \frac{16\ Ja}{(3Re_f)^{2/3}\ Pr_f}\right\}^{1/2}\right] .$$

Region I comes to an end when

$$\bar{\delta}_1 + \bar{\delta}_2 = \bar{\delta}_f \qquad 4.3.2$$

The extent of Region I, X_D, can be determined after solving the governing differential equations. Alternately it can be evaluated utilizing the profiles indicated in Equation 4.2.21. Substituting the profiles for δ_1, δ_2 from Equation 4.2.21 and the values of a_1 and a_2 from Equation 4.3.1 into Equation 4.3.2 yields

$$\left[\frac{36}{(3Re_f)^{1/3}\ Pr_f}\right]^{1/3} \bar{x}_D^{\,1/3} + \left[\frac{24}{(3Re_f)^{2/3}\ Pr_f}\right]^{1/2} \bar{x}_D^{\,1/2} = \bar{\delta}_f \ . \qquad 4.3.3$$

The above equation has to be solved numerically to obtain the value of X_D. Moreover it is clear that the extent of Region is only a function of the Reynolds number and the Prandtl number of the film.

The average Nusselt number in Region I is given by

$$Nu_I = \frac{-3\theta_w}{(1 - \theta_w)\left[\frac{36}{(3Re_f)^{1/3}\ Pr_f}\right]^{1/3} \bar{x}_D^{\,1/3}} \ . \qquad 4.3.4$$

In addition to the Reynold, Prandtl, Jakob numbers, condensation in Region II is dependent on a fourth parameter: the temperature of the plate. In Region II, simple expressions could not be obtained for the local or average Nusselt number; thus they had to be evaluated numerically.

It is important to determine the length of the plate over which the average Nusselt number is to be calculated. It has been reported [27] that for surface condensation the average film heat transfer coefficient on a tube with diameter, d, has the same magnitude as the average film heat transfer coefficient on a vertical plate with height $x = 2.5\ d$. The tube diameters of interest lie below one inch which corresponds to an equivalent nondimensional height of the plate of 1000. Thus the average Nusselt number was calculated over the height of the plate to a maximum of $x = 1000$.

Figure 4.3.1 presents the nondimensional interfacial temperature, θ_i, as function of the distance along the plate for different temperatures of the incoming film. As expected in Region I, as T_o increases T_i increases. However, in Region II, for a given T_w, a larger T_o results in a sharper decrease in θ_i. This is primarily due to the larger heat flux at the wall resulting from a larger temperature difference across the film. The faster depletion of the heat at the wall leads to a sharper decrease in θ_i.

Figure 4.3.2 presents the nondimensional interfacial temperature, plate for different temperatures of the wall. In Region I, θ_i remains the same for each of the wall temperatures. This is due to the fact that condensation in Region I is dependent only on the cooling capacity of the film and independent of the wall temperature. However in Region

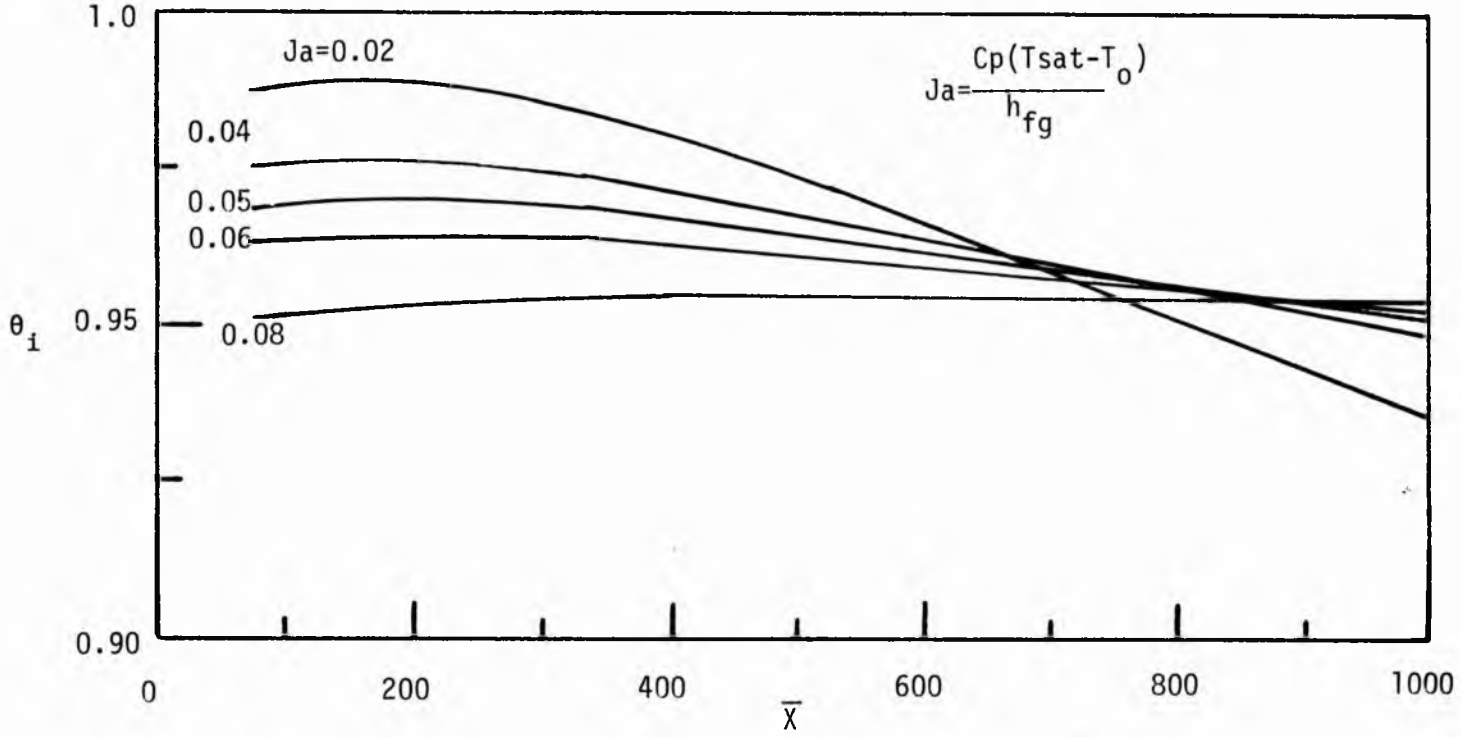

Figure 4.3.1. Interfacial temperature as a function of $\bar{X}$ for different Ja. $T_{sat}=600^{o}R$, $T_{w}=500^{o}R$.

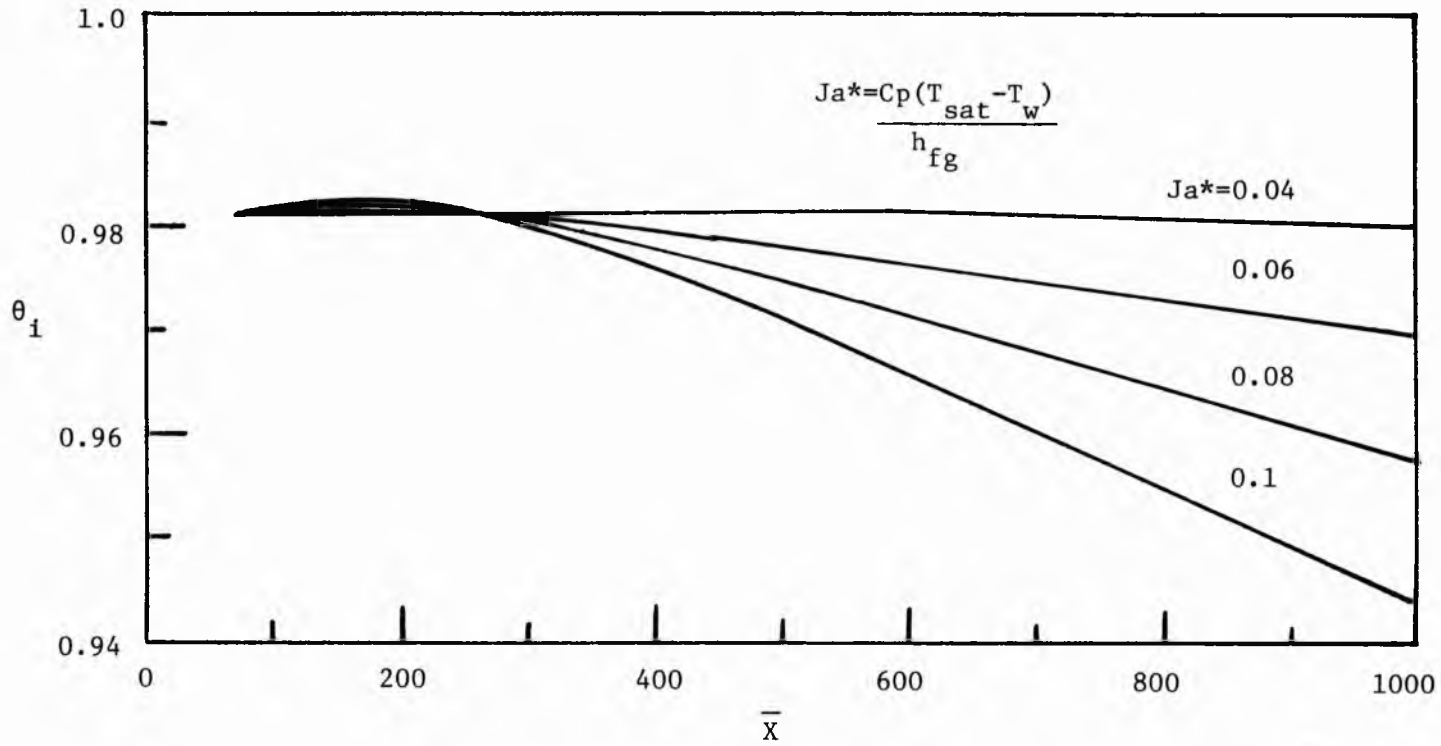

Figure 4.3.2. Nondimensional interfacial temperature as a function of $\bar{X}$ for different Ja*. T_{sat}=600°R, T_o=570°R.

II the plate wall maintained at low temperature acts as the heat sink. As a result θ_i decreases. As expected for lower wall temperatures there is a sharper decrease in θ_i in Region II. Furthermore it is noticed that in the beginning of Region II for a short distance θ_i increases instead of decreasing. This can be attributed to the fact that in the beginning of the Region II, the influence of the wall is not felt immediately by the interface. The distance between the points A and B is the distance required for the interface to feel the effect of the plate wall. This distance is strictly a function of the hydrodynamics of the film.

Figure 4.3.3 shows the variation of θ_i with X for different Reynolds numbers of the film. For low film velocities the interfaces are significantly affected by the low wall temperature. As a result there is a sharper decrease in θ_i. However, for a larger Reynolds number (>100) there is little decrease in θ_i in Region II. In fact the low temperature wall seems to have very little effect on the interfacial temperature.

Figures 4.3.4 through 4.3.6 present the integrated average Nusselt number as a function of x for different incoming film temperatures, wall temperatures and Reynolds numbers. The results agree with the expected trends. For example, a lower wall temperature leads to a larger temperature difference across the film leading to a higher heat transfer at the wall. It is to be noted that a higher heat transfer at the wall does not necessarily mean a higher condensation rate. For example consider the case of a high Reynolds numbers. For a high Reynolds number the interfacial temperature remains fairly high and does not decrease significantly in Region II. This leads to a high temperature difference

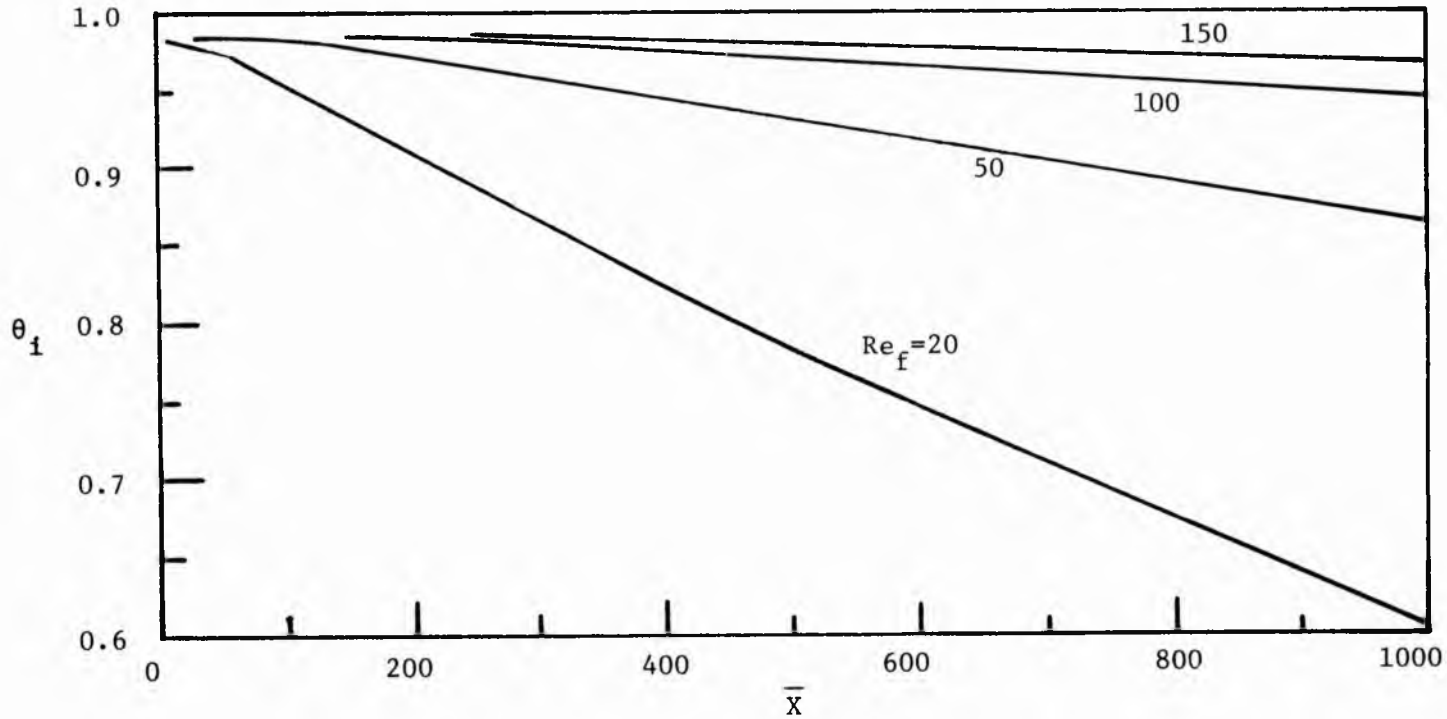

Figure 4.3.3. Nondimensional interfacial temperature as a function of $\overline{X}$ for different Reynolds numbers. T_{sat}=600°R, T_o=570°R, T_w=500°R.

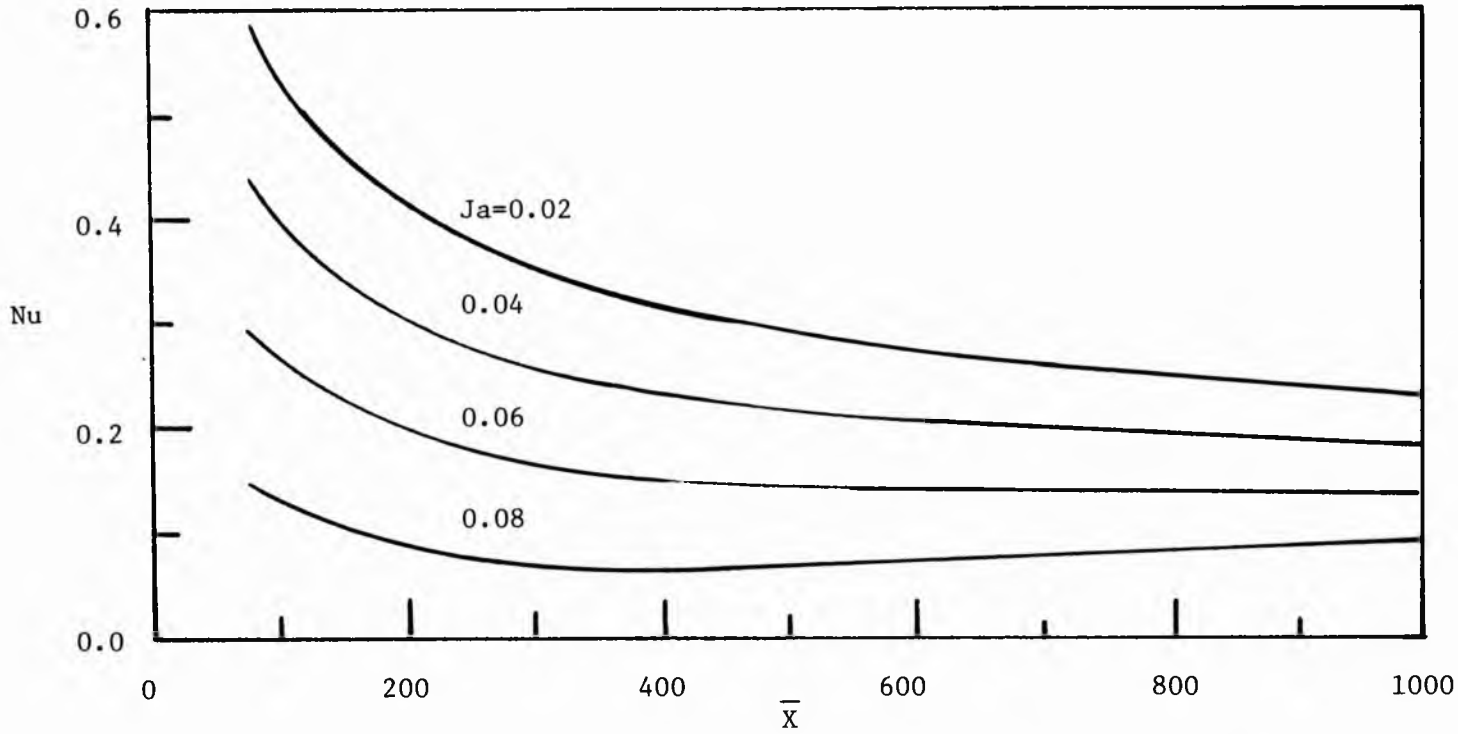

Figure 4.3.4. Integrated average Nusselt number as a function of $\overline{X}$ for different Ja. T_{sat}=600°R, T_w=500°R.

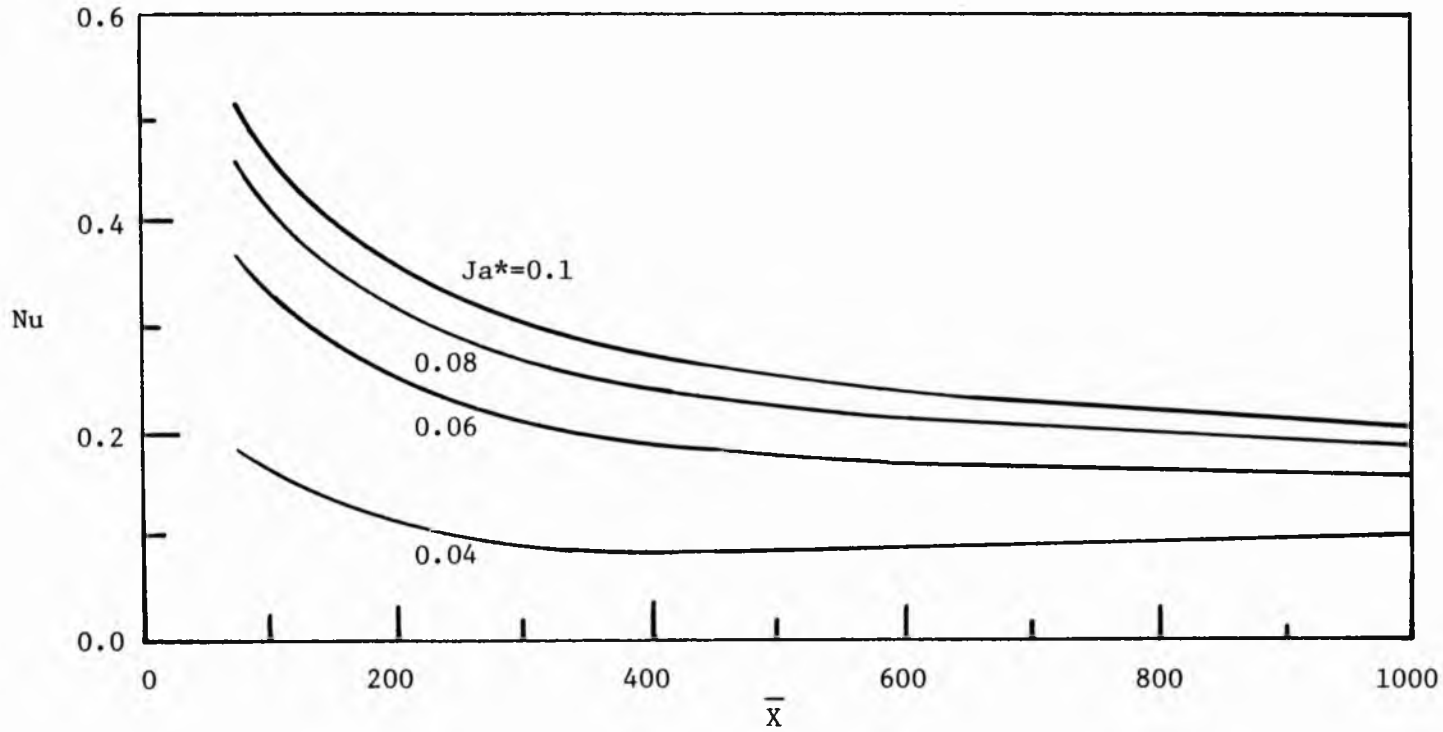

Figure 4.3.5. Integrated average Nusselt number as function of $\overline{X}$ for different Ja*. T_{sat}=600°R, T_o=570°R.

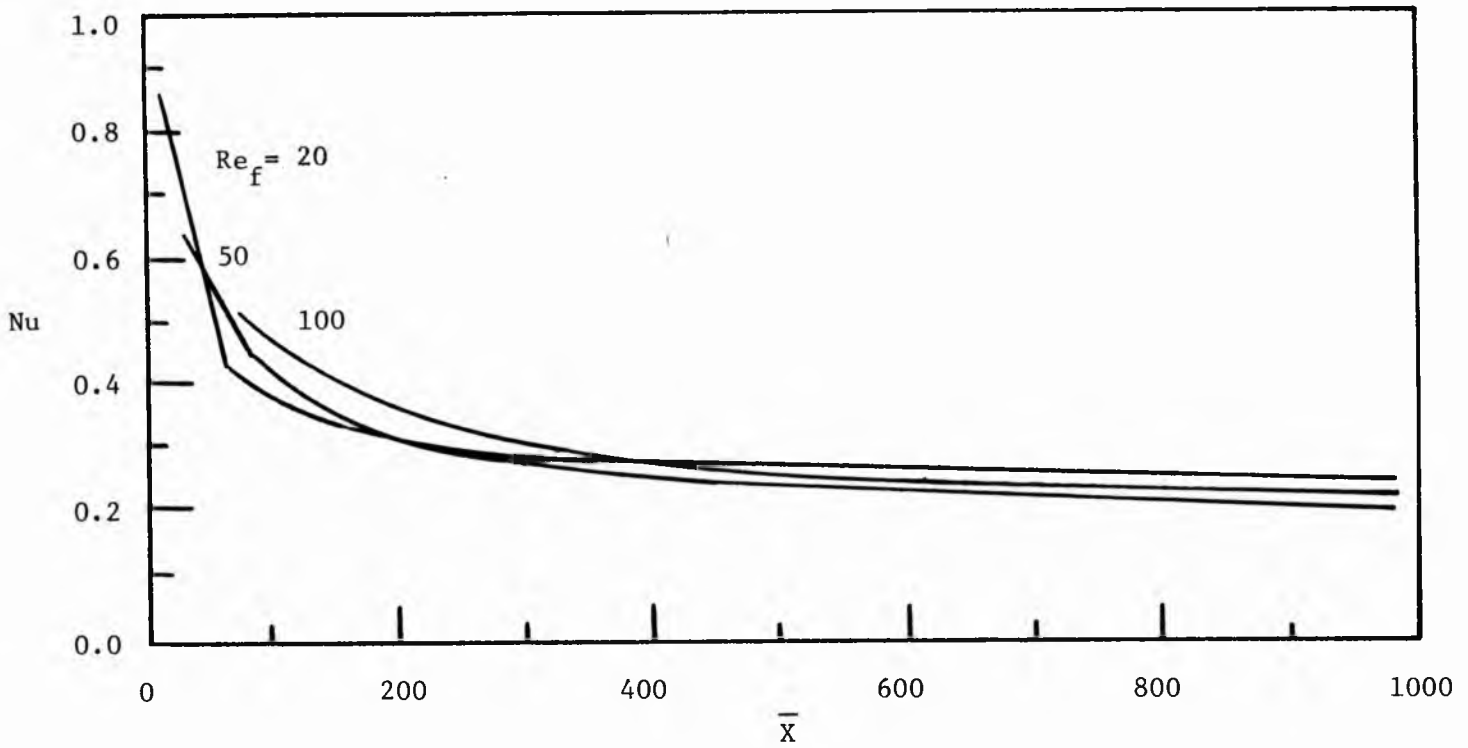

Figure 4.3.6. Integrated average Nusselt number as a function of $\overline{X}$ for different Reynolds numbers. T_{sat}=600°R, T_o=570°R, T_w=500°R.

across the film leading to a high heat transfer at the wall. However, a large interfacial temperature leads to a low temperature driving force for condensation leading to reduced condensation rate. The heat transfer at the wall is being treated as it is this quantity that has been reported in other theoretical and experimental works.

Case B $T_w < T_o = T_{sat}$

Examination of the governing differenetial Equation 4.2.36 indicates that the heat transfer in Region I is dependent on the Prandtl number and the thickness of the film. Equation 4.2.3 states that the thickness of the film is strictly a function of the Reynolds number. It has been shown that in Region I the thermal boundary layer growth can be expressed as

$$\bar{\delta}_1 = a_1 \bar{x}^{1/3} \quad . \qquad 4.3.5$$

On evaluating the value of a_1 at $x = 0$ it was found to be

$$a_1 = \left[\frac{36}{Pr_f \, \delta_f} \right]^{1/3} . \qquad 4.3.6$$

From Equation 4.2.3 an expression can be obtained for the nondimensional thickness of the flm.

$$\bar{\delta}_f = (3 \, Re_f)^{1/3} \qquad 4.3.7$$

Substituting Equation 4.3.7 into 4.3.6 yields

$$a_1 = 2.922 \, Pr_f^{-1/3} \, Re_f^{-1/9} \quad . \qquad 4.3.8$$

The extent of Region I is determined as

$$\bar{x}_D = \left(\frac{\bar{\delta}_f}{a_1}\right)^3 = \frac{(3Re_f)^{4/3} Pr_f}{36} \quad . \qquad 4.3.9$$

Utilizing the above expressions for a_1 and X_D the average Nusselt number in Region I can be obtained as

$$Nu_I = \frac{3}{a_1 \bar{x}_D^{1/3}} \quad . \qquad 4.3.10$$

No simple expressions could be obtained for the local or average Nusselt number in Region II. Thus, they had to be evaluated using numerical techniques.

Figure 4.3.7 shows the variation of the nondimensional interfacial temperature with the distance along the plate in Region II. For low Reynolds numbers there is a significant decrease in θ_i as x increases. However, for high Reynold numbers, which lead to high film velocities, the nondimensional interfacial temperature decreases very slowly with x. Thus, the conditions in Region II are almost the same as in Region I. It appears that the wall maintained at a low temperature has insignificant effect on the interfacial temperature θ_i. The present problem was analyzed utilizing a linear temperature profile in the film. For a large Reynolds number the following expression was obtained for the integrated Nusselt numbers over Regions I and II

$$Nu = \frac{0.028\ Re_f\ Pr_f + 0.693\ Re_f^{-1/3}\ (\bar{x} - \bar{x}_D)}{x} \quad . \qquad 4.3.11$$

The above expression does not contain the Jakob number indicating that at higher Reynold numbers the integrated average Nusselt number is independent of the wall temperature.

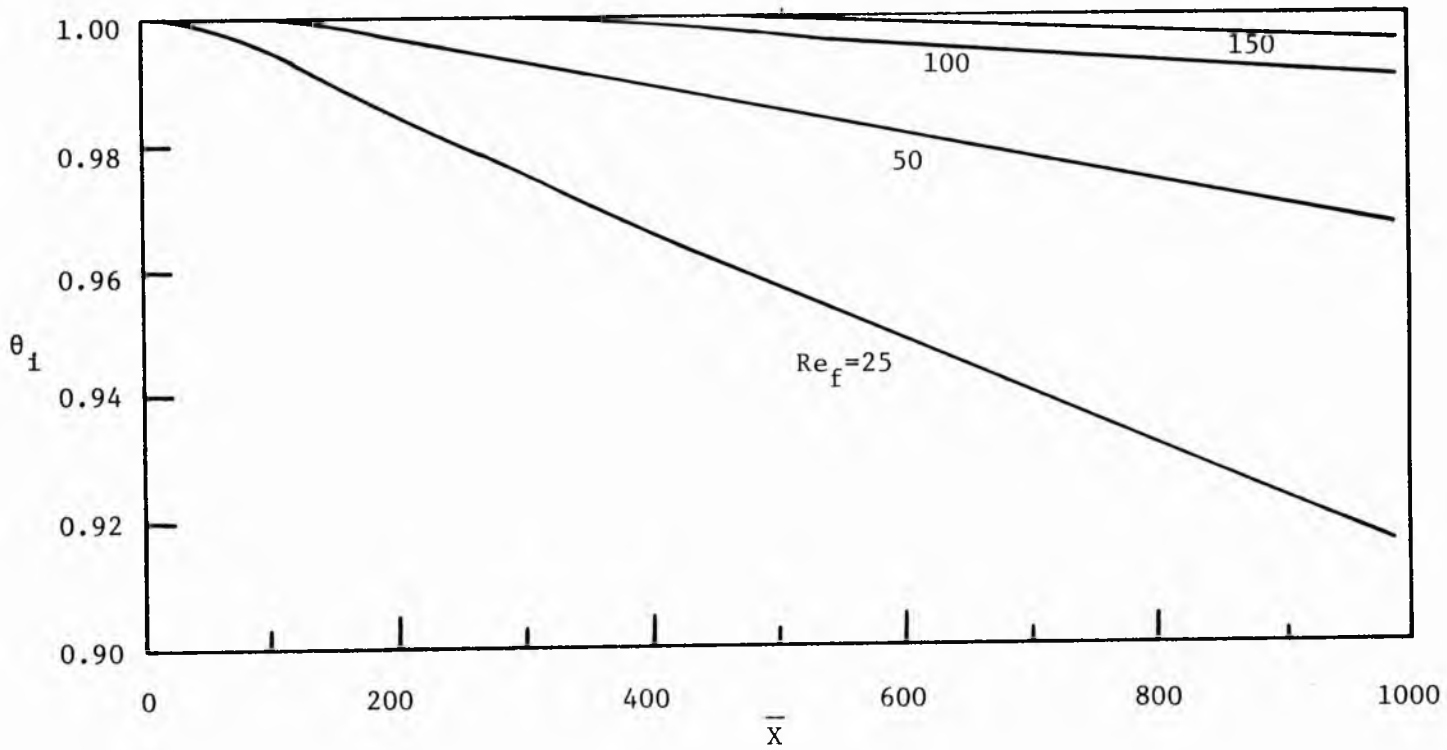

Figure 4.3.7. Nondimensional interfacial temperature as a function of $\overline{X}$ for different Reynolds numbers.

Figure 4.3.8 presents the variation of the nondimensional interfacial temperature with the distance along the plate for different temperatures of the wall. The results follow the expected trends. A lower wall temperature results in a faster removal of heat at the wall leading to a faster decrease in θ_i.

Figure 4.3.9 presents the integrated average Nusselt number as function of x for different Re_f. As noted earlier for a lower Reynolds number the interfacial temperature drops faster along the length of the plate. As a result the heat flux at the wall decreases leading to a lower average Nusselt number in Region II. However, in Region I a higher Reynolds number leads to a lower Nusselt number.

Figure 4.3.10 presents the integrated average Nusselt number as a function of x for different wall temperatures. It is observed that at higher Reynolds number (=100) the curves for $(T_{sat} - T_w)$ = 25, 50, 75°F fall on the same curve. This is in agreement with Equation 4.3.11 which states that at higher Reynolds numbers the average Nusselt number is independent of the wall temperature.

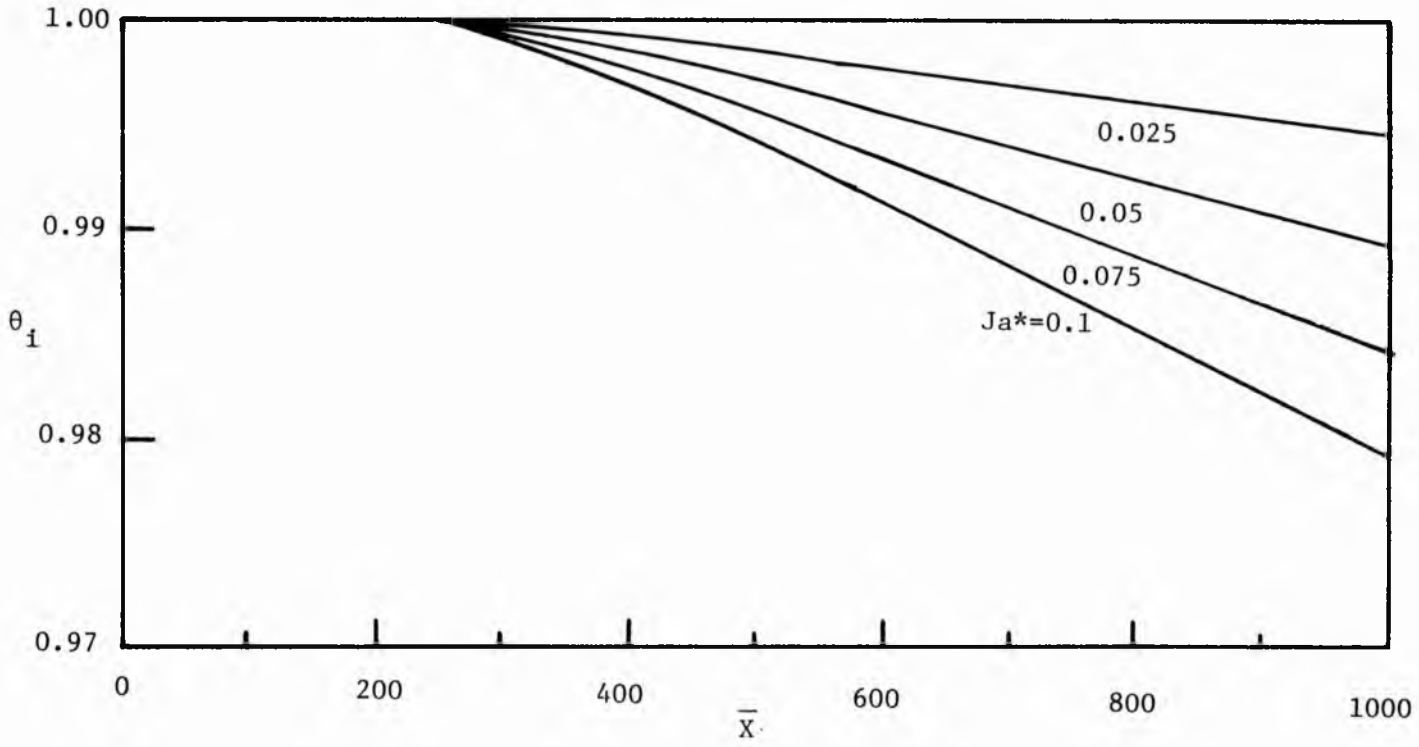

Figure 4.3.8. Nondimensional interfacial temperature as a function of $\overline{X}$ for different Ja*. T_{sat}=600°R.

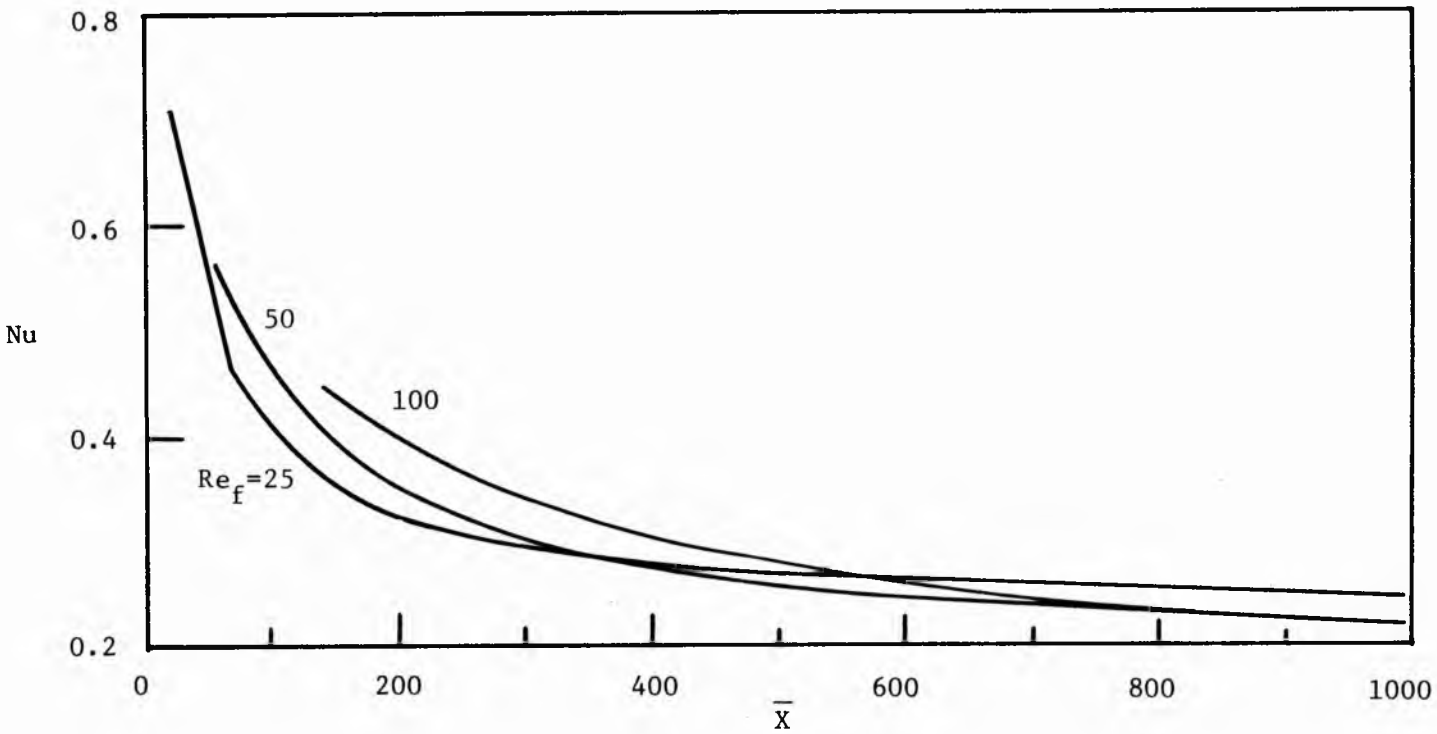

Figure 4.3.9. Integrated average Nusselt number as a function of $\overline{X}$ for different Reynolds numbers. T_{sat}=600°R.

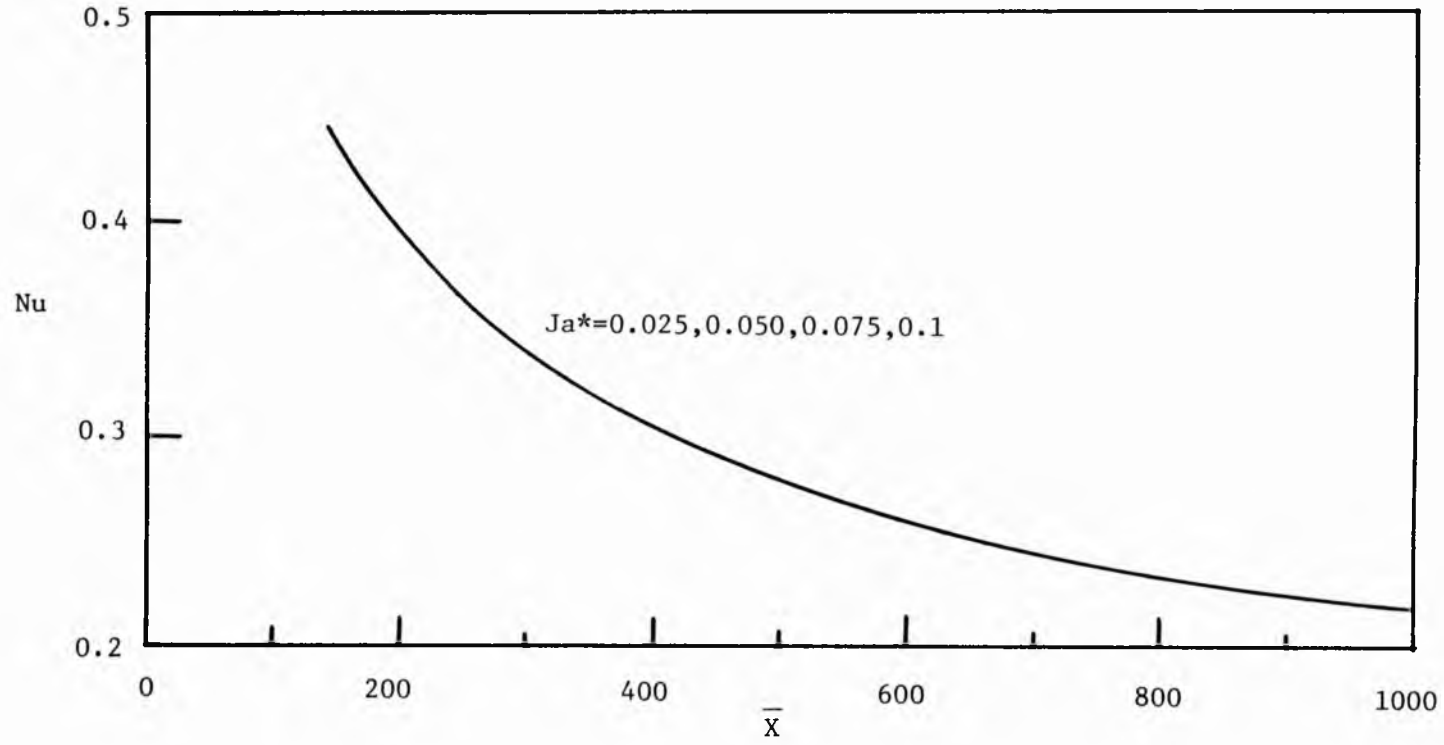

Figure 4.3.10. Integrated average Nusselt number as a function of of $\overline{X}$ for different Ja*. T_{sat}=600°R.

CHAPTER 5

CONDENSATION ON A THIN FILM FLOWING OVER A VERTICAL ISOTHERMAL PLATE IN PRESENCE OF A NONCONDENSIBLE GAS

5.1 Introduction

It is well known that the presence of a small amount of noncondensible gas in the condensing vapor can drastically reduce the condensation heat transfer. To understand the above phenomenon several investigators have dealt with the problem of laminar film condensation on an isothermal vertical surface. Sparrow and Lin [17] were the first to formulate a theory to predict the effects of noncondensible gases on laminar film condensation. Utilizing a similarity transformation they solved the coupled conservation equations of heat, mass and momentum transfer. They have shown that for condensation of steam, a mass fraction of air equal to half a percent can reduce the condensation heat transfer by over 50%. Minkowycz and Sparrow [6] studied the same problem in 1969. However, they examined the effects of interfacial resistance, free convection due to temperature gradients, mass and thermal diffusion and variable properties. They concluded that the effects of interfacial resistance and thermal diffusion were negligible. They further point out that the effects of noncondensible gases are accentuated at lower pressures. Rose [19] dealt with the same problem utilizing an integral approach. Al-Diwany [28] performed experimental

studies on laminar film condensation in the presence of a noncondensible gas. In all of the above studies it was concluded that the presence of a small amount of noncondensible gas drastically reduced the condensation heat transfer.

Although sizeable work of experimental and analytical nature has been reported on the effects of noncondensible gases on condensation on bare surfaces, little attention has been focused on the effects of noncondensible gases on direct contact condensation processes. Thus, it was decided to analyze the effects of noncondensible gases on condensation on a thin film flowing over an isothermal vertical surface.

The only work reported that is close to the problem is condensation on an immiscible film flowing over an adiabatic vertical surface [9] which was treated by the author in 1983. The present problem is different as the vertical surface is isothermal instead of being adiabatic. In the present problem the isothermal wall acts as the heat sink, leading to an entirely different heat transfer performance. However, the basic method of approach to the problem remains the same.

5.2 Physical Model and Mathematical Formulation

Case A $T_w < T_o < T_{sat}$

The basic model for condensation on a thin film flowing over an isothermal vertical plate in the presence of a noncondensible gas is shown in Figure 5.2.1. The film with a mass flow rate m_f and a temperature T_o flows down a vertical isothermal flat plate. It enters a chamber filled with a vapor containing a small fraction of noncondensible gas. It is assumed that the pressure in the chamber is sufficiently low

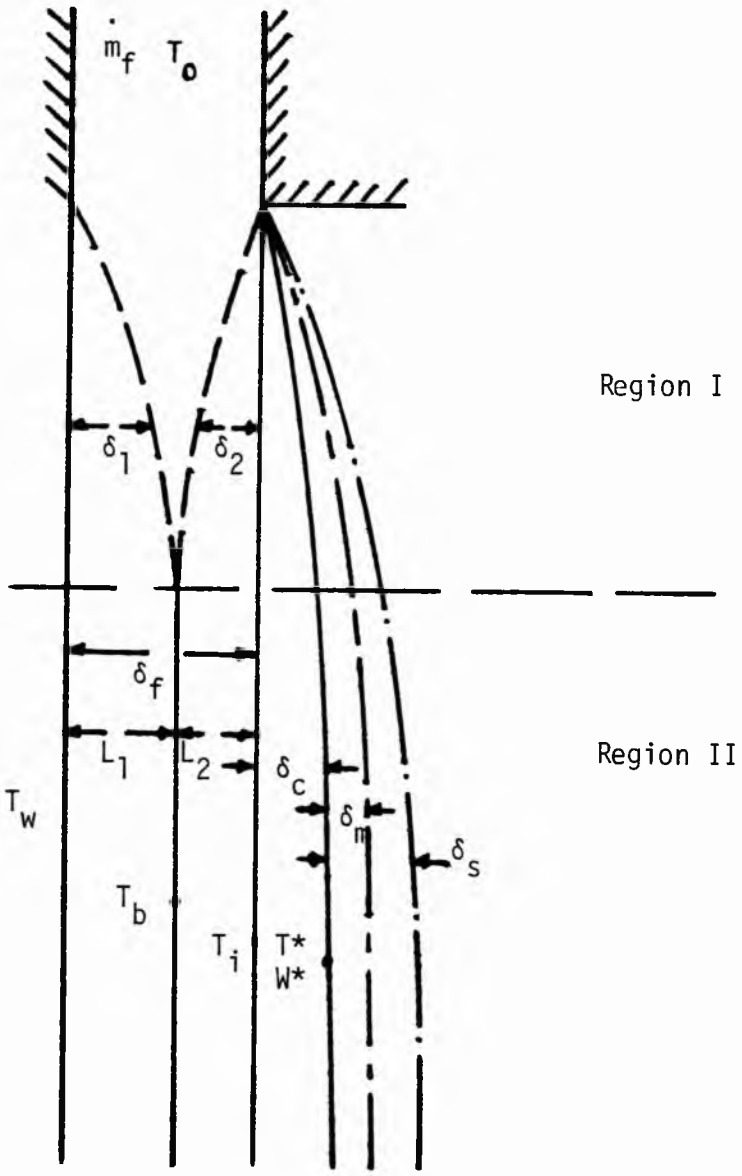

Figure 5.2.1. Physical model for condensation on a thin film flowing over an isothermal plate in the presence of a noncondensible gas when $T_w<T_o<T_{sat}$.

and the Jakob number, $C_p\ (T\infty - T_o)/hfg$, is small. This assures that the condensate layer is thin. It is assumed that the effects of superheating, thermal diffusion and diffusion thermo are negligible [6]. Fluid property variations are retained only in those places where they play an essential role in establishing the transport processes.

This problem as shown in Figure 5.2.1 can be divided into two regions. Region I defines a region where the thermal boundary layers are developing. As $T_o > T_w$, a thermal boundary layer, δ_1, grows from the wall towards the edge of the film. As $T\infty > T_o$, the vapor condenses on the edge of the film. As a result a second thermal boundary layer grows from the edge of the film towards the wall. At a point along the length of the plate, X_D, the two boundary layers meet. The region $0 < X < X_D$ is defined as Region I. In Region I in addition to the condensate layer, there are momentum and species boundary layers, which are brought about the by presence of the noncondensible gas.

Region II begins when the two thermal boundary layers δ_1 and δ_2 meet such that $\delta_1 + \delta_2 = \delta_f$. From this point onwards the entire film cools down. The isothermal plate acts as the heat sink instead of the coolant capacity of the film.

Region I

The mass flow rate per unit width for the film is

$$m_f = \int_0^{\delta_f} \rho_f\, u_f\, dy \qquad 5.2.1$$

where

$$u_f = \frac{g}{\nu_f} \left[\delta_f y - \frac{y^2}{2} \right] . \qquad 5.2.2$$

Utilizing Equations 5.2.1 and 5.2.2, there are obtained

$$\delta_f = \left[\frac{3m_f}{u_f} \right]^{1/3} \left(\frac{\nu_f^2}{g} \right)^{1/3} . \qquad 5.2.3$$

The integral form of energy equation for boundary layer δ_1 is

$$\frac{d}{dx} \int_0^{\delta_1} \rho_f \, u_f \, Cp_f \, (T_1 - T_o) dy = - k_f \left. \frac{\partial T_1}{\partial y} \right|_{y = 0} \qquad 5.2.4$$

and for the boundary layer δ_2, the energy equation is

$$\frac{d}{dx} \int_{\delta_f - \delta_2}^{\delta_f} \rho_f \, u_f \, Cp_f \, (T_2 - T_o) \, dy = k_f \left. \frac{\partial T_2}{\partial y} \right|_{y = \delta_f} . \qquad 5.2.5$$

As the Jakob number is small, the energy equation for the condensate layer is

$$h_{f_g} \frac{d}{dx} \int_{\delta_f}^{\delta_f + \delta_c} \rho_f \, u_c \, dy = k_f \left. \frac{\partial T_c}{\partial y} \right|_{y = \delta_f} . \qquad 5.2.6$$

The boundary conditions governing the temperature profile in boundary layer δ_1 are

$$T_1 = T_w \text{ at } y = 0$$

$$T_1 = T_o; \quad \frac{\partial T_1}{\partial y} = 0 \text{ at } y = \delta_1 . \qquad 5.2.7$$

These conditions lead to

$$T_1 - T_o = (T_w - T_o)\left(1 - \frac{y}{\delta_1}\right)^2 . \qquad 5.2.8$$

The boundary conditions for the temperature profile in boundary layer δ_2 are

$$T_2 = T_o; \quad \frac{\partial T_2}{\partial y} = 0 \text{ at } y = \delta_f - \delta_2$$

$$T_2 = T_i \text{ at } y = \delta_f . \qquad 5.2.9$$

These conditions lead to

$$T_2 - T_o = (T_i - T_o)\left(1 - \frac{\delta_f - y}{\delta_2}\right)^2 . \qquad 5.2.10$$

As the condensate layer is thin it is reasonable to assume a linear temperature profile. The boundary conditions are

$$T_c = T_i \text{ at } y = \delta_f$$
$$T_c = T^* \text{ at } y = \delta_c + \delta_f . \qquad 5.2.11$$

These conditions lead to

$$T_c = T_i + (T^* - T_i)\left(\frac{y - \delta_f}{\delta_c}\right) . \qquad 5.2.12$$

The compatibility of heat fluxes at the interface δ_f

$$k_f \left.\frac{\partial T_2}{\partial y}\right|_{y = \delta_f} = k_f \left.\frac{\partial T_c}{\partial y}\right|_{y = \delta_f} . \qquad 5.2.13$$

leads to the following expression for the interfacial temperature

$$T_i = \frac{T_o + \frac{1}{2}\frac{\delta_2}{\delta_c} T^*}{1 + \frac{1}{2}\frac{\delta_2}{\delta_c}} . \qquad 5.2.14$$

Defining a nondimensional temperature

$$\theta = \frac{T - T_o}{T_\infty - T_o} \qquad 5.2.15$$

the nondimensional interfacial temperature can be expressed as

$$\theta_i = \frac{\frac{1}{2}\frac{\bar{\delta}_2}{\bar{\delta}_c}\theta^*}{1 + \frac{1}{2}\frac{\bar{\delta}_2}{\bar{\delta}_c}} . \qquad 5.2.16$$

Substituting Equations 5.2.8 and 5.2.2 into Equation 5.2.4 and nondimensionalizing the length term by $(\nu_f^2/g)^{1/3}$ leads to

$$\frac{d\bar{\delta}_1^3}{dx} = \frac{36}{Pr_f\,(\bar{\delta}_f - \frac{3}{10}\,\bar{\delta}_1)} . \qquad 5.2.17$$

Substituting Equations 5.2.2 and 5.2.10 into Equation 5.2.5 and nondimensionalizing the length term by $(\nu_f^2/g)^{1/3}$ yields

$$\frac{d\bar{\delta}_2^2}{d\bar{x}} = \frac{\frac{24}{Pr_f} - 2\bar{\delta}_2\,(\bar{\delta}f^2 - \frac{\bar{\delta}_2^2}{10})\,\frac{1}{\bar{\theta}i}\,\frac{d\theta_i}{d\bar{x}}}{(\bar{\delta}_f^2 - \frac{3}{10}\,\bar{\delta}_2^2)} . \qquad 5.2.18$$

The velocity in the condensate layer is equal to the edge velocity of the film

$$u_c = u_f \Big|_{y = \delta_f} = \frac{g}{2\nu_f} \delta_f^2 \qquad 5.2.19$$

Substituting Equations 5.2.19 and 5.2.12 into Equation and non-dimensionalizing the length terms by $(\nu_f^2/g)^{1/3}$ results in

$$\frac{d\bar{\delta}_c^2}{d\bar{x}} = \frac{4}{3^{2/3}} \frac{Ja}{(Re_f)^{2/3} Pr_f} (\theta^* - \theta_i) . \qquad 5.2.20$$

Utilizing Equation 5.2.16, Equation 5.2.20 becomes

$$\frac{d\bar{\delta}_c^2}{d\bar{x}} = \frac{4}{3^{2/3}} \frac{Ja}{(Re_f)^{2/3} Pr_f} \frac{\theta^*}{1 + \frac{1}{2}\frac{\bar{\delta}_2}{\bar{\delta}_c}} . \qquad 5.2.21$$

The conservation equations to be satisfied in the gas vapor boundary layer are the conservation of mass for the mixture, conservation of species of one of the components and the conservation of energy and momentum. As the energy transferred due to conduction and convection in the gas-vapor region is very small relative to that liberated as latent heat, the vapor energy equation will not be considered.

The local concentration of gas and vapor is expressed in terms of their respective mass fractions W_g and W_v

$$W_g = \frac{\rho_g}{\rho}; \; W_v = \frac{\rho_v}{\rho} \qquad 5.2.22$$

$$\rho = \rho_v + \rho_g \; ; \; W_v + W_g = 1 \quad .$$

As W_v and W_g are dependent on each other, one of them can be eliminated from the problem. In this analysis W_g is retained and its sub-

script is dropped. The partial pressure of the vapor and the total pressure are related by the expression

$$\frac{P_v}{P} = \frac{1 - W}{1 - W\,(1 - M_v/M_g)} \quad . \qquad 5.2.23$$

As the Jakob number is small and the pressure across the boundary layer is assumed to be constant, the variation in h_{f_g} is small. Under the above assumptions the Clausius Clapreyon Equation can be integrated

$$\int_{P_v^*}^{P_{v\infty}} \frac{dP}{P} = \int_{T^*}^{T_{s\infty}} \frac{h_{f_g}}{R} \frac{dT}{T^2} \qquad 5.2.24$$

where T^* and Ts_∞ are the saturation temperatures of the vapor corresponding to the partial pressure Pv^* and Pv_∞, respectively.

Upon performing the indicated integration in Equation 5.2.24, an expression is obtained for the interfacial temperature between the condensate and the gas vapor boundary layers.

$$T^* = \frac{Ts_\infty}{1 + \frac{T_{s\infty} R}{h_{f_g}} \ln \frac{P_{v\infty}}{P_v^*}} \qquad 5.2.25$$

where utlizing Equation 5.2.23

$$\frac{P_{v\infty}}{P_v^*} = \left\{ \frac{1 - W_\infty}{1 - W_\infty \left(1 - \frac{M_v}{M_g}\right)} \right\} \left\{ \frac{1 - W^* \left(1 - M_v/M_g\right)}{1 - W^*} \right\} \quad . \qquad 5.2.26$$

In terms of the nondimensional temperature Equation 5.2.25 is given as

$$\Theta^* = \frac{\Theta_{s_\infty} - \frac{T_o\, T_{s\infty}\, R}{h_{f_g}(T_\infty - T_o)} \ell n \frac{P_{v\infty}}{P_v^*}}{1 + \frac{T_{s\infty}\, R}{h_{f_g}} \ell n \frac{P_{v\infty}}{P_v^*}} \quad . \qquad 5.2.27$$

The conservation equations for mass, momentum and species are

$$\frac{\partial u}{\partial x} + \frac{\partial v}{\partial y} = 0$$

$$u \frac{\partial u}{\partial x} + v \frac{\partial u}{\partial y} = \nu \frac{\partial^2 u}{\partial y^2} \qquad 5.2.28$$

$$u \frac{\partial w}{\partial x} + v \frac{\partial w}{\partial y} = D \frac{\partial^2 w}{\partial y^2} \quad .$$

The integral form of equations for the conservation of momentum and species are

$$\frac{d}{dx} \int_{\delta_f + \delta_c}^{\delta_f + \delta_c + \delta_m} u^2 dy + u_c^2 \frac{d\delta_c}{dx} - u_c V^* = - \nu \left.\frac{\partial u}{\partial y}\right|_{y = \delta_f + \delta_c} \qquad 5.2.29$$

$$\frac{d}{dx} \int_{\delta_f + \delta_c}^{\delta_f + \delta_c + \delta_m} u(W - W_\infty)\, dy + u_c (W^* - W_\infty) \frac{d\delta_c}{dx}$$

$$- u_c V^* (W - W_\infty) = - D \left.\frac{\partial W}{\partial y}\right|_{y = \delta_f + \delta_c} \quad . \qquad 5.2.30$$

As quadratic profiles for velocity and concentration have been reported to yield good results it is necessary to satisfy the following boundary conditions:

$$u = u_c;\ W = W^* \text{ at } y = \delta_f + \delta_c$$

$$u = 0; \frac{\partial u}{\partial y} = 0 \text{ at } y = \delta_f + \delta_c + \delta_m$$

$$W = W_\infty \; ; \quad \frac{\partial W}{\partial y} = 0 \text{ at } y = \delta_f + \delta_c + \delta_s \; . \qquad 5.2.31$$

These conditions lead to the following profiles for velocity and concentration

$$u = \frac{u_c}{\delta_m^2} [\, \delta_f + \delta_c + \delta_m - y]^2 \qquad 5.2.32$$

$$W - W_\infty = \left(\frac{W^* - W_\infty}{\delta_s^2} \right) [\, \delta_f + \delta_c + \delta_s - y]^2 \; . \qquad 5.2.33$$

The conservation of mass at the interface $\delta_f + \delta_c$ leads to

$$\frac{d}{dx} \int_{\delta_f}^{\delta_f + \delta_c} \rho_f \, u_c \, dy = [\, \rho u \, \frac{d\delta}{dx} - \rho v]_{\delta_f + \delta_c} \; . \qquad 5.2.34$$

The interface between the condensate and the gas vapor mixture is impermeable to the noncondensible gas. Therefore,

$$[(\, \rho_g u \, \frac{d\delta}{dx} - \rho_g V) + D \, \frac{\partial w}{\partial y} \,]_{y = \delta_f + \delta_c} = 0 \; . \qquad 5.2.35$$

Combining equations 5.2.34 and 5.2.35 and eliminating v^* results in

$$\frac{\rho_c}{\rho_i} u_c \frac{d\delta_c}{dx} = \frac{2D}{W^*} \frac{W^* - W_\infty}{\delta_s} \; . \qquad 5.2.36$$

As the Jakob number is small the thermal driving for is relatively small. Therefore equation 5.2.36 can be reduced to

$$\frac{\rho_c}{\rho_\infty} u_c \frac{d\delta_c}{dx} = \frac{2D}{W^*} \left(\frac{W^* - W_\infty}{\delta_s} \right) . \qquad 5.2.37$$

This yields an expression for the concentration of the noncondensible gas at the interface $\delta_f + \delta_c$. Nondimensionalizing Equation 5.2.37 yields

$$W^* = \frac{W_\infty}{1 - \frac{3^{2/3}}{8} Re_f^{2/3} Pr_f \frac{\nu_f}{\nu_\infty} S_c \frac{\bar{\delta}_s}{\bar{\delta}_c} \frac{d\bar{\delta}_c^2}{d\bar{x}}} . \qquad 5.2.38$$

Substituting Equations 5.2.32 and the expression for v^* from Equation 5.2.34 into Equation 5.2.29 yields

$$\frac{d\bar{\delta}_m^2}{d\bar{x}} = \frac{40}{(3 Re_f)^{2/3} \frac{\nu_f}{\nu_\infty}} - 5 \frac{\rho_f}{\rho_\infty} \frac{\bar{\delta}_m}{\bar{\delta}_c} \frac{d\bar{\delta}_c^2}{d\bar{x}} . \qquad 5.2.39$$

Substituting Equation 5.2.33 and the expression for v^* from Equation 5.2.35 into Equation 5.2.30 and nondimensionalizing yields

$$\frac{d\bar{\delta}^2}{d\bar{x}} = \left[\frac{24 W_\infty}{(3 Re_f)^{2/3} S_c \frac{\nu_f}{\nu_\infty} W^*} - \frac{\bar{\delta}_s^3}{\bar{\delta}_m} (0.5 - 0.2 \frac{\bar{\delta}_s}{\bar{\delta}_m}) \frac{d\bar{\delta}_m^2}{d\bar{x}} \right.$$

$$\left. - \frac{\bar{\delta}_s^2}{(W^* - W_\infty} \left\{ 1 - \frac{1}{2} \frac{\bar{\delta}_s}{\bar{\delta}_m} + \frac{1}{10} \frac{\bar{\delta}_s^2}{\bar{\delta}_m^2} \right\} \frac{dw^*}{d\bar{x}} \right] \div \left(1 - \frac{\bar{\delta}_s}{\bar{\delta}_m} + \frac{3}{10} \frac{\bar{\delta}_s^2}{\bar{\delta}_m^2} \right) . \qquad 5.2.40$$

Equations 5.2.17, 5.2.18, 5.2.21, 5.2.39 and 5.2.40 defind the condensation in Region I. They can be solved numerically after establishing the values of the first derivatives at x = 0. As can be seen from the figure the initial conditions are $\delta_1(x=0)=0$; $\delta_2(x=0)=0$; $\delta_c(x=0)=0$; $\delta_m(x=0)=0$;

and $\delta_s(x=0)=0$. Alternately, they may be solved assuming a series of solution. It may be shown that the solutions are satisfied by the expressions

$$\begin{aligned}
\bar{\delta}_1 &= a_1 \bar{x}^{1/3} + \ldots \\
\bar{\delta}_2 &= a_2 \bar{x}^{1/2} + \ldots \\
\bar{\delta}_c &= a^3 \bar{x}^{1/2} + \ldots \\
\bar{\delta}_m &= a_4 \bar{x}^{1/2} + \ldots \\
\bar{\delta}_x &= a_5 \bar{x}^{1/2} + \ldots
\end{aligned} \qquad 5.2.41$$

The solutions for Region I ends when $\delta_1 + \delta_2 = \delta_f$.

Region II

Region II begins when $\delta_1 + \delta_2 = \delta_f$. From this point onwards the isothermal plate acts as the heat sink.

At the end of Region I let

$$\bar{\delta}_1 = \bar{L}_1 \; ; \quad \bar{\delta}_2 = \bar{L}_2$$

$$\text{and} \quad C_1 = \frac{\bar{\delta}_1}{\bar{\delta}_f} \; ; \; C_2 = \frac{\bar{\delta}_2}{\bar{\delta}_f} \qquad 5.4.42$$

such that $c_1 + c_2 = 1$.

In the beginning of Region II an inflexion point occurs at $y = L_1$; where the slope $\frac{\partial T}{\partial y} = 0$. Therefore the heat transfer in Region II is analyzed in two zones; $0 < y < L_1$ and $L_1 < y < \delta_f$.

The energy equation for the film is

$$\frac{d}{dx} \int_0^{L_1} u_f \; T_1 \; dy = \frac{k_f}{\rho_f \; Cp_f} \left[\left. \frac{\partial T_1}{\partial y} \right|_{y = L_1} - \left. \frac{\partial T_1}{\partial y} \right|_{y = 0} \right] \qquad 5.2.43$$

for $0 < y < L_1$

and

$$\frac{d}{dx}\int_{L_1}^{\delta_f} u_f \, T_2 \, dy = \frac{k_f}{\rho_f \, Cp_f}\left[\left.\frac{\partial T_2}{\partial y}\right|_{y=\delta_f} - \left.\frac{\partial T_2}{\partial y}\right|_{y=L_1}\right] \qquad 5.2.44$$

for $L_1 \leq y \leq \delta_f$.

The boundary conditions for the temperature profile in $0 \leq y \leq L_1$ are

$$T_1 = T_w \text{ at } y = 0$$

$$T_1 = T_b \; ; \; \frac{\partial T_1}{\partial y} = -\frac{q}{k} = -\beta(x) \text{ at } y = L_1 \; . \qquad 5.2.45$$

These conditions lead to

$$T_1 = T_w + 2\left(T_b - T_w + \frac{\beta L_1}{2}\right)\frac{y}{L_1} - \left(T_b - T_w + \beta L_1\right)\frac{y^2}{L_1^2} \; . \qquad 5.2.46$$

The boundary conditions governing the temperature profile in $L_1 < y < \delta_f$ are

$$T_2 = T_b(x); \; \frac{\partial T_2}{\partial y} = -\frac{q}{k} = -\beta(x) \text{ at } y = L_1$$

$$T_2 = T_i \text{ at } y = \delta_f = L_1 + L_2 \; . \qquad 5.2.47$$

These conditions lead to

$$T_2 = T_b - \beta(y - L_1) + \left(T_i - T_b + \beta L_2\right)\left(\frac{y - L_1}{L2^2}\right)^2 \; . \qquad 5.2.48$$

The condensate layer temperature profile remains as

$$T_c = T_i + (T^* - T_i)\,\frac{(y - \delta_f)}{\delta_c} \quad . \qquad 4.2.49$$

The compatibility of heat fluxes at the interface δ_f leads to the following expression for the nondimensional interfacial temperature

$$\theta_1 = \frac{\theta^* \bar{L}_2 + 2\theta_b \bar{\delta}_c - \bar{\beta} \bar{L}_2 \bar{\delta}_c}{2\bar{\delta}_c + \bar{L}_2} \qquad 5.2.50$$

Substituting Equations 5.2.2 and 5.2.46 into Equation 5.2.43 and nondimensionalizing the length terms by $(\nu f^2/g)^{1/3}$ leads to

$$\left[\frac{\left(\frac{5}{3} - \frac{3}{5} c_1\right)}{\left(\frac{1}{3} - \frac{c_1}{10}\right)}\right] \frac{d\theta_b}{d\bar{x}} + c_1 \bar{\delta}_f \frac{d\bar{\beta}}{d\bar{x}} = \frac{-8\left[\theta_b - \theta_w + \bar{\beta} c_1 \bar{\delta}_f\right]}{Pr_f\, c_1{}^3\, \bar{\delta}_f{}^4 \left(\frac{1}{3} - \frac{c_1}{10}\right)} . \qquad 5.2.51$$

Substituting Equations 5.2.2 and 5.2.48 into Equation 5.2.44 and nondimensionalizing the length terms by $(\nu_f{}^2/g)^{1/3}$ leads to

$$M_1 \frac{d\theta_b}{d\bar{x}} - M_2 \delta_f \frac{d\bar{\beta}}{d\bar{x}} + M_3 \frac{d\theta_i}{dx} = \frac{2}{Pr_f} \frac{\left[\theta_i - \theta_b + \bar{\beta} \bar{L}_2\right]}{(1-C_1)\, \bar{\delta}_f{}^4} \qquad 5.2.52$$

where

$$M_1 = \frac{2c_1c_2}{3}\left(1 - \frac{c_1}{2}\right) + \frac{c_2{}^2}{4}(1 - c_1) - \frac{c_2{}^3}{15} \qquad 5.2.53$$

$$M_2 = \frac{c_1c_2{}^2}{6}\left(1 - \frac{c_1}{2}\right) + \frac{c_2{}^3}{12}(1 - c_1) \quad \frac{c_2{}^4}{20}$$

$$M_3 = \frac{c_1c_2}{6}\left(1 - \frac{c_1}{2}\right) + \frac{c_2{}^2}{4}(1 - c_1) \quad \frac{c_2{}^3}{10} .$$

The condensate layer energy equation, the momentum and species equation in the gas vapor region remain the same as Equations 5.2.20, 5.2.39 and 5.2.40, respectively.

Thus Equations 5.2.51, 5.2.52, 5.2.20, 5.2.39 and 5.2.40 define the condensation in Region II. The initial conditions are β and $\theta_b = 0$. The initial values for δ_c, δ_m, δ_s are those obtained at the end of Region I.

Case B $T_w < T_o = T_{sat}$

Figure 5.2.2 shows the physical model for condensation on a vertical isothermal plate in the presence of a noncondensible gas when incoming film is at the same temperature as the saturation temperature of the vapr. As the film temperature is the same as the saturation temperature, no condensation takes place. However, as the film temperature is greater than the temperature of the plate, a thermal boundary layer grows from the wall towards the edge of the film. The region where the thermal boundary layer develops is called as Region I. Region I comes to end when $\delta_1 = \delta_f$. From this point onward the film edge temperature decreases. As the film edge temperature is less than the saturation temperature, condensation takes place. Due to the presence of the noncondensible gas, in the gas vapor zone, a momentum and species boundary layer are established. The region where the film edge temperature drops leading to condensation is termed as Region II.

Region I

The integral form of the energy equation for the boundary layer δ_1 and the velocity profile remain the same as Equations 5.2.2 and 5.2.4. However, the boundary conditions for the temperature profile change to

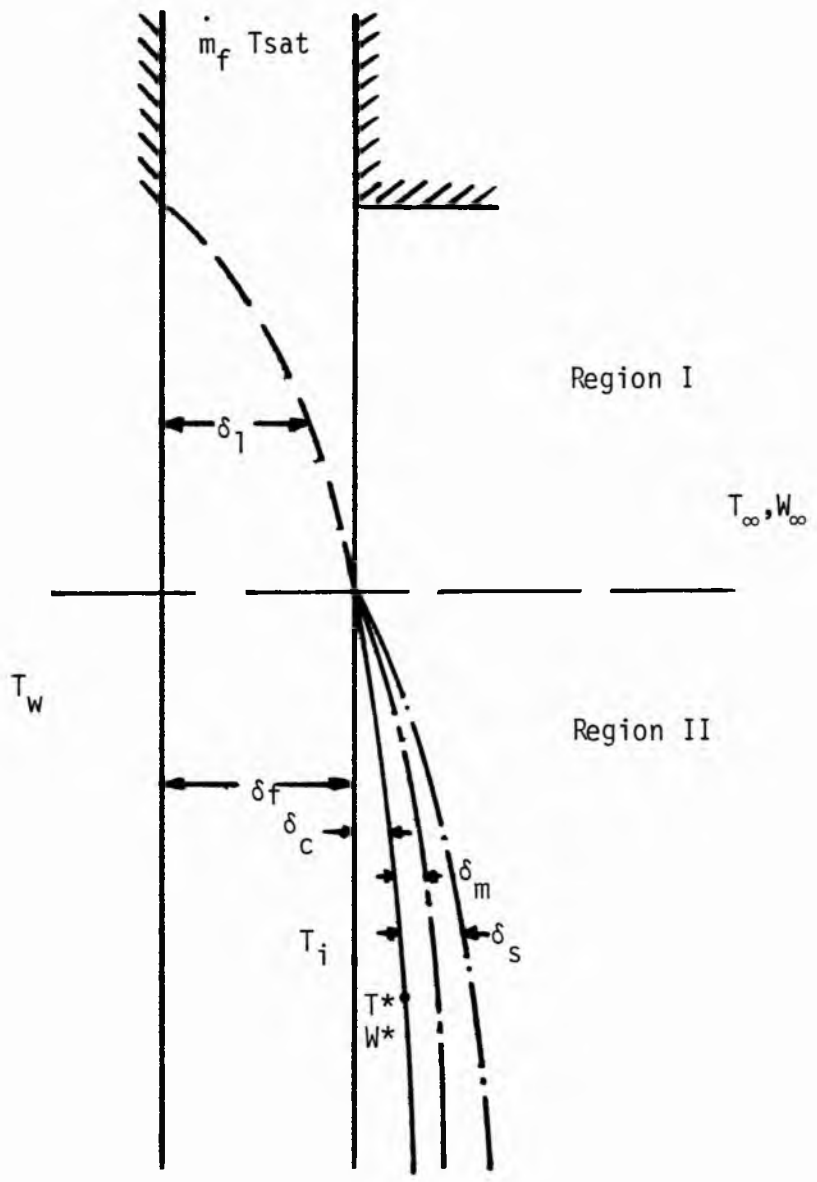

Figure 5.2.2. Physical model for condensation on a thin film flowing over an isothermal vertical plate in the presence of a noncondensible gas when $T_w < T_o = T_{sat}$.

$$T_1 = T_w \text{ at } y = 0$$

$$T_1 = T_{sat} \; ; \; \frac{\partial T_1}{\partial y} = 0 \text{ at } y = L_1 \quad . \tag{5.2.54}$$

These conditions lead to

$$T_1 - T_{sat} = (T_w - T_{sat}) \left(1 - \frac{y}{\delta_1}\right)^2 \quad . \tag{5.2.55}$$

Substituting Equations 5.2.54 and 5.2.2 into Equation 5.2.4 and nondimensionalizing the length terms by $(\nu_f^2/g)^{1/3}$ leads to

$$\frac{d\bar{\delta}_1^3}{d\bar{x}} = \frac{36}{Pr_f(\bar{\delta}_f - \frac{3}{10}\bar{\delta}_1)} \quad . \tag{5.2.56}$$

Equation 5.2.55 describes the heat transfer in Region I. It can be solved numerically after establishing the value of the first derivative at x = 0. For extremely small values of x it can be shown that

$$\bar{\delta}_1 \; a_1 \; \bar{x}^{1/3} + \ldots \tag{5.2.57}$$

Region I comes to an end when $\delta_1 = \delta_f$.

Region II

Region II begins as the film edge temperature at $y = \delta_f$ drops below the saturation temperature of the vapor. As a result, condensation begins. A condensate layer, δ_c, forms on the edge of the film. Due to the presence of noncondensible gas in the condensing vapor a separate momentum and species equations are established in the gas vapor region.

The boundary conditions for the temperature profile in the film are

$$T_1 = T_w \text{ at } y = 0$$

$$T_1 = T_i \; ; \; \frac{\partial T_1}{\partial y} = -\frac{q}{k} = -\beta \text{ at } y = \delta_f \quad . \qquad 5.2.58$$

These conditions lead to

$$T_1 = T_w + [\,2(T_i - T_w) + \beta\delta_f]\frac{y}{\delta_f} - [(T_i - T_w) + \beta\delta_f]\frac{y^2}{\delta_f^2} \quad . \qquad 5.2.59$$

The energy equation for the film is

$$\frac{d}{dx}\int_0^{\delta_f} u_f\, T_1\, dy = \frac{k_f}{\rho_f\, C_{p_f}}\left[\left.\frac{\partial T_1}{\partial y}\right|_{y=\delta_f} - \left.\frac{\partial T_1}{\partial y}\right|_{y=0}\right] \qquad 5.2.60$$

Substituting Equation 5.2.2 and 5.2.58 into Equation 5.2.59 and nondimensionalizing the length terms by $(\nu_f^2/g)^{1/3}$ leads to

$$\frac{d}{d\bar{x}}\left[4\theta_i + \frac{7}{8}\,\bar{\beta}\,\bar{\delta}_f\right] = -\frac{30}{Pr_f}\left(\frac{\theta_i + \bar{\beta}\,\bar{\delta}_f}{\bar{\delta}_f^4}\right) \qquad 5.2.61$$

where

$$\left.\begin{aligned} \theta &= \frac{T - T_w}{T_\infty - T_w} \\ \text{and } \bar{\beta} &= \frac{\bar{\beta}\,(\nu_f^2/g)^{1/3}}{(T_\infty - T_w)} \end{aligned}\right\} \quad . \qquad 5.2.62$$

The temperature in the condensate layer remains as

$$T_c = T_i + (T^* - T_i) \left(\frac{y - \delta_f}{\delta_c}\right) . \qquad 5.2.63$$

The compatibility of heat fluxes at the interface $y = \delta_f$ leads to the following expression for the nondimensional interfacial temperature θ_i.

$$\theta_i = \theta^* + \bar{\beta}\,\bar{\delta}_c . \qquad 5.6.64$$

Substituting Equation 5.2.64 into Equation 5.2.61 yields

$$\frac{d\bar{\beta}}{d\bar{x}} = \frac{-\frac{30}{Pr_f \bar{\delta}_f^4}\left[\theta^* + \bar{\beta}\,(\bar{\delta}_f + \bar{\delta}_c)\right] - 4\frac{d\theta^*}{dx} - 4\,\bar{\beta}\frac{d\bar{\delta}_c}{d\bar{x}}}{4\,\bar{\delta}_c + \frac{7}{8}\bar{\delta}_f} . \qquad 5.2.65$$

The condensate energy equation remains as

$$\frac{d\bar{\delta}_c}{d\bar{x}} = \frac{2}{3^{2/3}} \frac{Ja}{Re_f^{2/3} Pr_f} \frac{\theta^* - \theta_i}{\bar{\delta}_c} . \qquad 5.2.66$$

Substituting Equation 5.2.64 into Equation 5.2.66 yields

$$\frac{d\bar{\delta}_c}{d\bar{x}} = \frac{2}{3^{2/3}} \frac{Ja}{Re_f^{2/3} Pr_f}\,\bar{\beta} . \qquad 5.2.67$$

The nondimensional interfacial temperature, θ^*, at $y = \delta_f + \delta_c$ remains as

$$\theta^* = \frac{\theta_{s\infty} - \dfrac{RT_o T_{s\infty}}{(T_\infty - T_o\ h_{f_g}} \ell n\ \dfrac{Pv_\infty}{Pv^*}}{1 + \dfrac{RT_{s\infty}}{h_{f_g}}\ \ell n\ \dfrac{Pv_\infty}{Pv^*}} \quad . \qquad 5.2.68$$

where

$$\frac{Pv_\infty}{PV^*} = \left[\frac{1 - W_\infty}{1 - W_\infty\ (1 - M_v/M_g)}\right]\ \left[\frac{1 - W^*\ (1 - M_v/M_g)}{1 - W^*}\right] \quad . \qquad 5.2.69$$

The interfacial concentration of noncondensible gas remains as

$$W^* = \frac{W_\infty}{1 - \dfrac{3^{2/3}}{4}\ Re_f^{2/3}\ \dfrac{\nu_f}{\nu_\infty}\ \delta c\ \dfrac{\rho_f}{\rho_\infty}\ \bar{\delta}_s\ \dfrac{d\bar{\delta}_c}{dx}} \quad . \qquad 5.2.70$$

The governing differential equations for conservation of momentum and species in the gas vapor mixture remain as

$$\frac{d\bar{\delta}_m^2}{dx} = \frac{40}{(3\ Re_f)^{2/3}\ \dfrac{\nu_f}{\nu_\infty}} - 10\ \frac{\rho_f}{\rho_\infty}\ \bar{\delta}_m\ \frac{d\bar{\delta}_c}{d\bar{x}} \qquad 5.2.71$$

$$\frac{d\bar{\delta}_s^2}{d\bar{x}} = \left[\frac{24\ W_\infty}{(3\ Re_f)^{2/3}\ S_c\ \dfrac{\nu_f}{\nu_\infty}\ w^*} - \frac{\bar{\delta}_s^3}{\bar{\delta}_m^3}\ \left(\frac{1}{2} - \frac{1}{5}\ \frac{\bar{\delta}_s}{\bar{\delta}_m}\right)\ \frac{d\bar{\delta}_m^2}{d\bar{x}}\right.$$

$$\left. - \frac{2\ \bar{\delta}_2^2}{(w^* - w_\infty)}\left(1 - \frac{1}{2}\ \frac{\bar{\delta}_c}{\bar{\delta}_m}\ \frac{1}{10}\ \frac{\bar{\delta}_s^2}{\bar{\delta}_m^2}\right)\frac{dw^*}{d\bar{x}}\right] \div \left(1 - \frac{\bar{\delta}_s}{\bar{\delta}_m}\ \frac{3}{10}\ \frac{\bar{\delta}_s^2}{\bar{\delta}_m^2}\right) . \qquad 5.2.72$$

Heat Transfer Expressions

A heat transfer coefficient can be defined as

$$h(x) = \frac{k \left.\frac{\partial T}{\partial y}\right|_{y=0}}{(T_\infty - T_w)} \quad . \qquad 5.2.73$$

The local Nusselt number can be defined as

$$N_u\ (\bar{x}) = \frac{h(x)(\nu_f^2/g)^{1/3}}{k} \quad . \qquad 5.2.74$$

Case A $T_w \leq T_o \leq T_{sat}$

Substituting for h(x), the local Nusselt number in Region I becomes

$$N_u\ (\bar{x}) = - \frac{2\theta_w}{(1 - \theta_w)\ \bar{\delta}_1} \quad . \qquad 5.2.75$$

Substituting the expression for δ_1 from Equation 5.2.41 the local Nusselt number becomes

$$N_u\ (\bar{x}) = - \frac{2\theta_w}{(1 - \theta_w) a_1\ \bar{x}^{1/3}} \qquad 5.2.76$$

from which an average Nusselt number in Region I can be calculated as

$$Nu_I = - \frac{3\theta_w}{(1 - \theta_w) a_1\ \bar{x}^{1/3}} \quad . \qquad 5.2.77$$

The local Nusselt number in Region II is given by

$$Nu_{II}(x) = \frac{2\left[\theta_b - \theta_w + \frac{\bar{\beta}\bar{L}_1}{2}\right]}{\bar{L}_1 (1 - \theta_w)} \quad . \qquad 5.2.78$$

The average Nusselt number in Region II is expressed as

$$Nu_{II} = \frac{\int_{\bar{x}_D}^{\bar{x}} Nu_{II}(\bar{x})\, d\bar{x}}{(\bar{x} - \bar{x}_D)} \qquad 5.2.79$$

where

X_D is the extent of Region I.

The average Nusselt over the entire length of Regions I and II is given by

$$\overline{Nu} = \frac{Nu_I\, \bar{x}_D + Nu_{II}(\bar{x} - \bar{x}_D)}{\bar{x}} \quad . \qquad 5.2.80$$

Case B $T_w < T_o = T_{sat}$

The local Nusselt number in Region I is given by

$$Nu(\bar{x}) \frac{2.0}{\bar{\delta}_1} \quad . \qquad 5.2.81$$

Substituting for δ_1 the local Nusselt number can be expressed as

$$Nu(\bar{x}) = \frac{2}{a_1 \bar{x}^{1/3}} \qquad 5.2.82$$

from which an average Nusselt number in Region I can be calculated

as

$$Nu_I = \frac{3}{a_1 \bar{x}^{1/3}} \quad . \qquad 5.2.83$$

The local Nusselt number in Region II is given by

$$Nu_{II}\ (\bar{x}) = \frac{2\theta_i + \bar{\beta}\ \bar{\delta}_f}{\bar{\delta}_f} \quad . \qquad 5.2.84$$

The average Nusselt number in Region II is calculated as

$$Nu_{II} = \frac{\int_{\bar{x}_D}^{\bar{x}} Nu_{II}\ (\bar{x})\ d\bar{x}}{(\bar{x} - \bar{x}_D)} \quad . \qquad 5.2.85$$

The overall average Nusselt number over Regions I and II is given by

$$\overline{Nu} = \frac{Nu_I\ \bar{x}_D + Nu_{II}\ (\bar{x} - \bar{x}_D)}{\bar{x}} \qquad 5.2.86$$

where x_D is the extent of Region I.

In the present analysis the overall average Nusselt number is the quantity of prime importance.

5.3. Results and Discussion

Case A $T_w < T_0 < T_{sat}$

Examination of the governing differential equations indicates that condensation in Region I is dependent on eight nondimension parameters. They are

$$Pr_f,\ Re_f,\ Ja,\ w_\infty,\ S_c,\quad \frac{\nu_f}{\nu_\infty},\ \frac{M_v}{M_g},\ \frac{\rho_f}{\rho_\infty}\ . \tag{5.3.1}$$

Although the equations derived are valid for all fluid systems of interest, it was decided to restrict the study to that of steam condensing on a thin film of water. The reason for this restriction is the availability of other literatures for steam-air systems.

It was observed that simple expressions could be obtained for the coefficients of δ_1 and δ_2 as indicated in Equation 5.2.41. They are

$$a_1 = \left[\frac{36}{(3Re_f)^{1/3}\ Pr_f}\right]^{1/3} ;\ a_2 = \left[\frac{24}{(3Re_f)^{2/3}\ Pr_f}\right]^{1/2} . \tag{5.3.2}$$

No simple expressions could be obtained for the coefficients of δ_c, δ_m and δ_s. Thus they had to be evaluated numerically. They were determined to a high precision using the Meinback subroutine, Hybrd1 [29], developed at the Argonne National Laboratory, Chicago, Illinois The subroutine finds the zeros of a system of N nonlinear functions in n variables by a modification of the Powell hybrid method. The user must provide a subroutine which calculates the functions. The Jacobian is then calculated by a forward difference approximation.

Utilizing the expressions for δ_1 and δ_2 from Equations 5.2.41 and the values of the constants a_1 and a_2 from Equation 5.3.2, the following expression is obtained for X_D the extent of Region I.

$$\left[\frac{36}{(3Re_f)^{1/3}\ Pr_f}\right]^{1/3} \bar{x}_D^{\,1/3} + \left[\frac{24}{(3Re_f)^{2/3}\ Pr_f}\right]^{1/2} \bar{x}_D^{\,1/2} = \bar{\delta}_f\ . \tag{5.3.3}$$

The above equation has to be solved numerically to obtain the ex-

tent of Region I. It is observed that the extent of Region I is dependent on the Prandtl number and the Reynolds number of the film. The average Nusselt number in Region I is given by

$$Nu_I = \frac{-3\theta_w}{(1 - \theta_w)\left[\frac{36}{(3Re_f)^{1/3} Pr_f}\right]^{1/3} \bar{x}_D^{1/3}} \cdot \qquad 5.3.4$$

In addition to eight parameters noted in Equation 5.3.1, condensation in Region II is dependent on the nondimensional temperature of the vertical plate. No simple expressions could be obtained for the local or average Nusselt numbers in Region II; thus they had to be evaluated numerically. As noted in the previous chapter in section 4.3, the maximum nondimensional length of the plate of interest over which condensation heat transfer is examined is 1000.

The presence of noncondensible gases in the condensing vapor leads to complex transport processes. Thus to understand these processes one has to examine the behavior of the interfacial concentration of the noncondensible gas, its effect on the interfacial temperature and the Nusselt number.

Figure 5.3.1 presents the concentration of the noncondensible gas at the interface $\delta_f + \delta c$ as a function of the distance along the plate for different incoming film temperatures. It is observed that a lower T_0 leads to a high W^* in Region I. This can be explained as follows. A lower T_0 provides a higher temperature driving force for condensation. As a result more vapor and noncondensible gas are drawn towards the interface $\delta_f + \delta_c$. To counterbalance this increased inflow of the noncondensible gas, a higher outflow is required which results

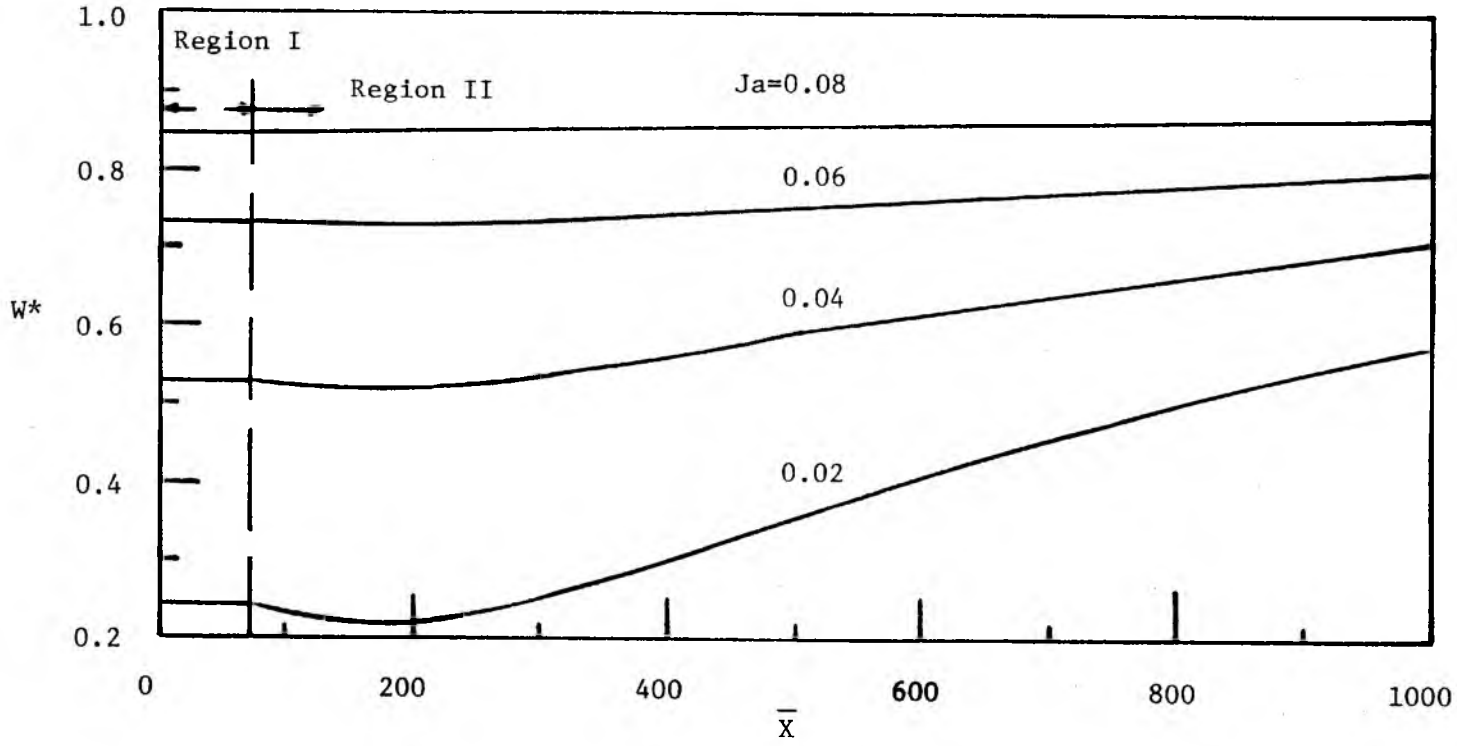

Figure 5.3.1. Inter concentration of noncondensible gas as a function of $\bar{X}$ for different Ja. T_{sat}=600°R, T_w=500°R.

in a higher W*. In Region II there is only a slight increase in W*. This is is due to the small difference between T_o and T_w. For a larger T_o, the concentration of the noncondensible gas, W*, is small in Region I. However, in Region II there is a considerable increase in W*. This is due to the larger difference between T_o and T_w which leads to significantly higher cooling of the interface.

Figure 5.3.2 presents W* as a function of x for different T_w. It is observed that W* is independent of T_w in Region I. This is due to that fact that the condensation in Region I is dependent only on the cooling capacity of the film. But in Region II as the wall temperature decreases, W* increases. A lower T_w leads to a faster cooling of the interface at $\delta_f + \delta_c$. Thus the thermal driving force increases, leading to a higher W*. This phenomenon has been observed in several studies on surface condensers [6,17,18,19]. As noted in the pure vapor case, for a short-distance in Region II, W* decreases instead of increasing. This phenomenon can be attributed to the delayed influence of the cold wall on the interface.

Figure 5.3.3 shows the variation of W* with x for a different Reynolds number. It is observed that for a larger Reynolds number there is a lesser build up of noncondensible gases.

An increase in the interfacial concentration of noncondensible gases, W*, decreases the saturation temperature of the vapor, T*, at the interface $\delta_f + \delta_c$. This in turn leads to a smaller temperature T_i, at the interface $y = \delta_f$. This phenomenon is observed in Figure 5.3.4 which presents the nondimensional interfacial temperature θ_i as a function of x for different T_o. A lower T_o leads to a higher W* which in turn drastically reduces θ_i. This phenomenon is further ob-

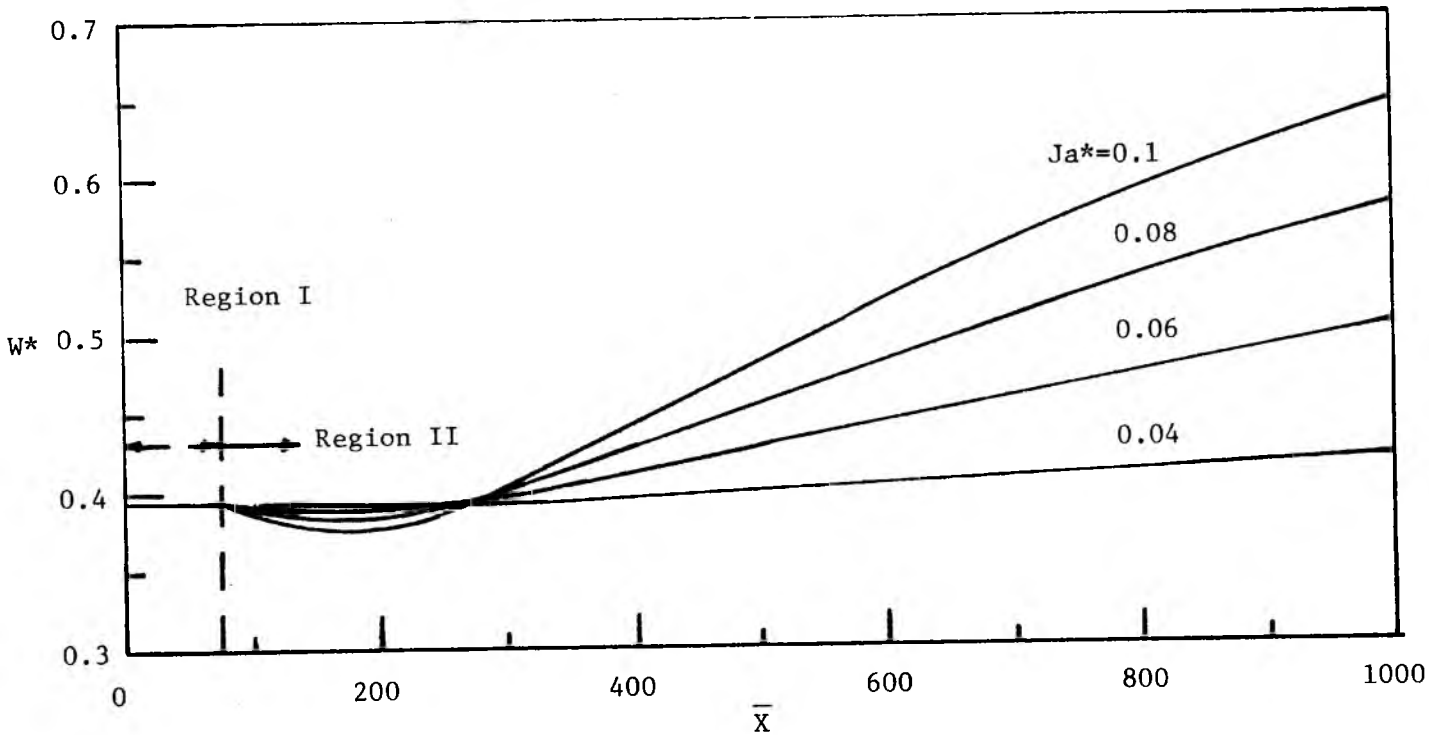

Figure 5.3.2. Interfacial concentration of noncondensible gas a function of $\overline{X}$ for different Ja*. T_{sat}=600°R, T_o=570°R.

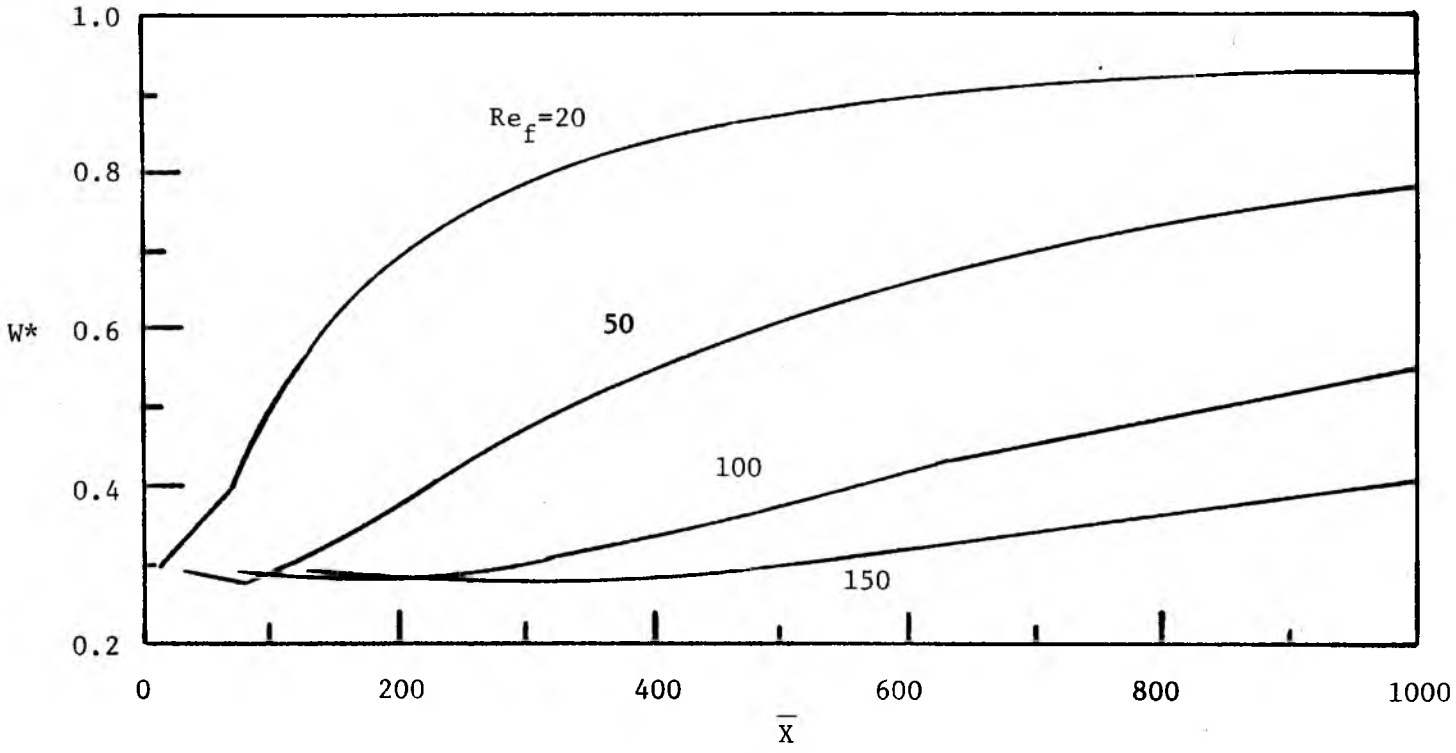

Figure 5.3.3. Interfacial concentration of noncondensible gas as a function of $\overline{X}$ for different Reynolds numbers. T_{sat}=600°R, T_o=570°R, T_w=500°R.

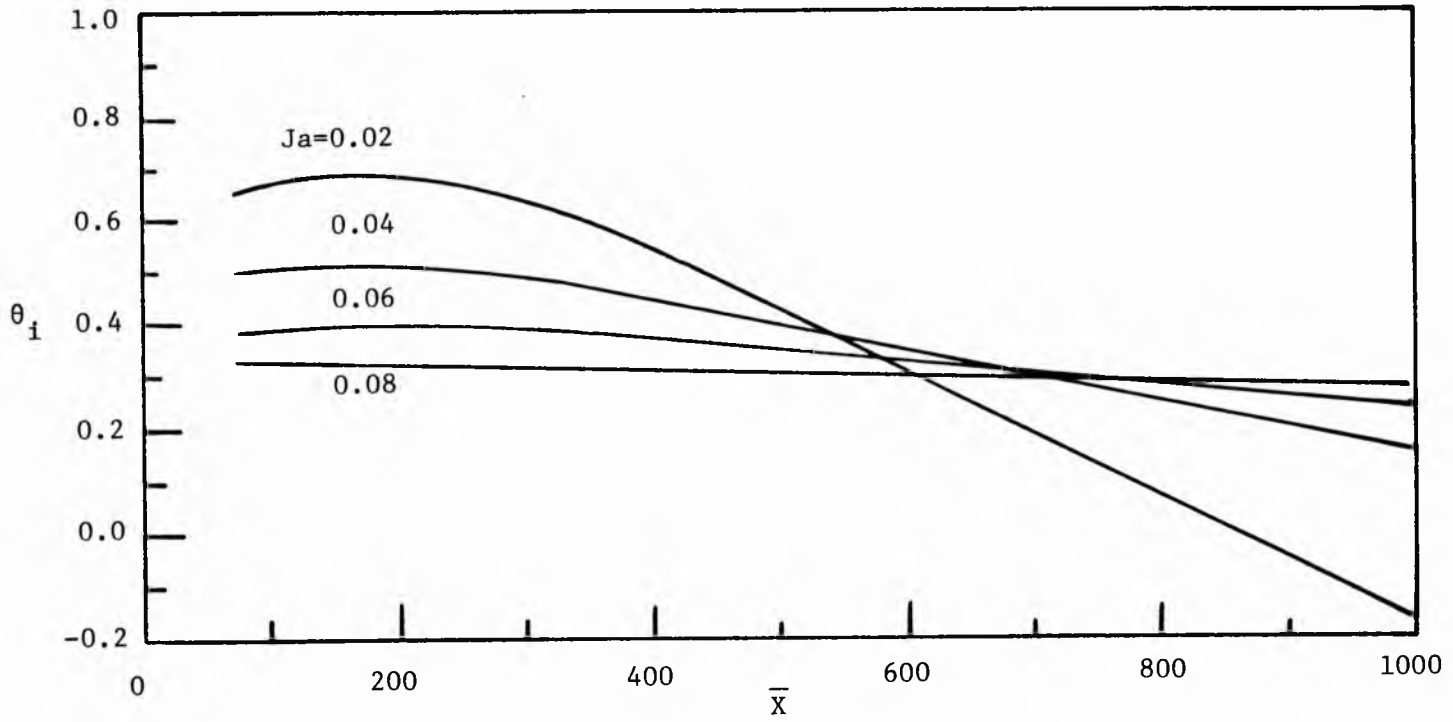

Figure 5.3.4. Nondimensional interfacial temperature as a function of $\bar{X}$ for different Ja. T_{sat}=600°R, T_w=500°R.

observed in Figures 5.3.5 and 5.3.6 which present θ_i as a function of x for different wall temperatures and Reynolds numbers, respectively.

In order to understand clearly the effects of noncondensible gas on condensation heat transfer it is important to examine the variation of the ratio of the Nusselt numbers for condensation with and without noncondensible gas with other parameters. Figure 5.3.7 presents the ratio of Nusselt numbers as a function of x for $w_\infty = 0.01$, $T_O = 570°R$ and $T_W = 520°R$. It is observed that for a short distance in Region II, the ratio is greater than one. In all of the previous analytical studies on bare surface, it has been reported that the ratio of Nusselt numbers is less than one. In order to understand the unusual behavior in the present problem, it is necessary to examine the temperature profile in the film. Figure 5.3.8 and 5.3.9 present the temperature profiles in the film for condensation with and without the presence of noncondensible gas respectively, a function of x. For the pure vapor case it is observed that in the beginning of Region II the temperature profile exists in two separate shapes. A convex profile is $0 < y < L_1$ and a concave quadratic profile is $L_1 < y < \delta_f$ with the slope being zero at $Y = L_1$. This is in agreement with the boundary conditions in Equations 5.2.45 and 5.2.46. Moreover, it is noticed that the convex profile has more height. This is due to the comparatively large θ_i (resulting from the absence of noncondensible gas). After a short distance into Region II the entire profile in $0 < y < \delta_f$ becomes concave. Further the slope of the profile at y = 0 decreases. As we proceed farther into Region II the concavity decreases. The temperature profile gradually tends to a linear shape. Moreover, the slope at y = 0 starts to increase. Thus, it is observed that as we proceed into Re-

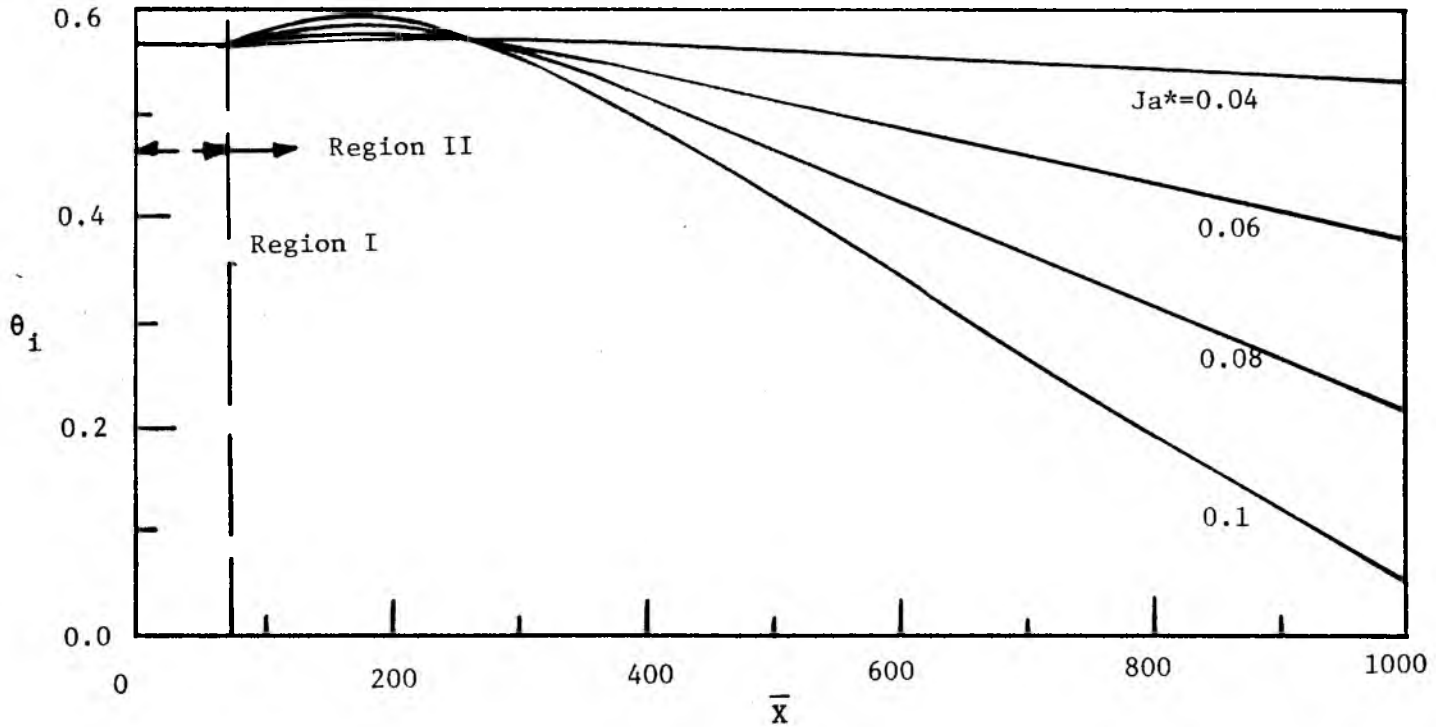

Figure 5.3.5. Nondimensional interfacial temperature as a function of $\overline{X}$ for different Ja*. T_{sat}=600°R, T_o=570°R.

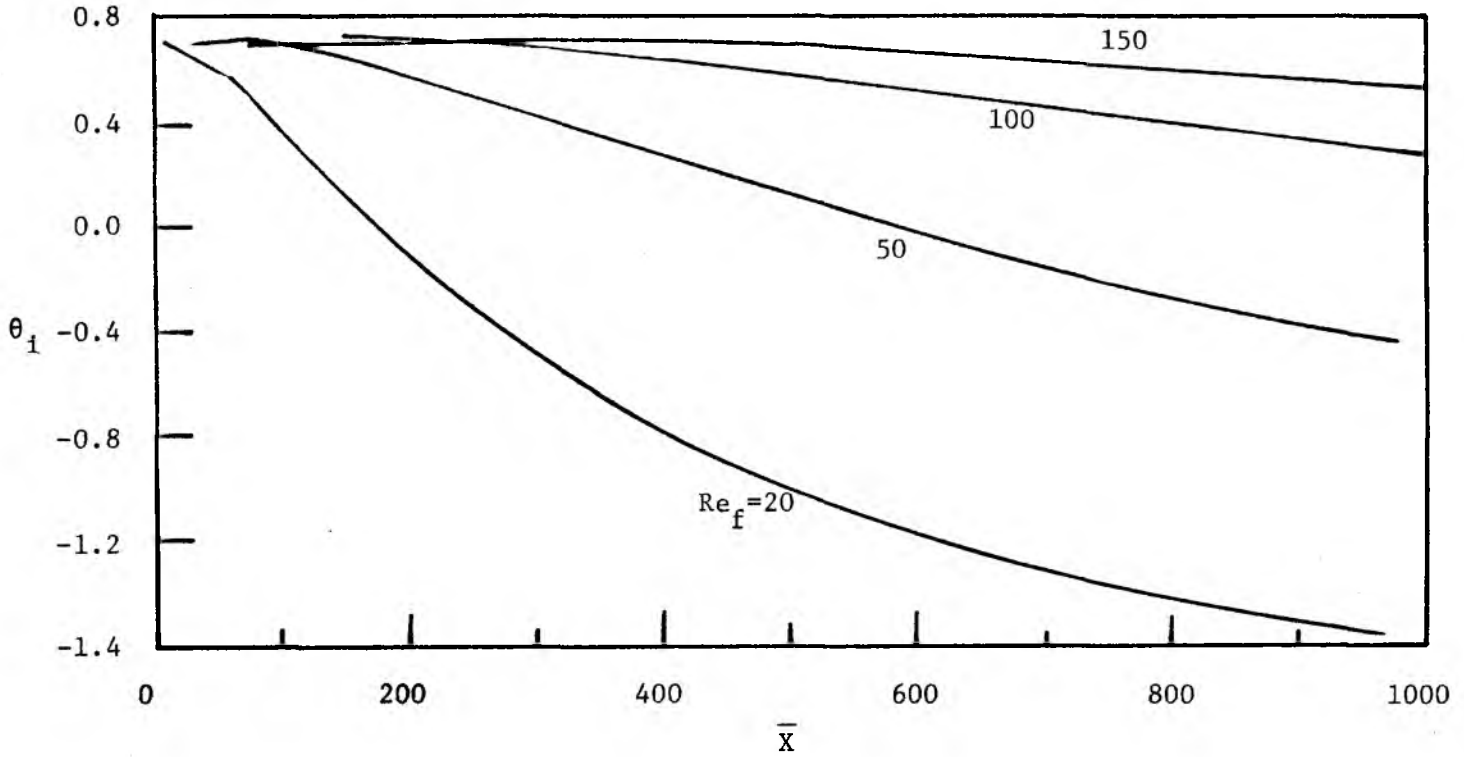

Figure 5.3.6. Nondimensional interfacial temperature as a function of $\bar{X}$ for different Reynolds numbers. T_{sat}=600°R, T_o=570°R, T_w=500°R.

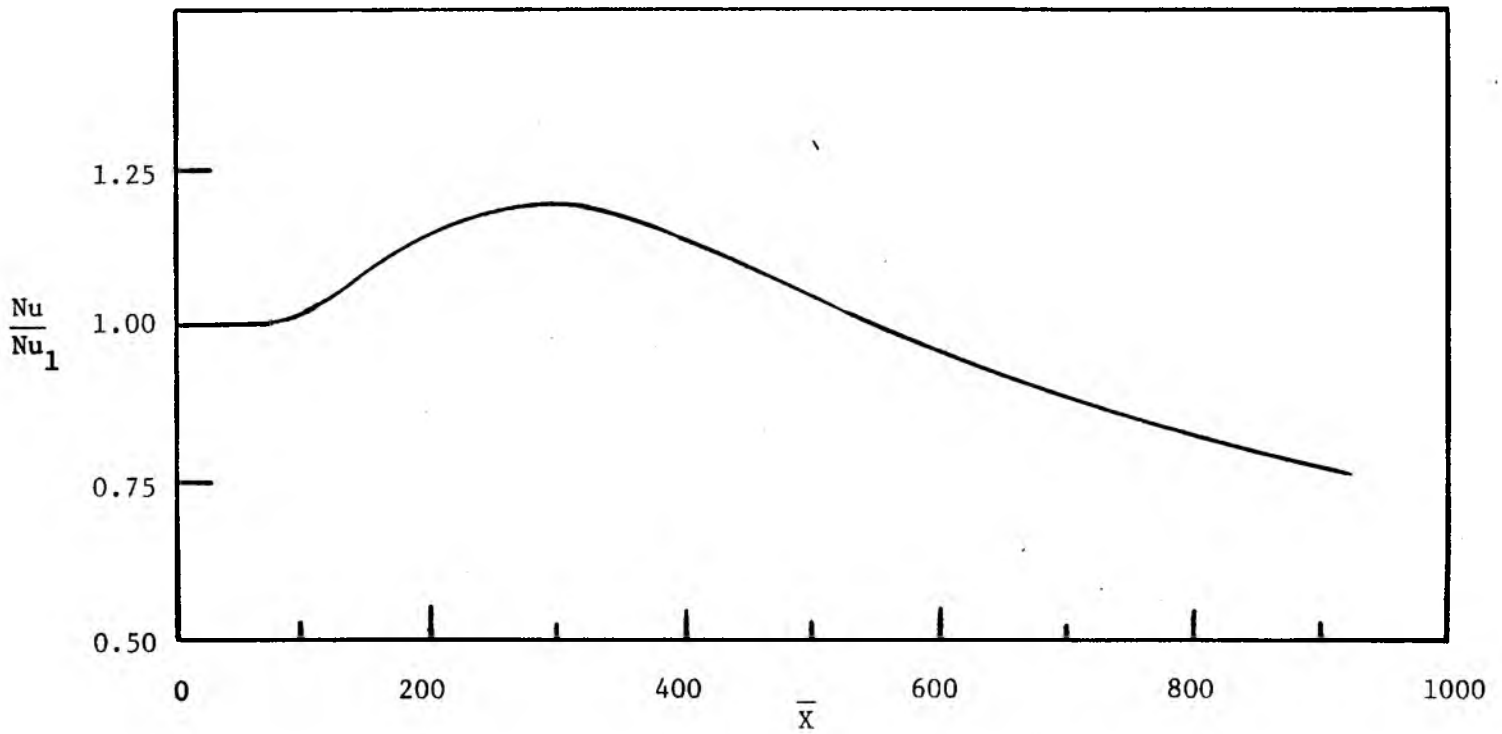

Figure 5.3.7. Ratio of Nusselt numbers for condensation with and without the presence of noncondensible gas as a function of X.

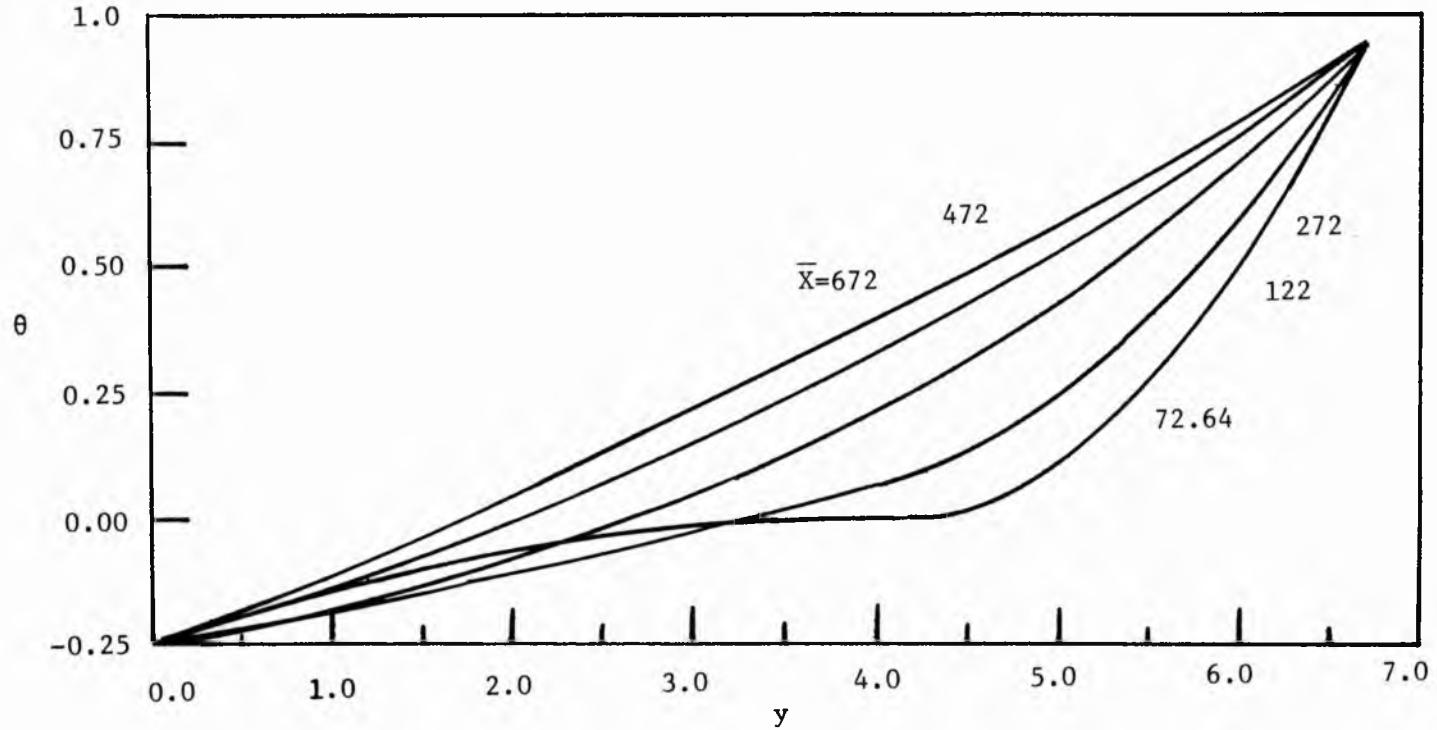

Figure 5.3.8. Temperature profile in the film at different values of $\overline{X}$. Pure vapor case.

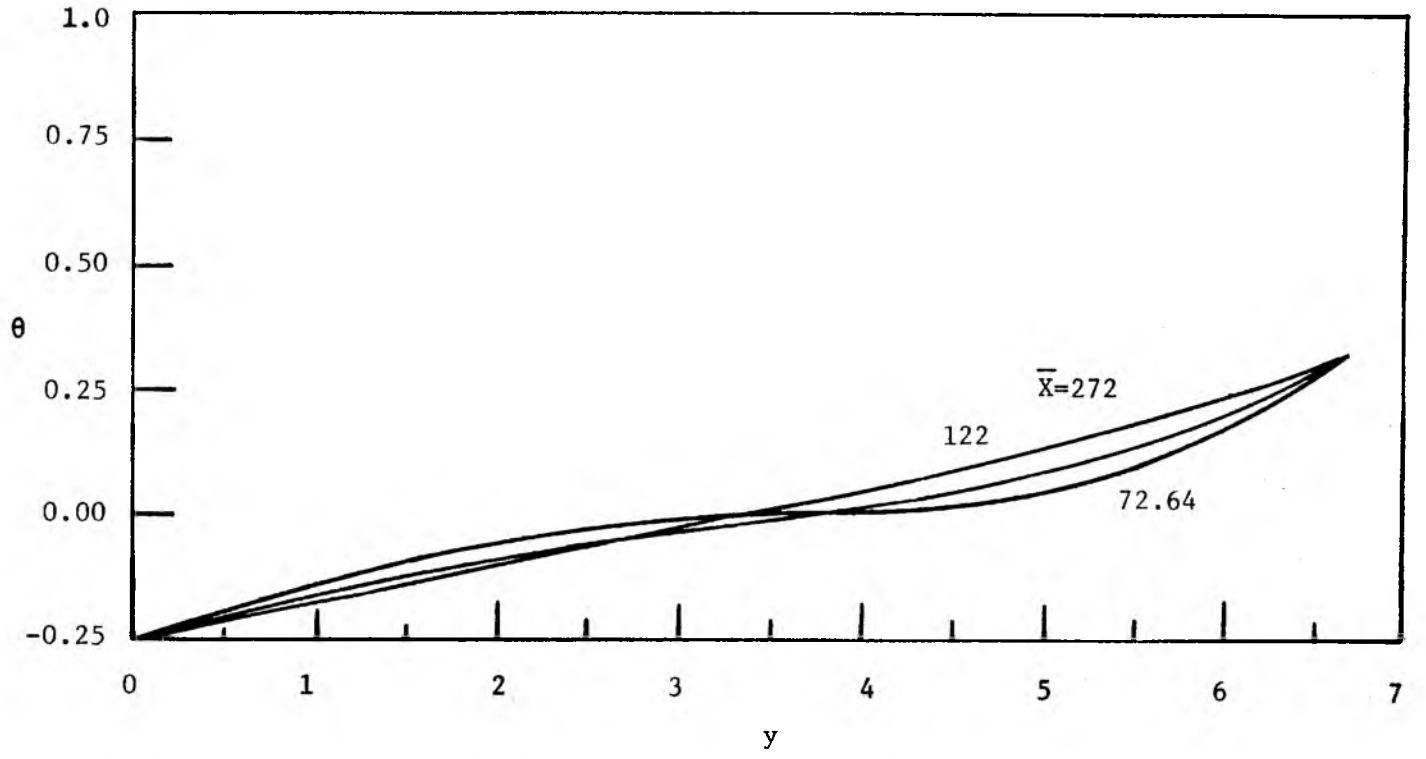

Figure 5.3.9. Temperature profile in the film at different values of X in the presence of noncondensible gas.

gion II the slope at y = 0 first decreases and then increases. The same behaviour is noted in Figure 5.3.9 for noncondensible gas being present, with one exception. The value of θ_i is much lower. This is due to presence of the noncondensible gas in the condensing vapor.

Figure 5.3.10 presents the temperature profile in the beginning of Region II for condensation with and without the presence of the noncondensible gas. It is observed that the slope of the profile at y = 0 is the same for both cases. Figure 5.3.10 presents the two profiles at x = 122. It is observed that the slope of the profile with noncondensible gases at x = 0 is greater than that for the pure vapor case. This is due to the larger convexity of the later curve. Figures 5.3.11, 5.3.12, and 5.3.13 present the two profiles at x = 272, 472 and 672 respectively. It is observed that at x = 272 the two slopes are almost the same. However, for x > 272, the slope at y = 0 for the pure vapor case exceeds that for the noncondensible gas case. This behaviour of the temperature profile leads to the ratio of Nusselt numbers in Figure 5.3.7 greater than 1.

Figures 5.3.14, 5.3.15, 5.3.16, and 5.3.17 show the variation of the ratio of Nusselt numbers for condensation with and without the presence of noncondensible gas with x for different incoming film temperature, wall temperatures, Reynolds number and free stream concentration of noncondensibles.

Case B $T_w < T_o < T_{sat}$

When the incoming film temperature is the same as the saturation temperature of the vapor, no condensation takes place in Region I. Equation 5.2.56 describes the heat transfer in Region I. The develop-

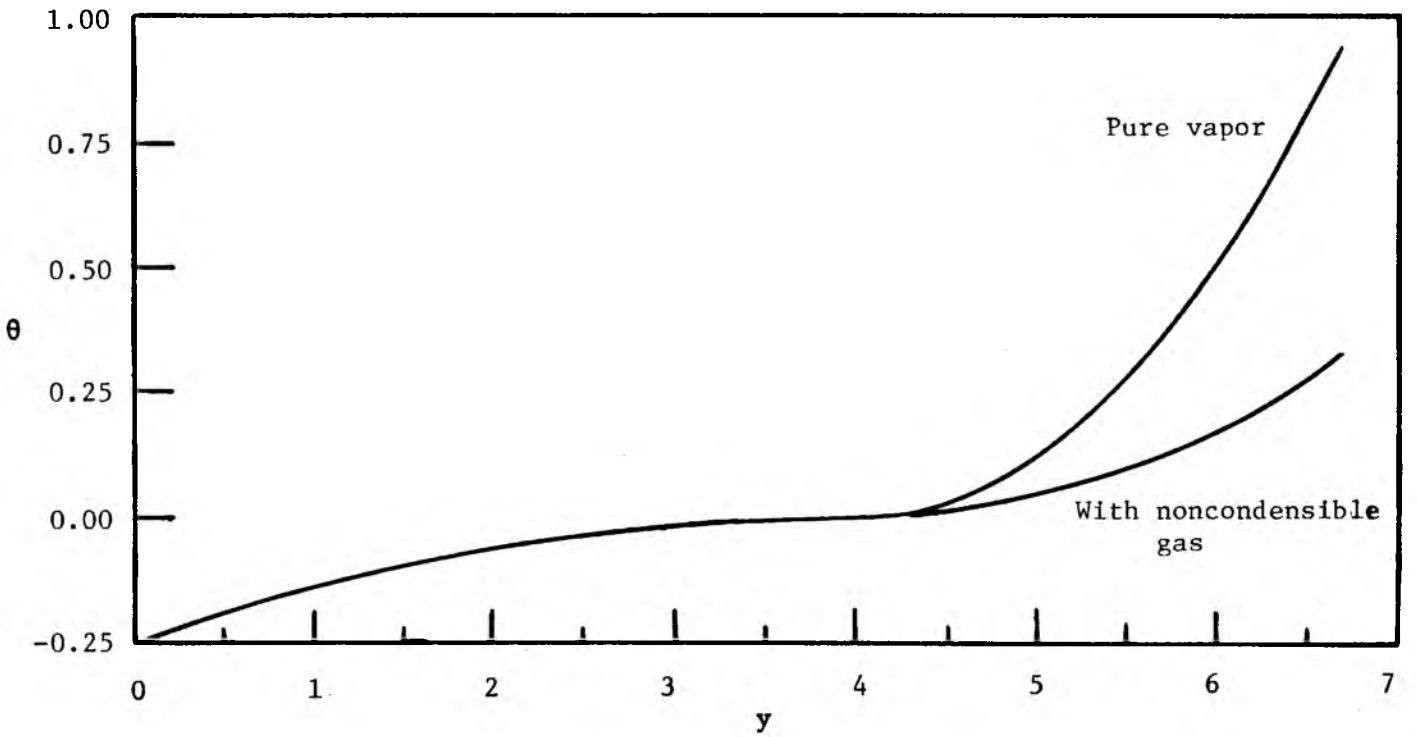

Figure 5.3.10. Comparison of temperature profile in the film for condensation with and without the presence of noncondensible gas at $\overline{X}$=72.64, at the beginning of Region II.

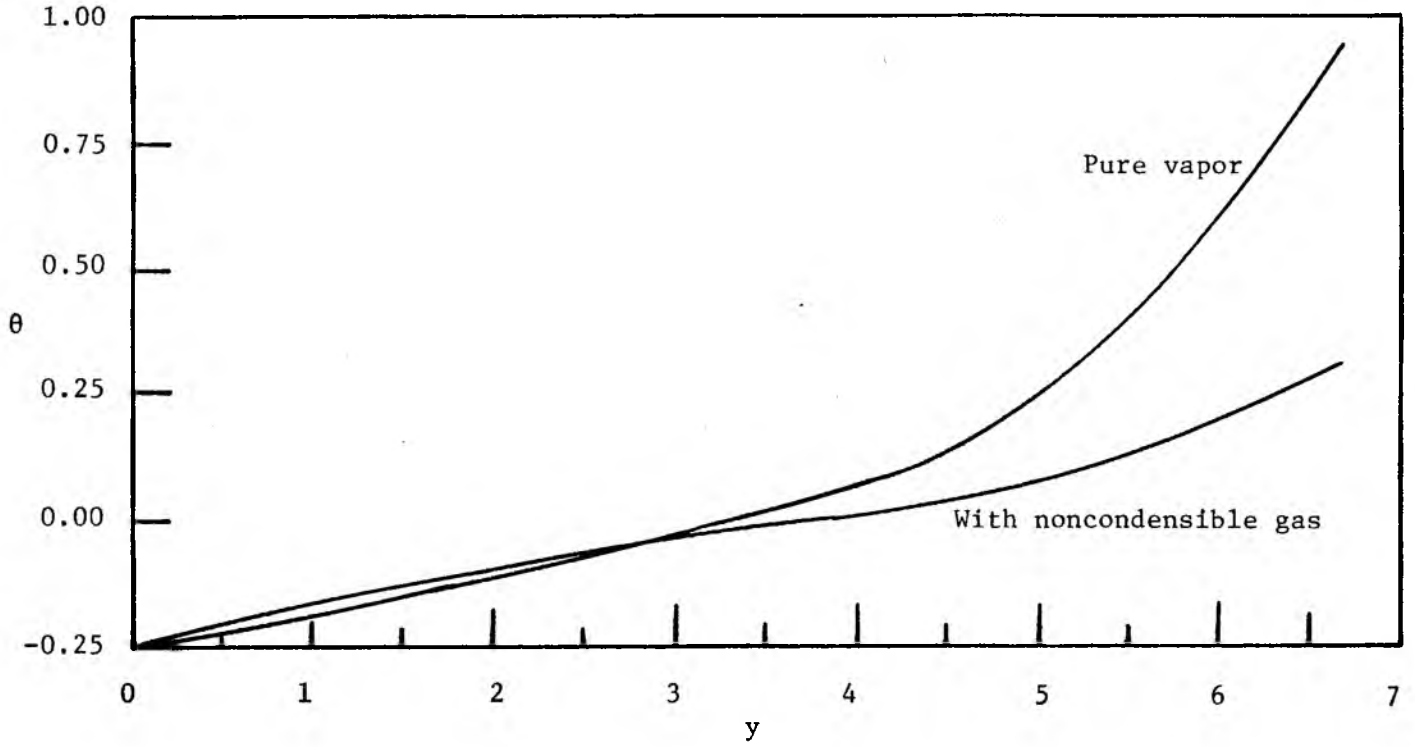

Figure 5.3.11. Comparison of temperature profile in the film for condensation with and without the presence of noncondensible gas at $\overline{X}$=122.

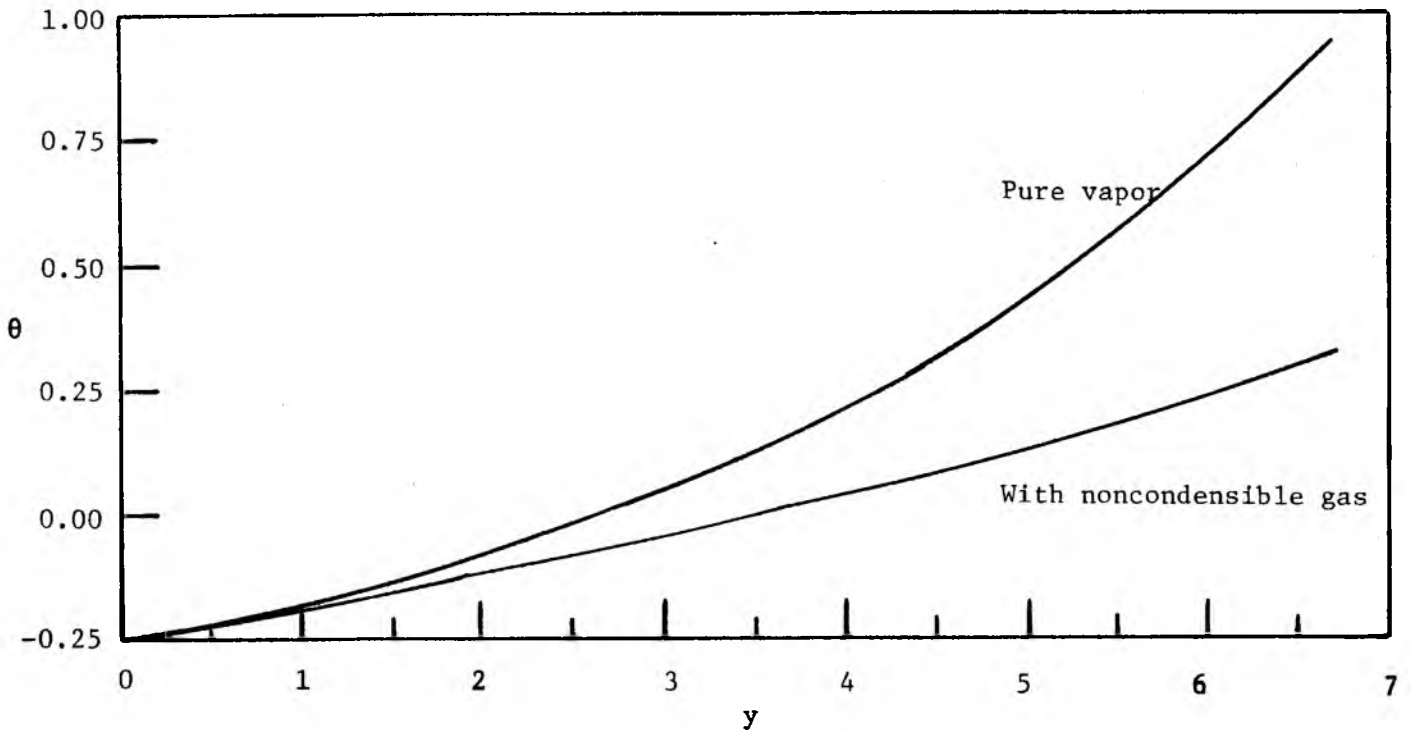

Figure 5.3.12. Comparison of temperature profile in the film for condensation with and without the presence of noncondensible gas at $\bar{X}$=272.

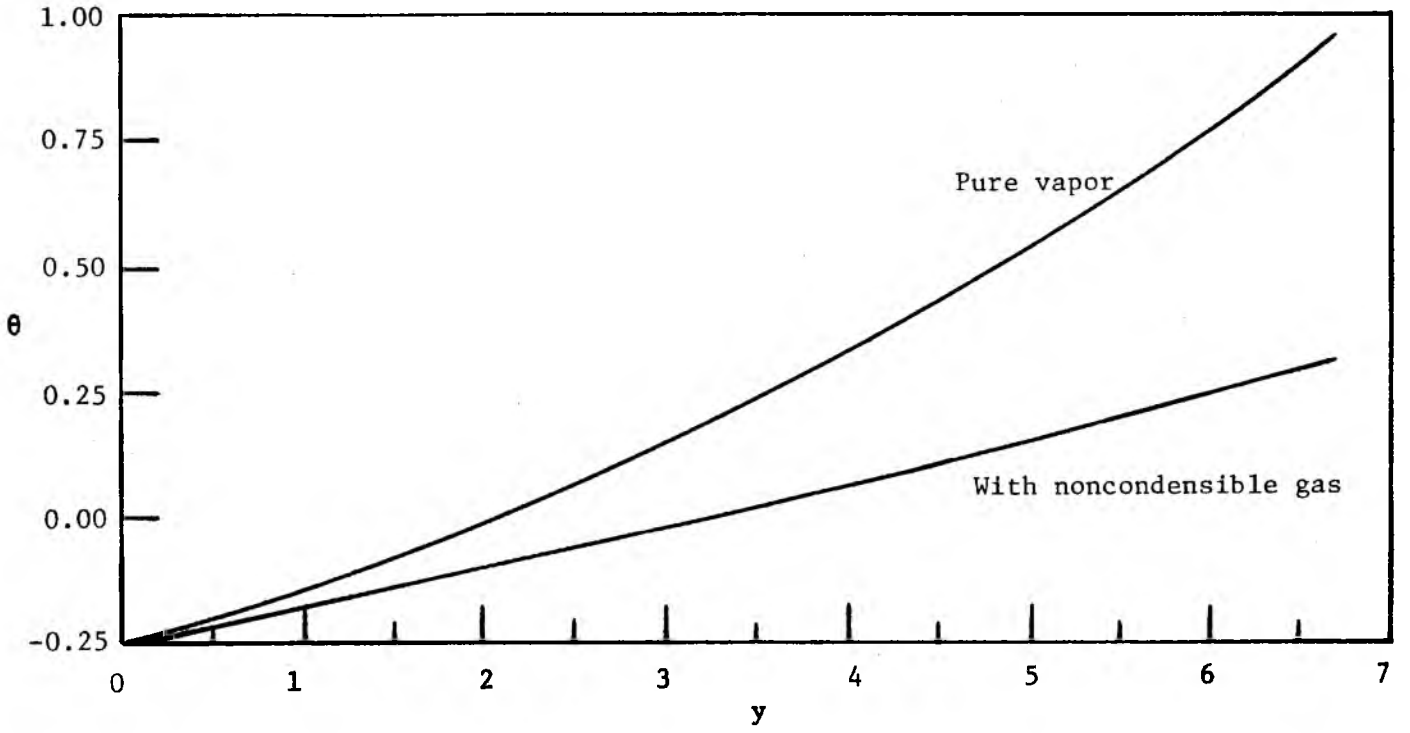

Figure 5.3.13. Comparison of the temperature profile in the film for condensation with and without the presence of noncondensible gas at $\bar{X}$=472.

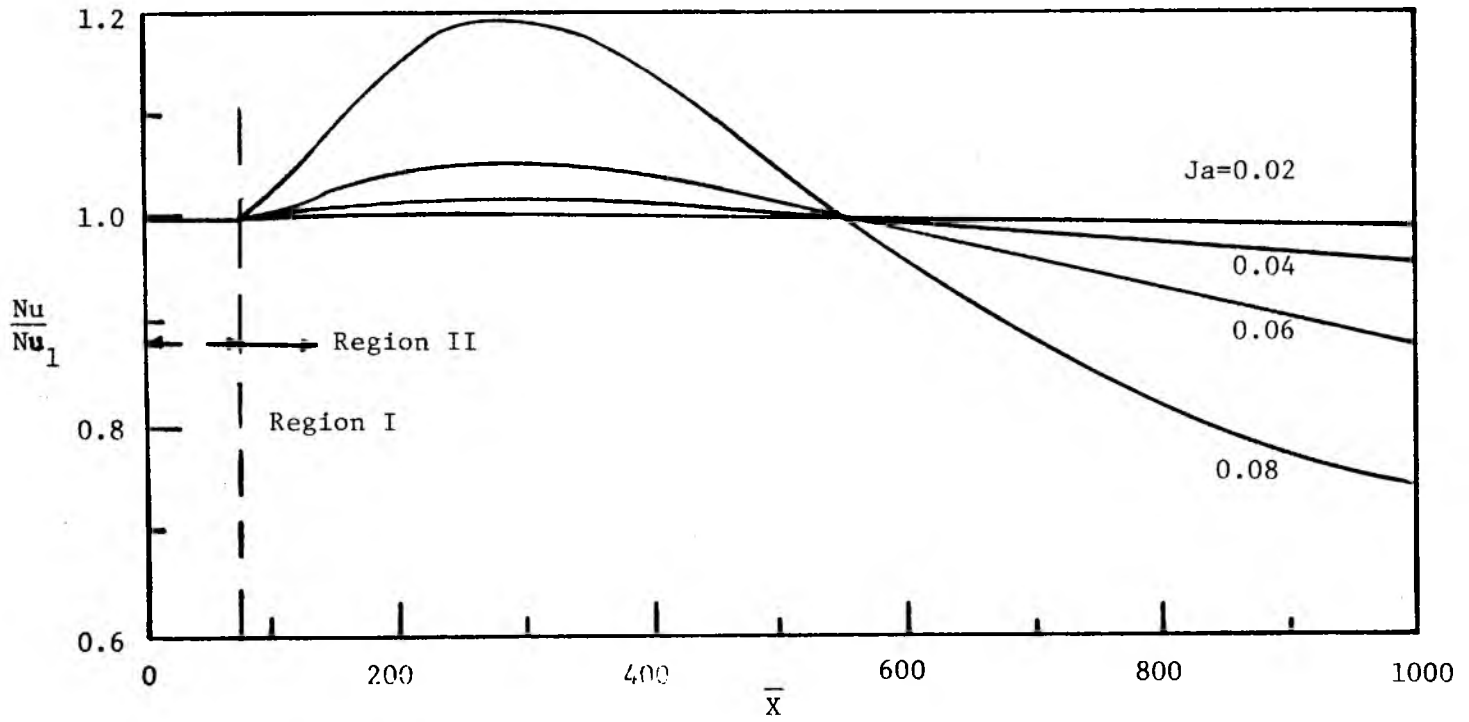

Figure 5.3.14. Ratio of average Nusselt numbers for condensation with and without the presence of noncondensible gas as a function of $\bar{X}$ for different Ja. T_{sat}=600°R, T_w=500°R, W_∞=0.01, Re_f=100.

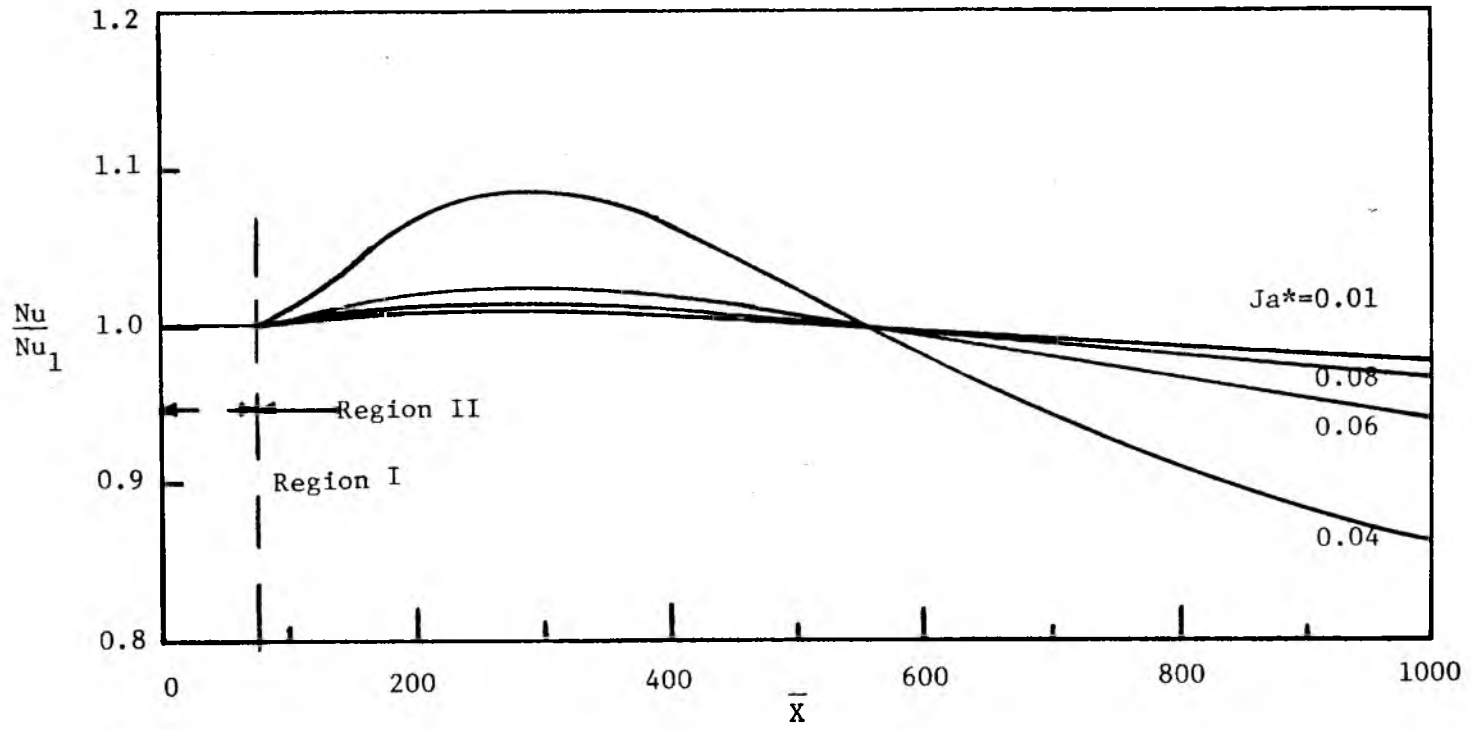

Figure 5.3.15. Ratio of average Nusselt number for condensation with and without the presence of noncondensible gas as a function of $\bar{X}$ for different Ja*. T_{sat}=600°R, T_o=570°R, W_∞=0.01, Re_f=100.

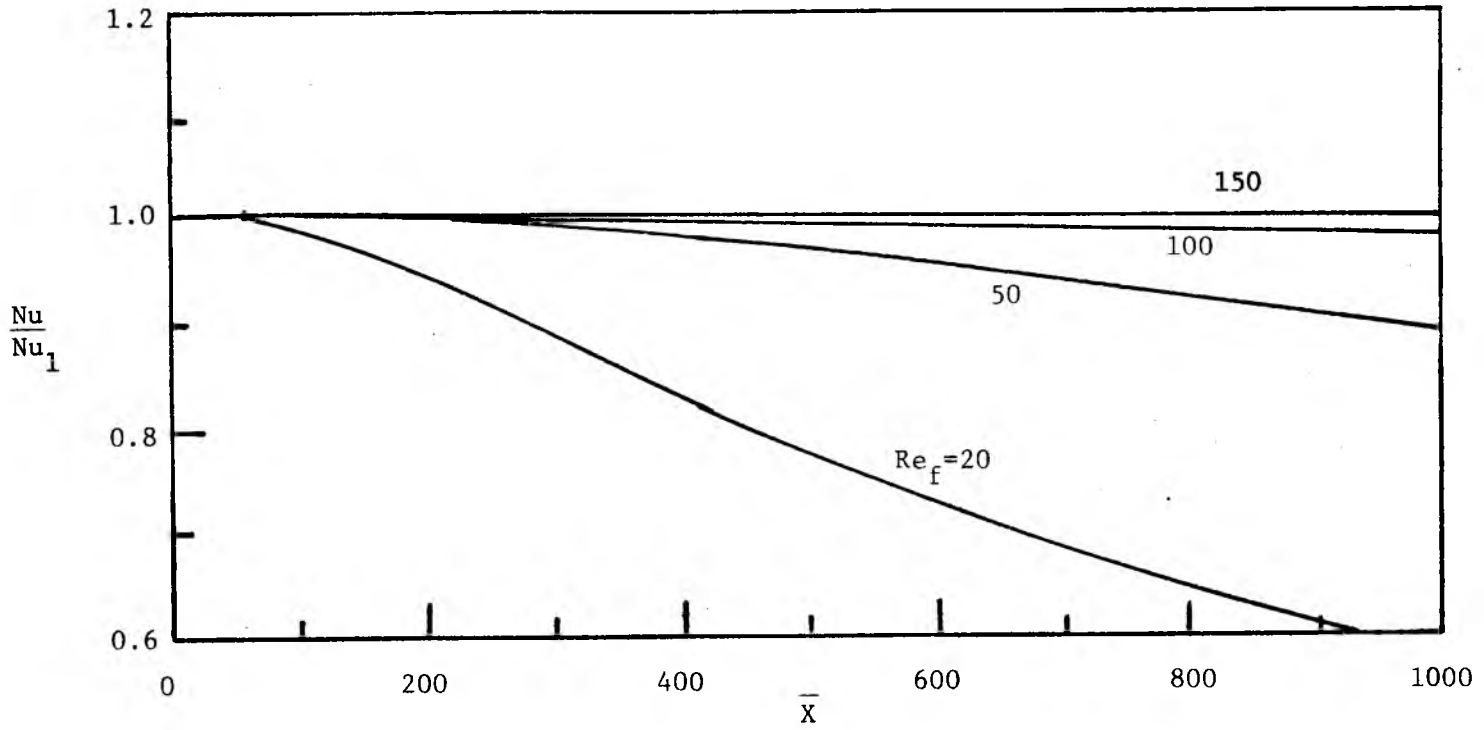

Figure 5.3.16. Ratio of average Nusselt numbers for condensation with and without the presence of noncondensible gas as a function of X for different Reynolds numbers. T_{sat}=600°R, T_w=500°R, T_o=570°R.

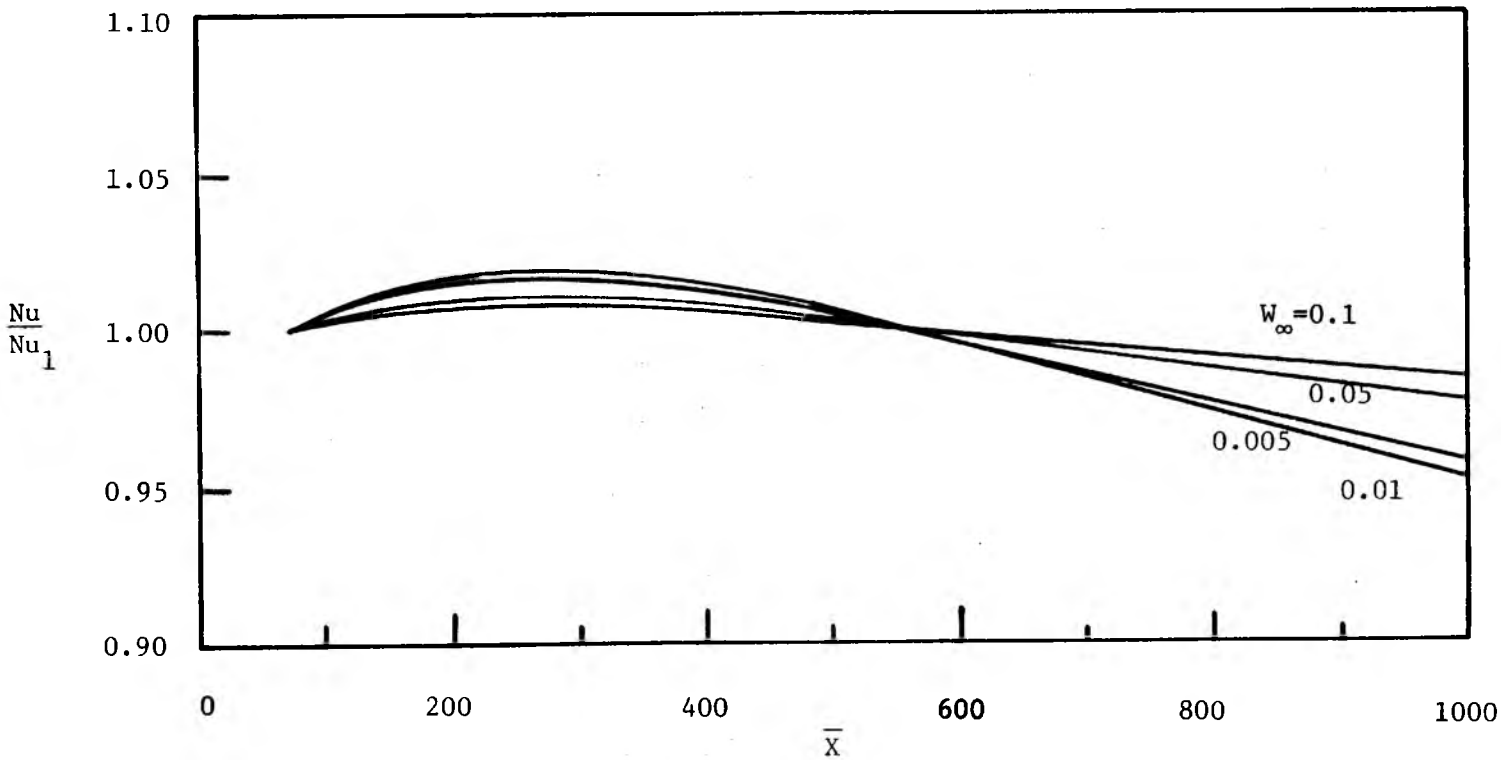

Figure 5.3.17. Ratio of Nusselt numbers for condensation with and without the presence of noncondensible gas as a function of $\bar{X}$ for different W_∞. T_{sat}=600°R, T_o=570°R, Re_f=100.

ment of the thermal boundary layer is described by

$$\delta_1 = a_1 x^{1/3} \quad . \qquad 5.3.5$$

For small values of x, a_1 can be calculated from Equation 5.2.56 as

$$a_1 = \left[\frac{36}{\delta_f Pr_f}\right]^{1/3} = \left[\frac{}{(3Re_f)^{2/3} Pr_f}\right]^{1/3} . \qquad 5.3.6$$

The extent of Region I is evaluated by solving Equation 5.2.55. Alternately it can be defined as

$$\bar{x}_D = \left(\frac{\bar{\delta}_f}{a_1}\right)^{1/3} \qquad 5.3.7$$

Thus the average Nusselt number in Region I can be expressed as

$$Nu_I = a_1 \bar{x}_D^{1/3} = \left[\frac{3}{(3Re_f)^{1/3} Pr_f}\right]^{1/3} \left[\frac{3}{36} (3Re_f)^{4/3} Pr_f\right]^{1/3} . \qquad 5.3.8$$

As Region II begins the film edge temperature drops below the saturation temperature of the vapor. As a result condensation begins. This leads to a build up of noncondensible gas at the interface $y = \delta_f + \delta_c$. Figure 5.3.18 presents the interfacial concentration of noncondensible gas, W*, as a function of x for different wall temperatures. It is seen that as the wall temperature decreases there is a sharper decrease in W*. This phenomenon can be explained as follows. A lower wall temperature leads to a faster cooling of the interface at $y = \delta_f + \delta_c$. This leads to an increase in the thermal driving force (T_{sat_∞} - T*) for

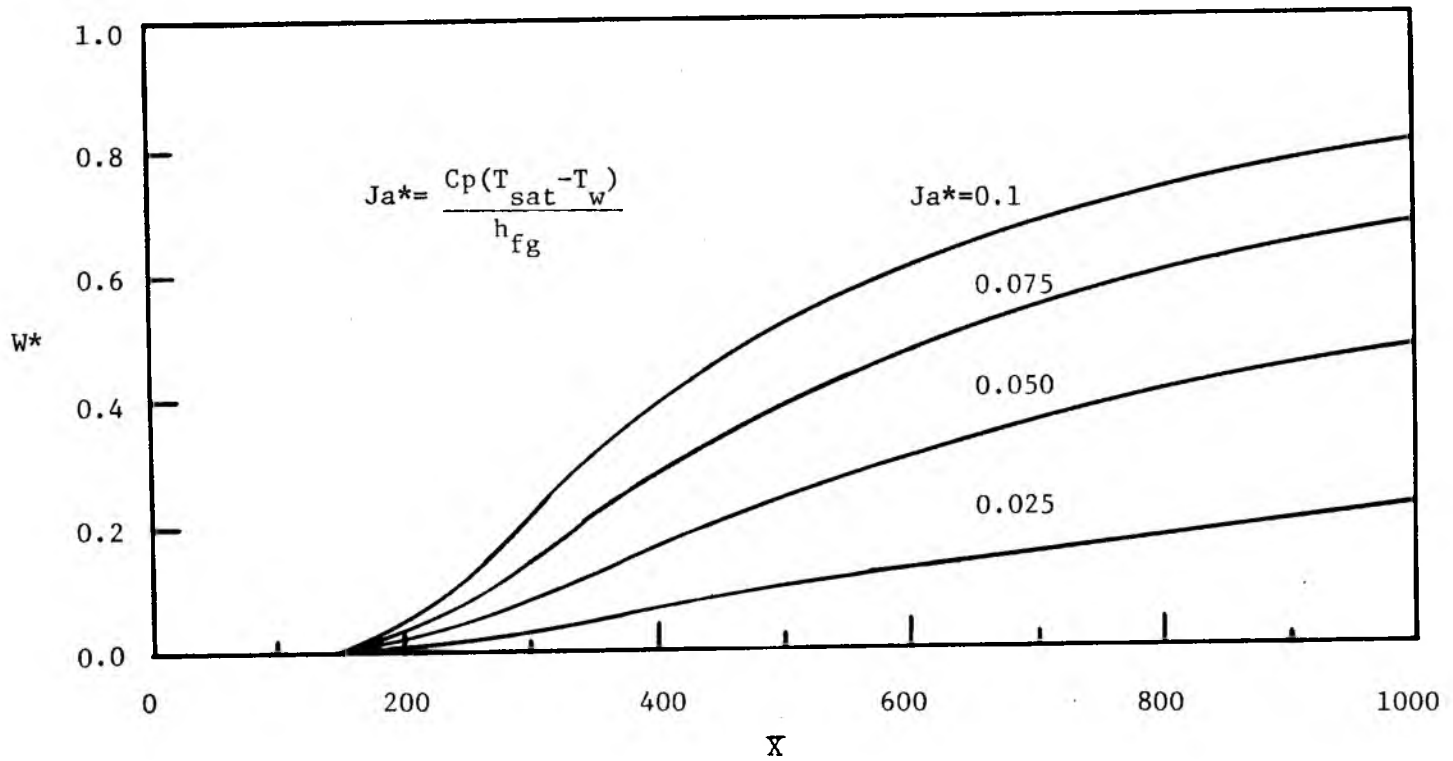

Figure 5.3.18. Interfacial concentration of noncondensible gas as a function of $\bar{X}$ for different ja*. T_{sat}=600°R, W_{∞}=0.01.

condensation. As a result more vapor and noncondensible gas are drawn towards the interface $\delta_f + \delta_c$. To counterbalance this increase in the inflow of the noncondensible gases, a higher outflow is required which results in an increase in the concentration of the noncondensible gas, W*, at the interface $\delta_f + \delta_c$.

Figure 5.3.19 presents the interfacial concentration of noncondensible gas a function of x for different Reynolds. A low Reynolds number indicates a lower film velo city. Thus the walls cools the interface faster leading to an increase in W*. It is obvious that a higher free stream concentration of noncondensible gas would lead to a higher interfacial concentration W*. This is readily seen in Figure 5.3.20 which prsents W* as a function of x for different W_∞.

Figures 5.3.21 through 5.3.23 present the interfacial temperature θ_i as a function of x for different wall temperatures, Reynolds numbers and free stream concentration of noncondensible gas. For all cases θ_i is equal to one in Region I, but it decreases in Region II. For high Reynolds numbers as seen in Figure 5.3.22 there is no appreciable decrease in θ_i. It was observed that at high Reynolds numbers the cold wall did not have significant effect on the interfacial temperature. Thus it can be concluded at high Reynolds numbers that neither the wall temperature nor the condensible gases have a significant effect on the interfacial temperature.

Figures 5.3.24, 5.3.25, 5.3.26 present the ratio of the Nusselt numbers for condensation with and without the presence of the noncondensible gas as a function of x for different wall temperatures, Reynolds numbers and the free stream concentration of noncondensible gas respectively.

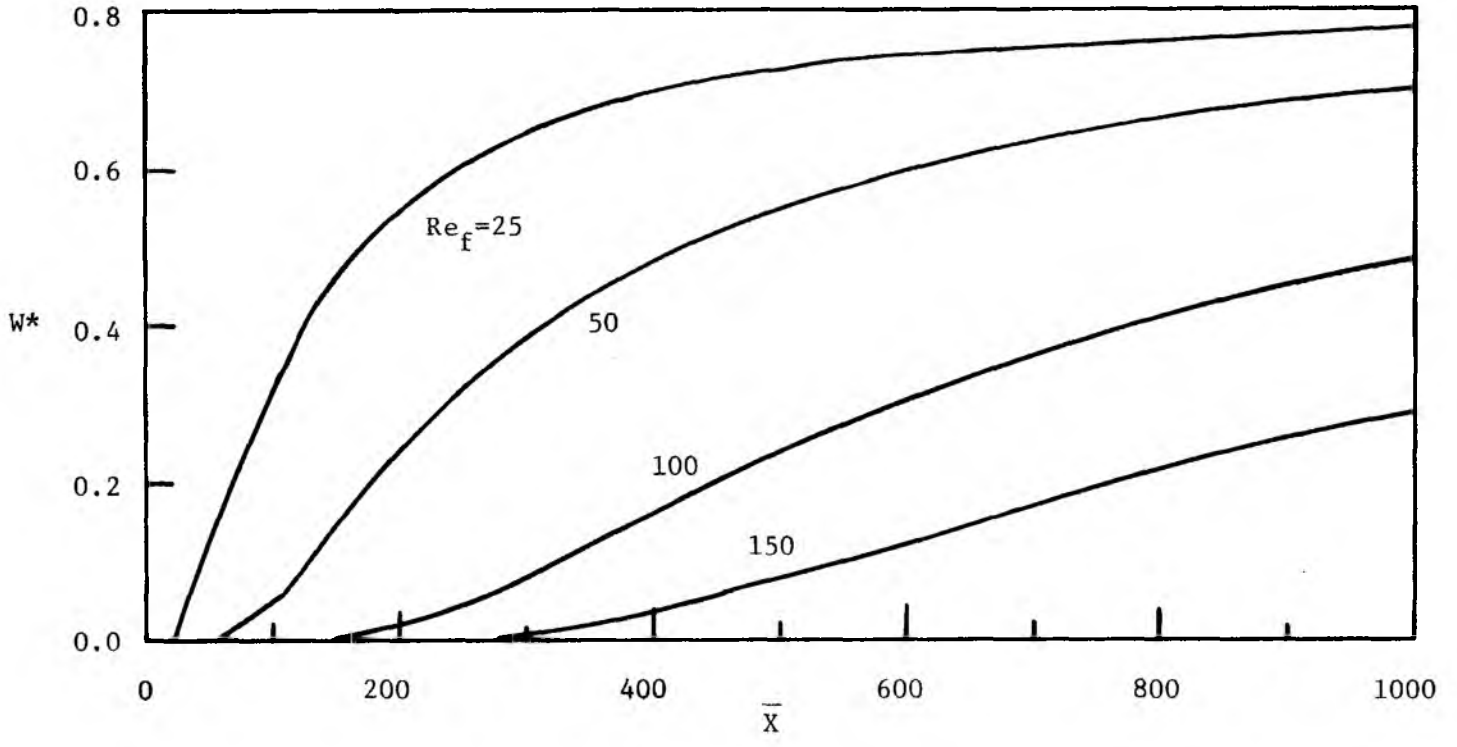

Figure 5.3.19. Interfacial concentration of noncondensible gas a function of $\bar{X}$ for different Reynolds numbers. T_{sat}=600°R, T_w=550°R, W_∞=.0.01.

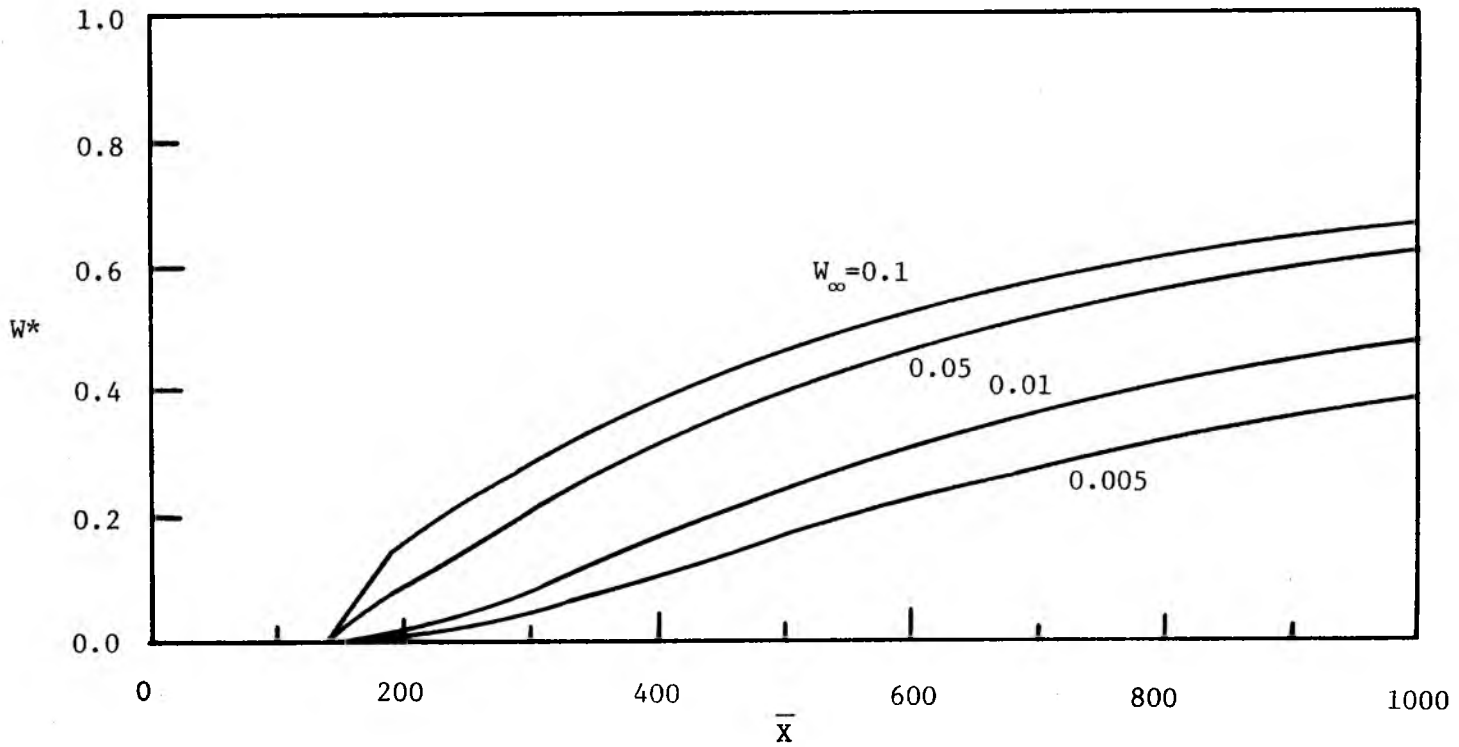

Figure 5.3.20. Interfacial concentration of noncondensible gas a function of $\bar{X}$ for different W_∞. T_{sat}=600°R, T_W=550°R, Re_f=100.

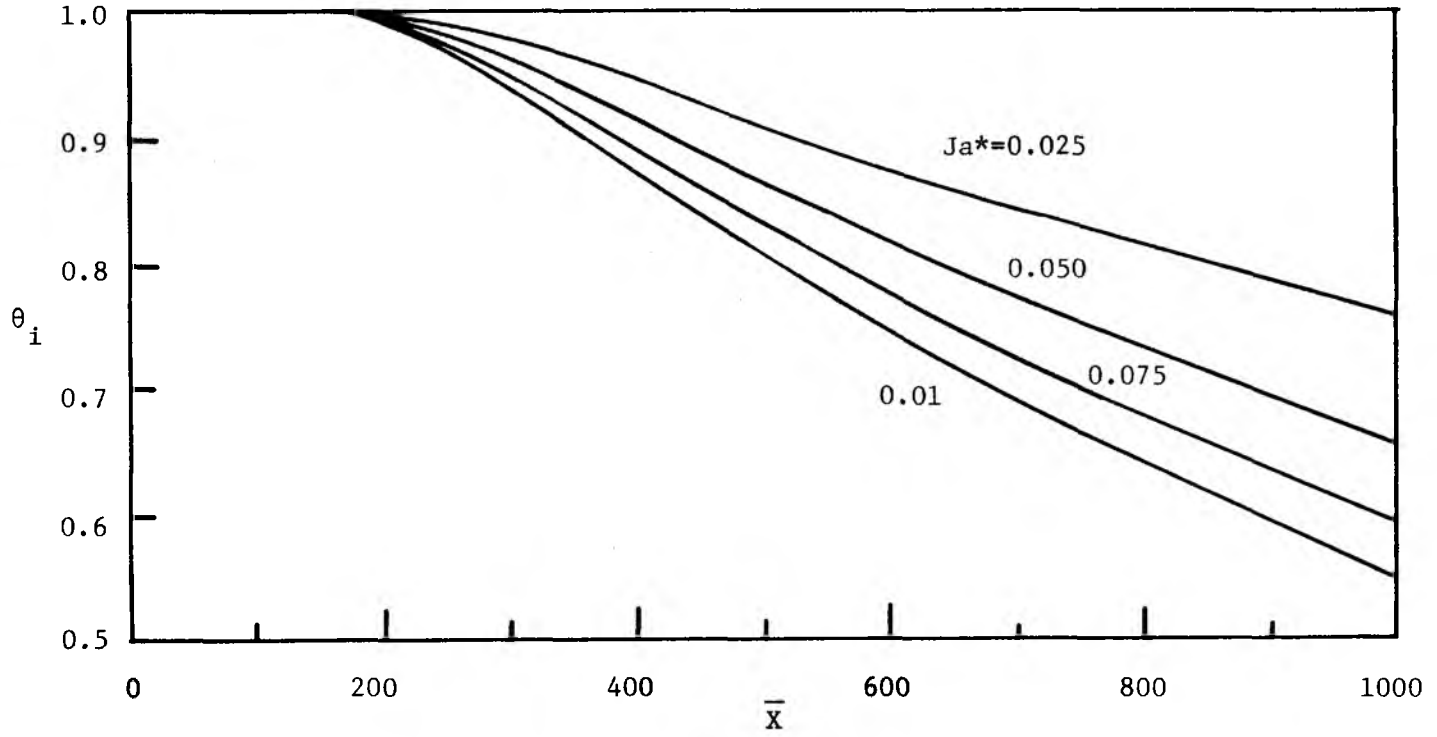

Figure 5.3.21. Nondimensional interfacial temperature as a function of $\overline{X}$ for different Ja*. T_{sat}=600°R, W_{∞}=0.01, Re_f=100.

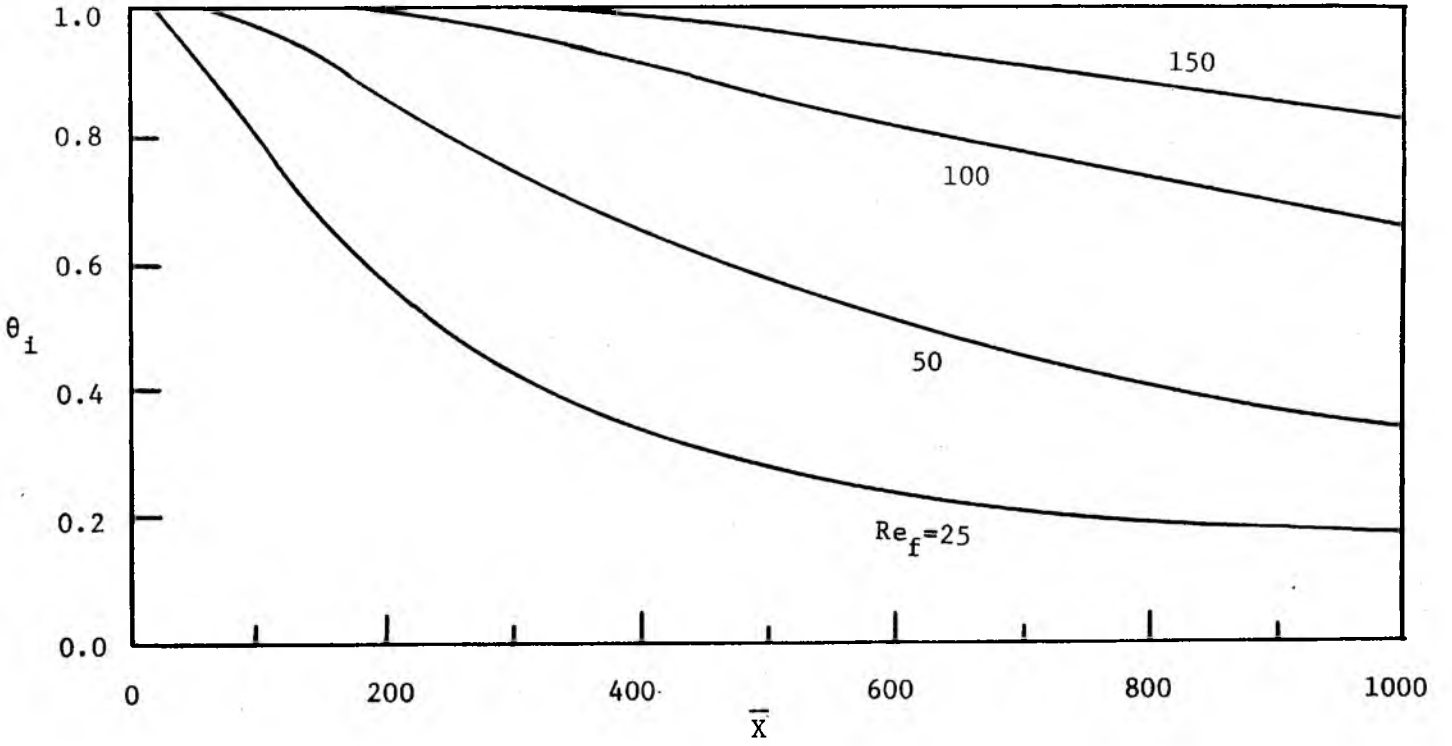

Figure 5.3.22. Nondimensional interfacial temperature as a function of $\overline{X}$ for different Reynolds numbers. T_{sat}=600°R, T_w=550°R, W_∞=0.01.

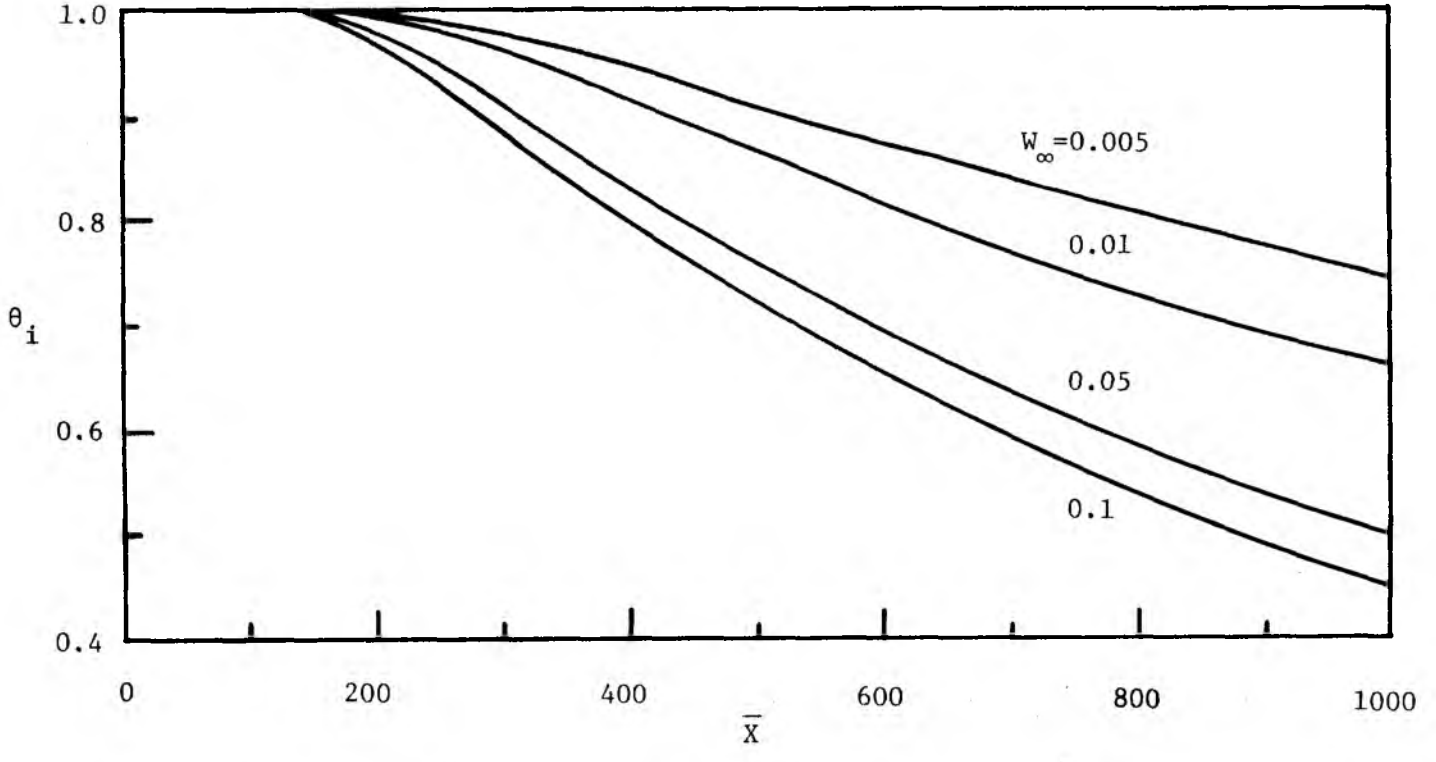

Figure 5.3.23. Nondimensional interfacial temperature as a function of $\overline{X}$ for different W_∞. T_{sat}=600°R, T_w=550°R, Re_f=100.

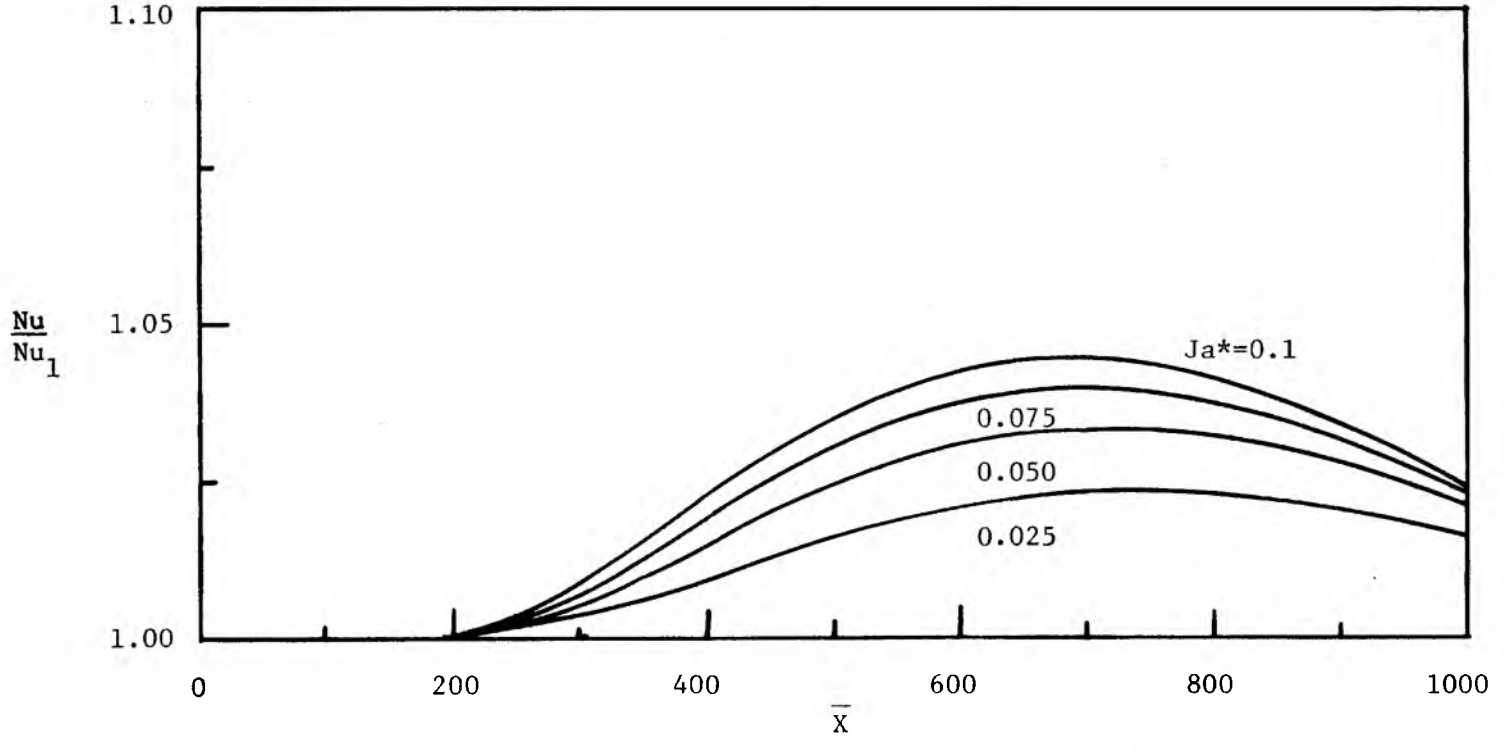

Figure 5.3.24. Ratio of Nusselt numbers for condensation with and without noncondensible gas a function of $\bar{X}$ for different Ja*. T_{sat}=600°R, W_{∞}=0.01.

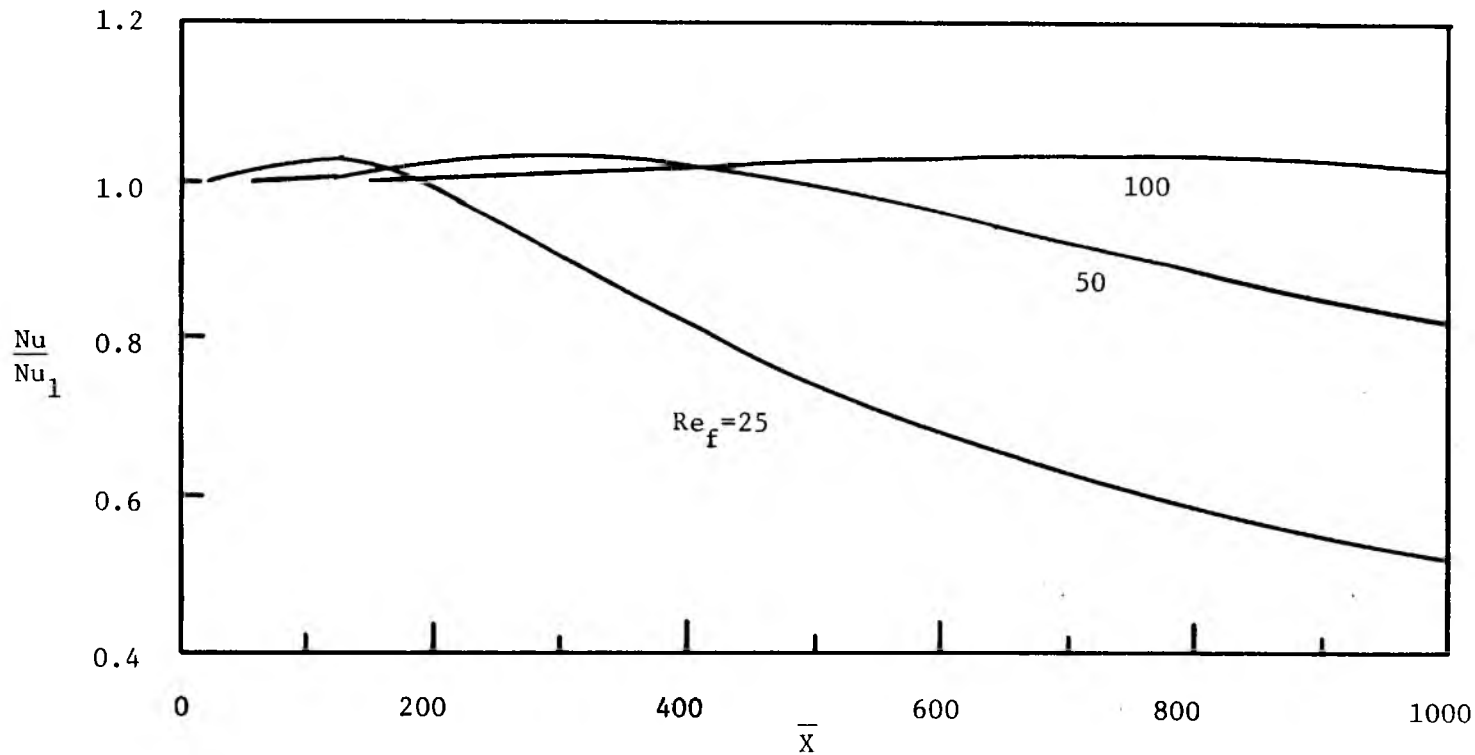

Figure 5.3.25. Ratio of Nusselt numbers for condensation with and without noncondensible gas a function of $\bar{X}$ for different Reynolds numbers. T_{sat}=600°R, T_w=550°R, W_∞=0.01.

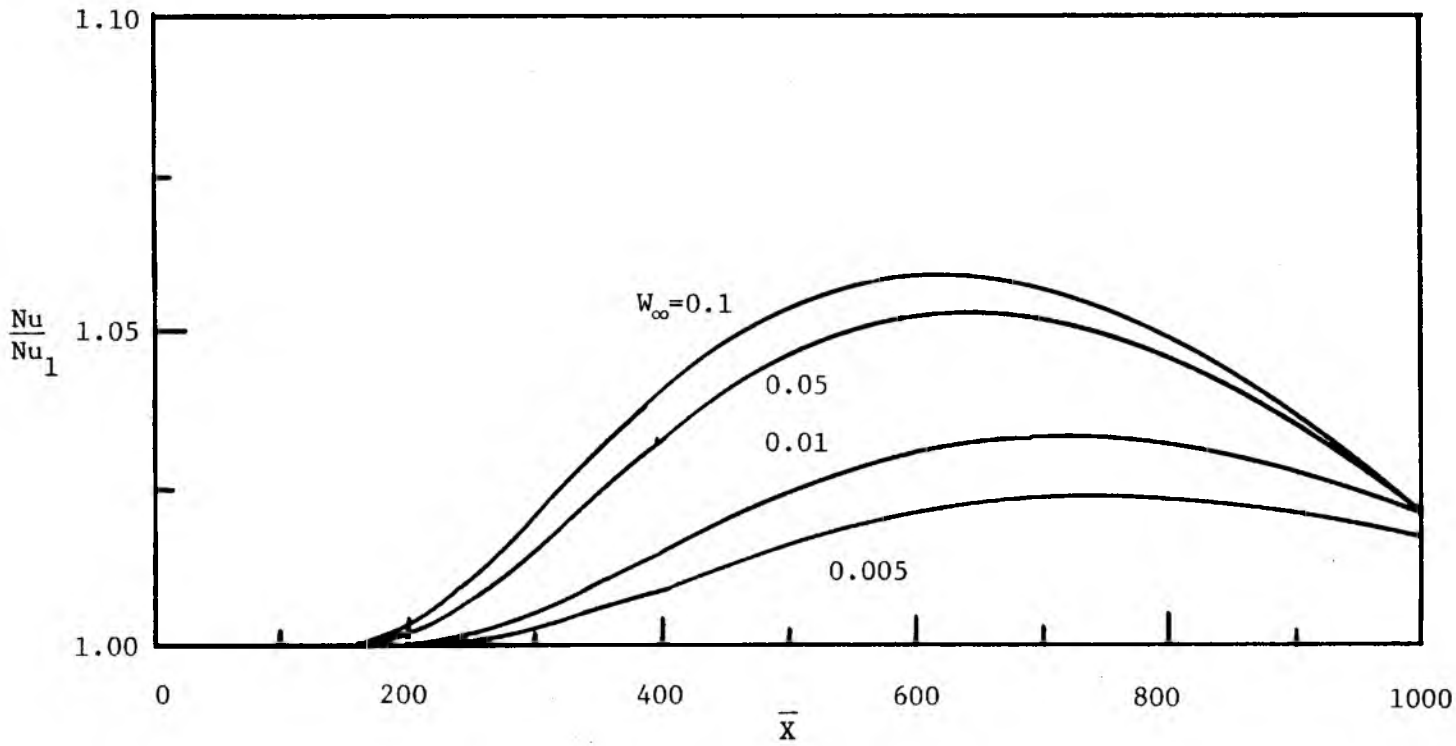

Figure 5.3.26. Ratio of Nusselt numbers for condensation with and without noncondensible gas as a function of $\bar{X}$ for different W_∞. T_{sat}=600°R, T_w=550°R, Re_f=100.

In all of the cases it is observed that in the beginning of Region I the ratio of Nusselt numbers is greater than one. Far away into Region II the ratio drops to a value less than one. In order to understand this behavior it is necessary to examine the temperature profile in the film. Figure 5.3.27 presents the temperature profile in the film at different locations in Region II. In the beginning of Region II at x = 55 the temperature profile is in the form of a quadratic. However, as x increases the profile, it tends to assume a linear profile. However, such a behavior is not observed in the case of condensation with noncondensible gas. At different values of x, the profile remains quadratic, as seen in Figure 5.3.28. This is due to the rapid decrease in θ_i due to the presence of noncondensible gas. It is observed that the profiles for condensation with and without the noncondensible gases will be same at the beginning of Region I. Figure 5.3.29 presents the two profiles at x = 155. It is observed that due to a lower θ_i, the slope of the profile at y = 0 for the noncondensible gas is greater than that for the pure vapor case. Figures 5.3.30 and 5.3.31 present the two profiles at x = 255 and 755 respectively. At x = 255 the two slopes at y = 0 are almost equal. However, at x = 755, the slope at y = 0 for the pure vapor case is higher than that for the case with noncondensible gas. This is due to the rapid suppression of the interfacial temperature. In the latter case, this results from the presence of the noncondensible gas.

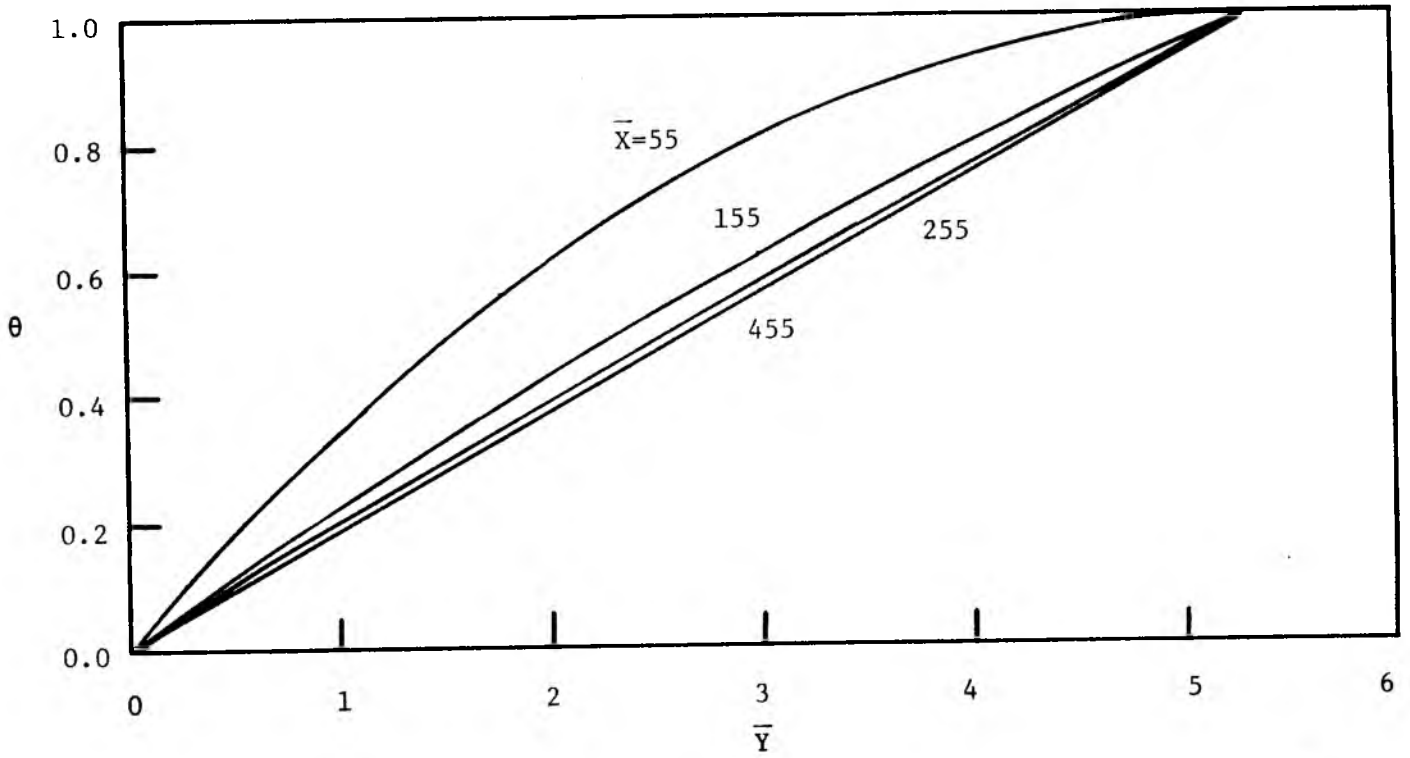

Figure 5.3.27. Nondimensional temperature in the film as a function of $\bar{Y}$ at different $\bar{X}$ location. T_{sat}=600°R, R_w=550°R.

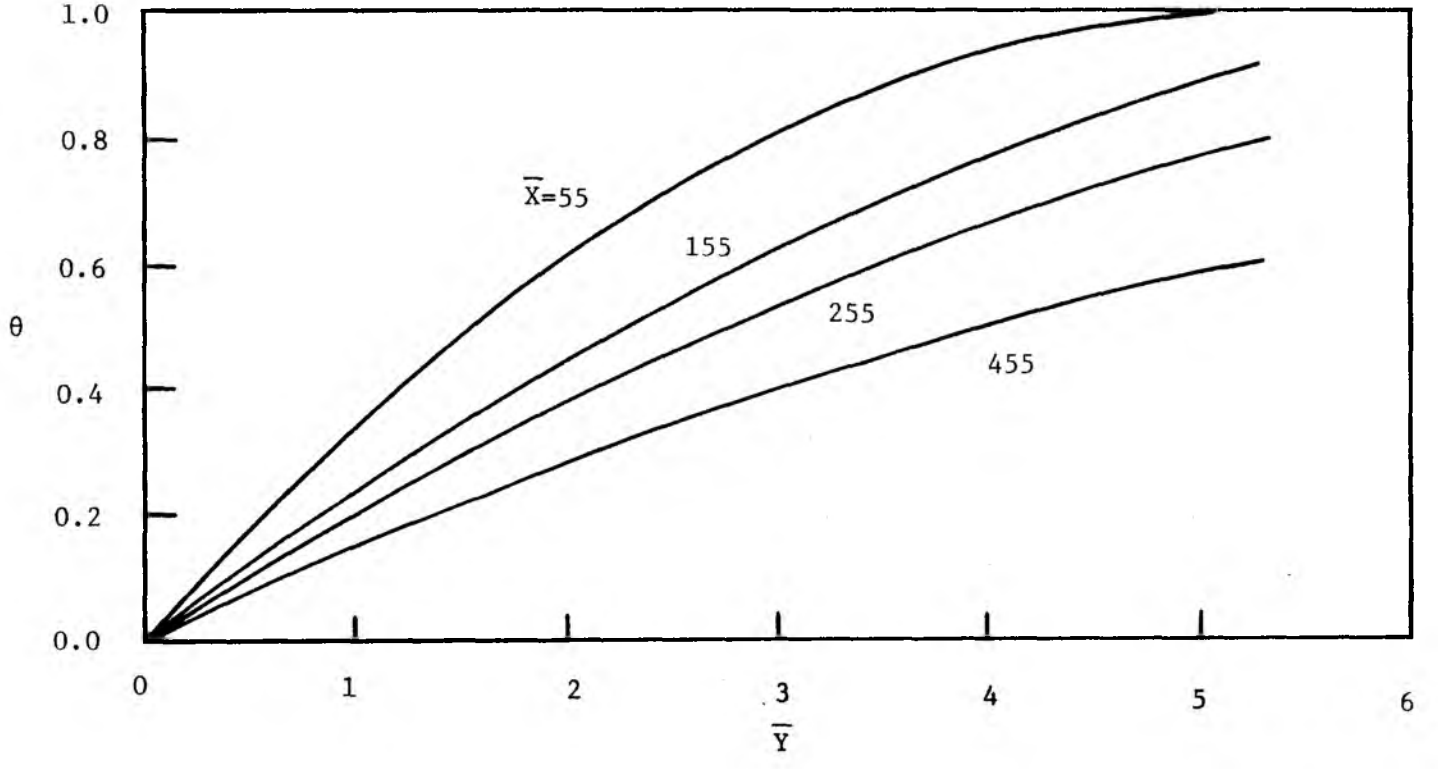

Figure 5.3.28. Nondimensional temperature in the film as a function of $\overline{Y}$ at different $\overline{X}$ locations. T_{sat}=600°R, T_w=550°R, W_∞=0.01, Re_f=50.

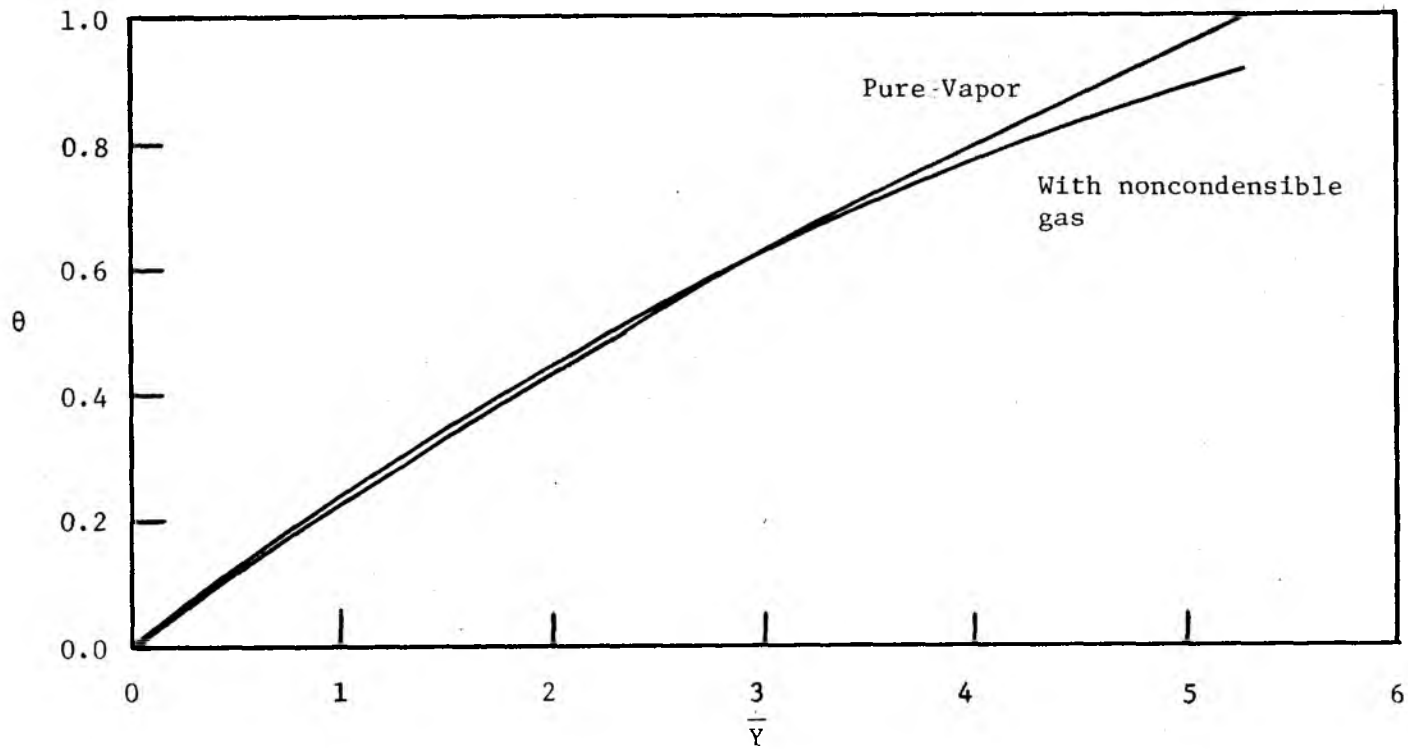

Figure 5.3.29. Nondimensional temperature in the film as a function of $\overline{Y}$ at $\overline{x}$=155. T_{sat}=600°R, T_w=550°R, Re_f=50, W_∞=0.01.

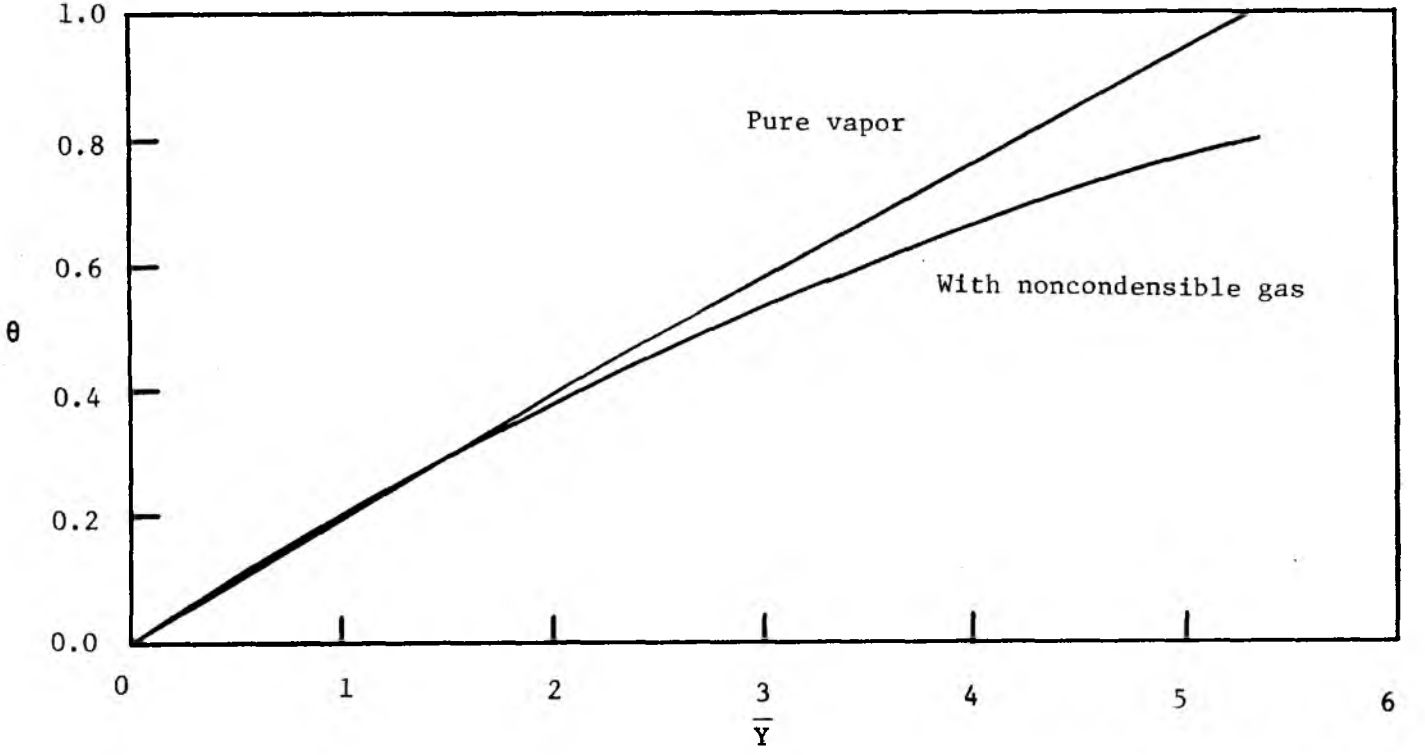

Figure 5.3.30. Nondimensional temperature in the film as a function of $\overline{Y}$ at $\overline{x}$=255. T_{sat}=600°R, T_w=550°R, Re_f=50, W_∞=0.01.

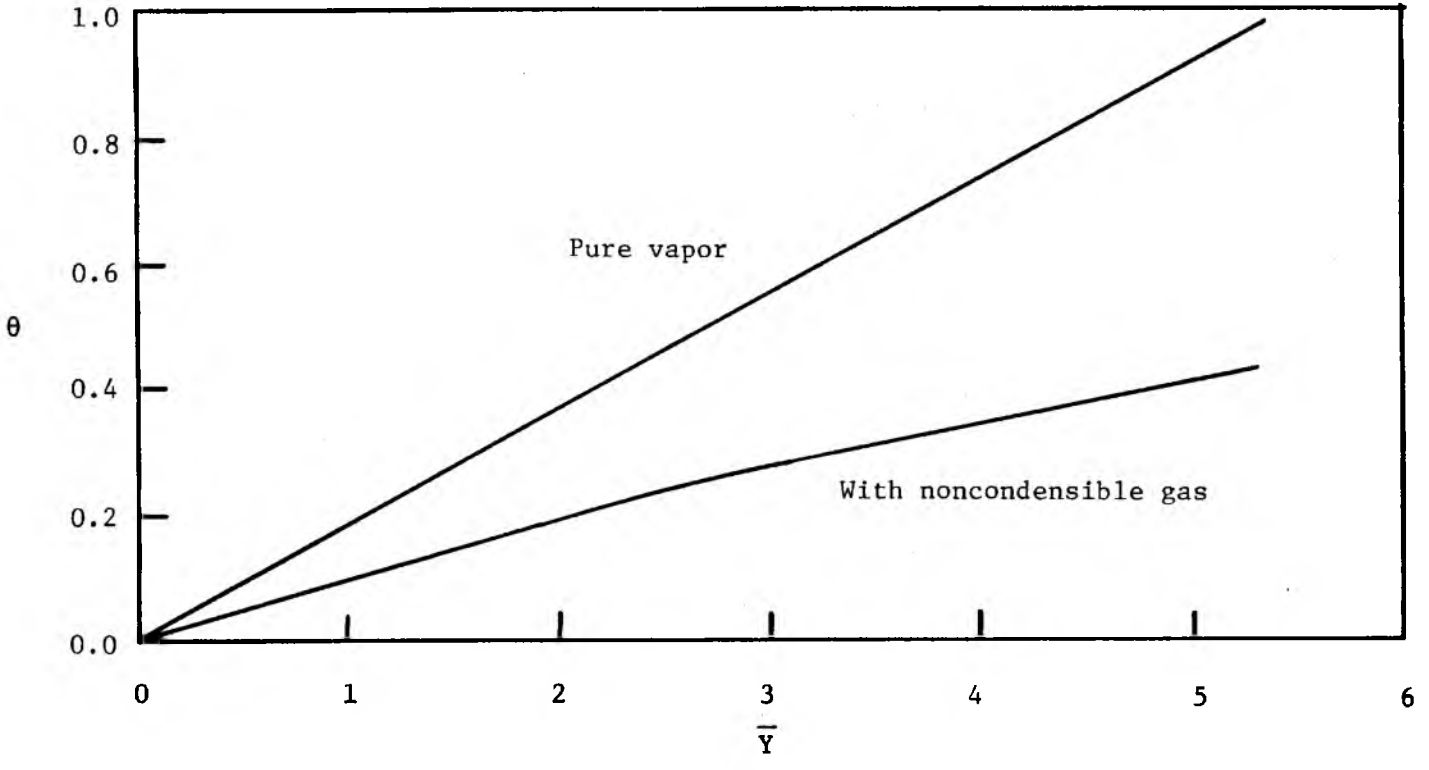

Figure 5.3.31. Nondimensional temperature in the film as a function of $\overline{Y}$ at $\overline{x}$=455. T_{sat}=600°R, T_w=550°R, Re_f=50, W_∞=0.01.

CHAPTER 6

CONDENSATION ON A THIN FILM FLOWING OVER SINGLE AND MULTILE HORIZONTAL ISOTHERMAL TUBES

6.1 Introduction

Since the pioneering work of Nusselt (22) numerous studies have been made of the problem of film condensation on flat plates and on tubes. In Nusselt's original analytical work the vapor was assumed to be quiescent, saturated, and free of noncondensibles. Further, he assumed that the thermal capacitance of the condensate film was negligible, the shear induced by the vapor was vanishingly small and that the interfacial resistance was also negligible. Beginning with Roshenow (23) the assumptions made by Nusselt were examined one at a time. Sparrow and co-workers (6,24,30) reported the influence of all of these assumptions for flow over a flat plate. Their results indicated that for a pure saturated vapor at low pressure, excluding liquid metals, the model of Nusselt was sufficient.

For a horizontal circular tube, the only analytical studies in addition to that of Nusselt (22) for laminar film condensation were due to Sparrow and Gregg (30) and Chen (31). The solution of Reference (30) was obtained by utilizing the boundary layer equation and casting the problem in terms of similarity variables. Of course, for a gravity driven flow of condensate a similarity solution does not exist except near the upper stagnation point. Chen (31) used an integral

boundary layer approach in which the governing equations were used to evaluate the temperature and velocity profiles. Chen's solution was cast in terms of two parameters which were essentially the Jakob number and the Jakob number divided by the Prandtl number. For these "two" parameters becoming vanishingly small his solution resulted in the identical results to those obtained by Nusselt (22). He showed that the Nusselt's solution did not hold for liquid metals. However, this fact had been previously indicated by Roshenow (23), Koh (32) and Sparrow and co-workers (6) for flat plate studies.

For the case of condensation on a vertical row of tubes, Chen (31) has been the only one to offer an improvement to Nusselt's theory, although experimental studies have been made by several investigators. The experimental results (33,34) have generally shown much higher heat transfer rates than predicted by either Nusselt or Chen. The phenomenon has been attributed to splashing and nonuniform spilling, both of which are difficult to predict. These effects as well as vapor velocity over the tubes and the possible effects of waves on the condensate film could all attribute to the difference between the experimental results and the theory for a quiescent vapor.

Chen, in developing his theoretical model for multiple tube laminar film condensation, assumed that the Ja/Pr was vanishingly small and that the condensate leaving the first or upper tube was at a temperature only slightly below the saturation temperature. By the time it reached the second tube he assumed that it would have reached the saturation temperature. Thus, condensation on the second tube would not start until a thermal boundary layer penetrated the film of fluid that had dripped from the upper tube. His results

indicate that the average heat transfer for n tubes is higher than that of Nusselt and is dependent on the Jakob number, but is independent of the tube spacing due to his assumptions about the temperature of the condensate when it reaches the second and subsequent tubes. In the present analysis we evaluate the heat transfer to the falling sheet between the subsequent tubes as well as that for each tube and thus are free of Chen's assumption as to the condensate temperature as it falls onto the lower tubes. Our analysis reduces to that of Chen's for large tube pitch where his assumption would be realistic.

6.2 Physical Model and Mathematical Formulation

Model for the Second or a Subsequent Tube

The physical model for the second or a subsequent tube is shown in Figure 6.2.1. A liquid sheet at temperature T_o and mass flux m_f impinges without splashing on top of the horizontal tube and flows over it due to gravity. The Reynolds number for the sheet is such that the resulting film remains thin and laminar. The tube wall is held at a temperature T_w and the film is surrounded by a quiescent saturated vapor at temperature T_{sat}. Two possible cases are encountered. If the tube above is at a large distance above the tube being considered it is possible that $T_o = T_{sat}$. Since $T_w < T_{sat}$ a thermal boundary layer will grow outward from the tube wall until it is of thickness equal to that of the film. At this point the film surface temperature T_i will drop below T_{sat}, and condensation will commence. It is this situation that was analyzed by Chen (31) except that he assumed that the distance it would take for the thermal boundary layer to grow from the wall was negligible. A more general situation would

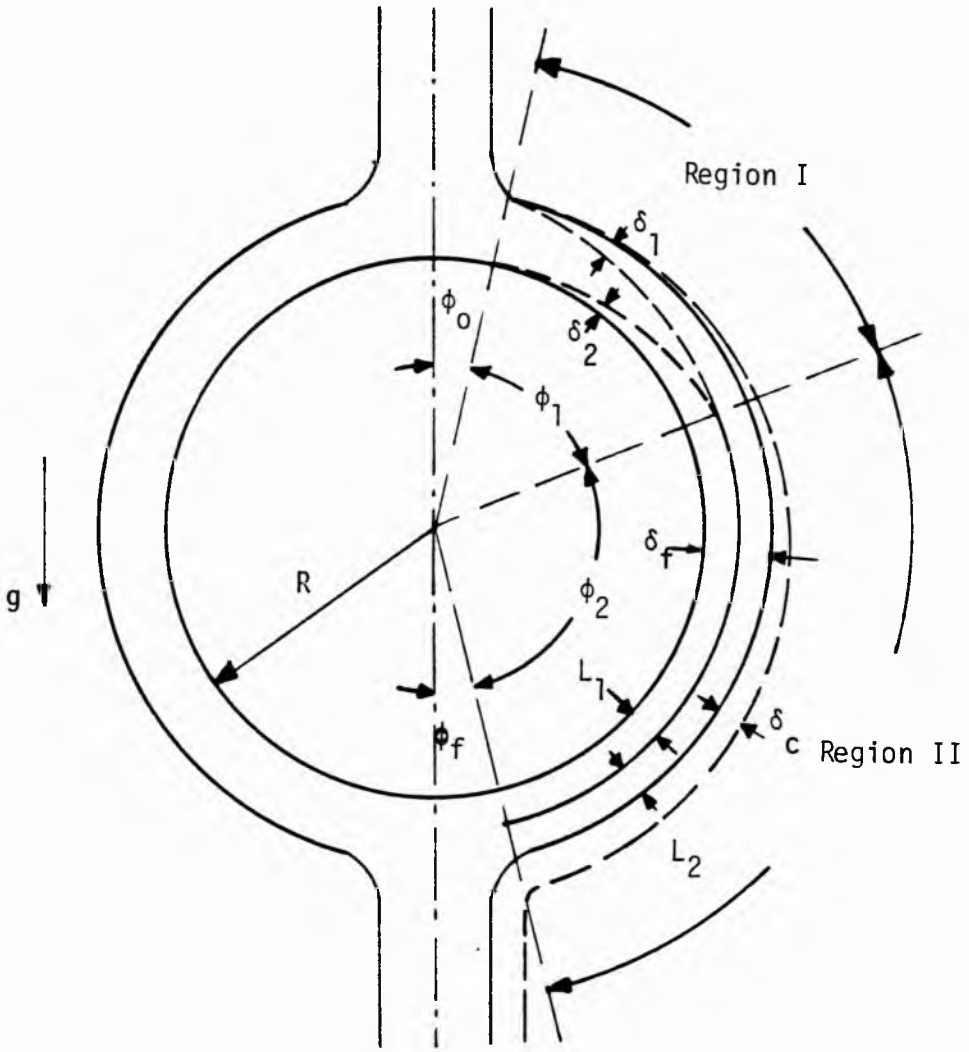

Figure 6.2.1. Physical model for condensation on second or subsequent tube.

apply when the tube pitch (distance between tubes) is small. For this case $T_{sat} > T_o > T_w$. As shown in Figure 6.2.1 condensation will be initiated immediately (at ϕ_o). A thermal boundary layer, δ_2, will grow into the film from the interface at the same time as a thermal boundary layer, δ_1, grows outward from the tube wall. Until the two boundary layers meet the only condensation will be that which occurs due to the heat capacitance of the film. The distance along the tube at which the two boundary layers meet, $\delta_1 + \delta_2 = \delta_f$, is called ϕ_1 and the region where only the film capacitance influences the condensate layer, δ_c, growth is called Region I. From the end of Region I until the film and condensate leave the tube is referred to as Region II. In this region the primary driving force for the condensation is the heat sink due to the wall being held at T_w. When the sheet is at a temperature T_o, below T_{sat}, condensation will occur along its entire length. However, in our model we assume perfect mixing when it impinges on the tube under consideration; thus, we consider the condensation to initiate at ϕ_o. In our analyses we assume that the film and condensate layer are laminar and free of surface waves. Further, we employ the remainder of the assumptions used by Nusselt, constant properties, negligible shear induced by the vapor, etc. These assumptions limit the analysis to low pressure and to the Jakob number $C_{p_f}(T_{sat} - T_w)/h_{fg}$ being small.

Utilizing the above assumptions the following analyses can be made for Regions I and II.

Region I

For the film which is due to the impinging sheet conservation of mass gives

$$\dot{m}_f = \int_0^{\delta_f} \rho_f \, u_f \, dy \quad . \tag{6.2.1}$$

The momentum equation, using Nusselt's assumptions, yields

$$u_f = \frac{g \sin\phi}{\nu_f} \left[\delta_f \, y - \frac{y^2}{2}\right] \tag{6.2.2}$$

thus

$$\delta_f = \left[\frac{3m_f}{\mu_f}\right]^{1/3} \left(\frac{\nu_f^2}{g}\right)^{1/3} \sin^{-1/3} \quad . \tag{6.2.3}$$

The integral form of the energy equation for the thermal boundary layer growing from the wall is

$$\frac{1}{R} \frac{d}{d\phi} \int_0^{\delta_1} \rho_f \, u_f \, C_{p_f} \, (T_1 - T_o) \, dy = - k_f \left.\frac{\partial T_1}{\partial y}\right|_{y=0} \tag{6.2.4}$$

and for the thermal boundary layer growing from the interface it is

$$\frac{1}{R} \frac{d}{d\phi} \int_{\delta_f - \delta_2}^{\delta_f} \rho_f \, u_f \, C_{p_f} \, (T_2 - T_o) \, dy = k_f \left.\frac{\partial T_2}{\partial y}\right|_{y=\delta_f} \quad . \tag{6.2.5}$$

The energy equation for the condensate layer assuming negligible thermal capacitance for this newly growing layer is

$$\frac{h_{fg}}{R} \frac{d}{d\phi} \int_0^{\delta_f + \delta_c} \rho_c \, u_c \, dy = k_f \left.\frac{\partial T_c}{\partial y}\right|_{y=\delta_f} \quad . \tag{6.2.6}$$

In the two thermal boundary layers growing in the film we assume quadratic temperature profiles which satisfy the temperature conditions at the edges and the temperature gradient at δ_1 or δ_2. The

resulting profiles are

$$T_1 - T_o = (T_w - T_o)\left(1 - \frac{y}{\delta_1}\right)^2 \qquad 6.2.7$$

and

$$T_2 = T_i + \frac{T_i - T_o}{\delta_2^2}\left[\delta_f^2 - 2\delta_f\,\delta_2 + 2y(\delta_2 - \delta_f) + y^2\right]. \qquad 6.2.8$$

The assumption of negligible thermal capacitance of the condensate layer implies a linear temperature profile

$$T_c = T_i + (y - \delta_f)\left(\frac{T_{sat} - T_i}{\delta_c}\right) \quad . \qquad 6.2.9$$

In the above equations T_i is the interfacial temperature between the film and the condensate layer. Compatibility of heat fluxes at the condensate layer-film interface leads to

$$T_i = \frac{T_o + 1/2\ \delta_2/\delta_c\ T_{sat}}{1 + 1/2\ \delta_2/\delta_c} \quad . \qquad 6.2.10$$

In Region I the condensate layer will be extremely thin as compared to δ_f; thus we will assume that the velocity in this layer will be that obtained from Equation 6.2.2 evaluated at $y = \delta_f$. This in fact assumes that the film is negligibly accelerated or decelerated due to the increased mass. This assumption is reasonable for $T_{sat} > T_o > T_w$ as we have previously assumed that $C_{p_f}(T_{sat} - T_w)/h_{fg} << 1$ and thus, $C_{p_f}(T_{sat} - T_o)/h_{fg} < C_{p_f}(T_{sat} - T_w)/h_{fg} << 1$.

Defining a dimensionless temperature

$$\theta = \frac{T - T_o}{T_{sat} - T_o} \qquad 6.2.11$$

the interfacial temperature becomes

$$\theta_i = \frac{1/2\ \bar{\delta}_2/\bar{\delta}_c}{1 + 1/2\ \bar{\delta}_2/\bar{\delta}_c}\ , \qquad 6.2.12$$

where the bar indicates nondimensionalizing with respect to the characteristic length $(\nu_f^2/g)^{1/3}$. Substituting the appropriate temperature and velocity profiles into Equations 6.2.4, 6.2.5 and 6.2.6 and nondimensionalizing the terms yields, respectively,

$$\frac{d\bar{\delta}_1^3}{d\phi} = \left[\frac{72}{Pr_f}\ \frac{\bar{R}}{\sin\phi} - \frac{3\bar{\delta}_f^3}{\tan\phi}\left(\frac{2}{3}\ \delta_f - \frac{\bar{\delta}_1}{5}\right)\right] \div \left(2\ \bar{\delta}_f - \frac{3}{5}\ \bar{\delta}_1\right) \qquad 6.2.13$$

$$\frac{d\bar{\delta}_2^2}{d\phi} = \left[\frac{24}{Pr_f}\ \frac{\bar{R}}{\sin\phi} - 2\bar{\delta}_2^2\left(\bar{\delta}_f^2 - \frac{\bar{\delta}_2^2}{10}\right)\frac{1}{\theta_i}\ \frac{d\theta_i}{d\phi} - \frac{2}{3}\ \frac{\bar{\delta}_2^2}{\tan\phi}\left(\bar{\delta}_f^2 - \frac{3}{10}\ \bar{\delta}_2^2\right)\right] \div \left(\bar{\delta}_f^2 - \frac{3}{10}\ \bar{\delta}_2^2\right) \qquad 6.2.14$$

and

$$\frac{d\bar{\delta}_c^2}{d\phi} = \frac{4}{3^{2/3}}\ \frac{Ja}{Re_f^{2/3}\ Pr_f}\ \frac{\bar{R}\ \sin^{-1/3}\phi}{(1 + 1/2\ \bar{\delta}_2/\bar{\delta}_c)} - \frac{2}{3}\ \frac{\bar{\delta}_c^2}{\tan\phi}\ . \qquad 6.2.15$$

Equations 6.2.12-6.2.15 describe the condensation in Region I. The

necessary boundary conditions as can be seen from Figure 1 are $\delta_1(\phi = \phi_o) = 0$, $\delta_2(\phi = \phi_o) = 0$ and $\delta_c(\phi = \phi_o) = 0$. The equations may be solved numerically after first establishing the values of the first derivatives of $\phi = \phi_o$. For very small values of $\phi - \phi_o$ it can be shown that

$$\delta_1 = a_1(\phi - \phi_o)^{1/3} + \ldots$$
$$\delta_2 = a_2(\phi - \phi_o)^{1/2} + \ldots \qquad 6.2.16$$
$$\delta_c = a_3(\phi - \phi_o)^{1/2} + \ldots$$

The solution for Region I ends when $\delta_1 + \delta_2 = \delta_f$.

Region II

After the two thermal boundary layers have merged, $\delta_1 + \delta_2 = \delta_f$, the entire film heats up. An inflection point occurs in the temperature profile at $y/\delta_f = \delta_1/\delta_f$. For $\phi = \phi_o + \phi_1$ this inflection point results in $\partial T/\partial y$ at $y/\delta_f = \delta_1/\delta_f$ equal to zero. The inflection persists at larger values of ϕ although the slope is no longer zero. In order to most easily deal with this situation the integral energy equation for the film is best solved in two parts, i.e., $y/\delta_f \leq \delta_1(\phi_o + \phi_1)/\delta_f = C_1$ and $C_1 \leq y/\delta_f \leq 1$.

The energy equation for the film can be written as

$$\frac{1}{R}\frac{d}{d\phi}\int_0^{C_1\delta_f} u_f\, T_1\, dy = \frac{k_f}{\rho_f C_{p_f}}\left[\left.\frac{\partial T_1}{\partial y}\right|_{y=C_1\delta_f} - \left.\frac{\partial T_1}{\partial y}\right|_{y=0}\right] \qquad 6.2.17$$

$$\frac{1}{R}\frac{d}{d\phi}\int_{C_1\delta_f}^{\delta_f} u_f\, T_2\, dy = \frac{k_f}{\rho_f C_{p_f}}\left[\left.\frac{\partial T_2}{\partial y}\right|_{y=\delta_f} - \left.\frac{\partial T_2}{\partial y}\right|_{y=C_1\delta_f}\right]. \qquad 6.2.18$$

The temperature profile to be used in Equation 6.2.17 must satisfy the conditions:

$$y = 0 \qquad T_1 = T_w$$

$$y = C_1 \delta_f \qquad T_1 = T_b = T_2, \frac{\partial T_1}{\partial y} = \frac{\partial T_2}{\partial y} = -\beta(\phi) \ . \qquad 6.2.19$$

These conditions lead to

$$T_1 = T_w + 2(T_b - T_w + \frac{\beta C_1 \delta_f}{2}) \frac{y}{C_1 \delta_f}$$

$$- (T_b - T_w + \beta C_1 \delta_f) (\frac{y}{C_1 \delta_f})^2 \ . \qquad 6.2.20$$

For T_2 the boundary conditions in y are:

$$y = C_1 \delta_f \qquad T_2 = T_b - \frac{\partial T_2}{\partial y} = \beta \ .$$

$$y = \delta_f \qquad T_2 = T_i$$

These lead us to

$$T_2 = T_b - \beta(y - C_1 \delta_f) + (T_i - T_b + \beta\delta_f(1$$

$$- C_1)) [\frac{(y - C_1 \delta_f)}{(1 - C_1) \delta_f}]^2 \ . \qquad 6.2.21$$

In addition the velocity profile in the film and condensate becomes

$$u_f = \frac{g \sin\phi}{\nu_f} [(\delta_f + \delta_c) y - \frac{y^2}{2}] \qquad 6.2.22$$

for $0 \leq y \leq \delta_f + \delta_c$.

Utilizing the temperature and velocity profiles given in Equations

6.2.19-6.2.21, and Equations 6.2.17 and 6.2.18 yield the following nondimensional equations respectively

$$\frac{[5/3 - 3/5\ C_1]}{[1/3 - C_1/10]} \frac{d\theta_b}{d\phi} - \frac{1}{3} \frac{\bar{C}_1\ \bar{\delta}_f\ \beta}{\tan\phi} + C_1\ \bar{\delta}_f \frac{d\bar{\beta}}{d\phi} = - \frac{8}{Pr_f\ C_1{}^3\ \bar{\delta}_f{}^4} \frac{\bar{R}}{\sin\phi(1/3 - C_1/10)} [\theta_b - \theta_w + \bar{\beta}\ C_1\ \bar{\delta}_f] \qquad 6.2.24$$

and

$$\frac{M_1}{M2} \frac{d\theta_b}{d\phi} + \frac{M_3}{M_2} \frac{d\theta_i}{d\phi} + \frac{1}{3} \frac{\bar{\beta}\bar{\delta}_f}{\tan\phi} - \delta_f \frac{d\bar{\beta}}{d\phi} = = \frac{2}{Pr_f\ M_2} \frac{\bar{R}}{\bar{\delta}_f{}^4(1 - C_1)} \frac{\theta_i - \theta_b + \bar{\beta}\ \bar{\delta}_f(1 - C_1)}{\sin\phi} \qquad 6.2.25$$

where

$$\left.\begin{aligned} M_1 &= (C_1 - \frac{C_1{}^2}{2}) \frac{2}{3} (1 - C_1) + (1 - C_1)^3 \frac{11}{60} \\ M_2 &= (C_1 - \frac{C_2{}^2}{2}) \frac{(1 - C_1)^2}{6} + (1 - C_1)^4 \frac{7}{120} \\ M_3 &= (C_1 - \frac{C_1{}^2}{2}) \frac{(1 - C_1)}{3} + (1 - C_1)^3 \frac{3}{20} \end{aligned}\right\} \qquad 6.2.26$$

The compatability of heat fluxes at the condensate layer-film interface leads to

$$\theta_i = \frac{\bar{\delta}_f(1 - C_1)\ (1 - \bar{\beta}\bar{\delta}_c) + 2\theta_b\ \bar{\delta}_c}{2\bar{\delta}_c + (1 - C_1)\ \bar{\delta}_f} . \qquad 6.2.27$$

The condensate energy equation is

$$\frac{d\bar{\delta}_c^2}{d\phi} = \frac{4}{3^{2/3}} \frac{Ja}{Re_f^{2/3} Pr_f} \frac{\bar{R}(1 - \theta_i)}{\sin^{1/3}\phi} - \frac{2}{3} \frac{\bar{\delta}_c^2}{\tan\phi} \quad . \qquad 6.2.28$$

The solution of Equations 6.2.2-6.2.28 will define the condensation in Region II. The boundary conditions for this region are those at the end of Region I; i.e.,

$$\theta_b = 0, \qquad \beta = 0,$$

$$\delta_c = \delta_{c_{\phi = \phi_o + \phi_1}}, \quad \theta_L = \theta_{L_{\phi = \phi_o + \phi_1}}.$$

Heat Transfer Coefficient

The purpose of a heat transfer coefficient is to define the surface area needed to provide a given amount of condensation or temperature rise in the coolant. Thus, for the current problem it is necessary to define the heat per unit area as:

$$q'' = h(\phi)(T_{sat} - T_w) = + k_c \left.\frac{\partial T}{\partial y}\right|_{y=0} \qquad 6.2.30$$

which yields

$$h_I(\phi) = \frac{2k}{\delta_1} \frac{(T_o - T_w)}{T_{sat} - T_w} \text{ in Region I} \qquad 6.2.31$$

and

$$h_{II}(\phi) = \frac{2k(T_b - T_w + \beta C_1 \delta_f/2)}{C_1 \delta f(T_{sat} - T_w)} \text{ in Region II} \quad . \qquad 6.2.32$$

The average heat transfer coefficient is

$$\bar{h} = \left[\int_{\phi_o}^{\phi_o+\phi_1} h_I(\phi)\, d\phi + \int_{\phi_o+\phi_1}^{\phi_o+\phi_1+\phi_2} h_{II}(\phi)\, d\phi \right] / (\phi_1 + \phi_2) \quad . \qquad 6.2.33$$

Condensation on a Vertical Row of Tubes

Condensation on the upper most tube, as shown in Figure 6.2.2, in a vertical row of horizontal tubes can be analyzed by the theory of Nusselt (22) or Chen (31). The condensate leaving the upper tube is hypothesized here as falling as a continuous sheet until it impinges on the second tube. While the condensate traverses the distance to the second tube condensation occurs on the sheet. Jacobs and Nadig (21) have recently solved the problem of condensation on such a sheet. If we assume that the fluid in the sheet becomes well mixed as it impinges on the second tube the model developed earlier in this paper is applicable for the analysis of the heat transfer as the fluid layer flows around the tube. If the condensate leaving the second tube again falls as a sheet and impinges on the third tube and so on, we find that the heat transfer for multiple tubes can be analyzed by repeatedly using the model of Jacobs and Nadig for condensation on a falling sheet and the present model. In the analysis the mean temperature of the fluid leaving a tube and impinging on the next is successively changed in the models as one works downward through the row of tubes.

Since all of the heat transfer must ultimately be absorbed by the coolant, it is only necessary to evaluate the average heat transfer coefficient on the surface of each successive tube, add them together and divide by the total number of tubes in the vertical row in order to determine the average heat transfer coefficient for that number of tubes. The theory of Nusselt is used for the first tube's h and the present analysis is used for the successive tubes. The model of Jacobs and Nadig (21) is only used to determine the value of T_o for each tube. This value will depend on the tube spacing as

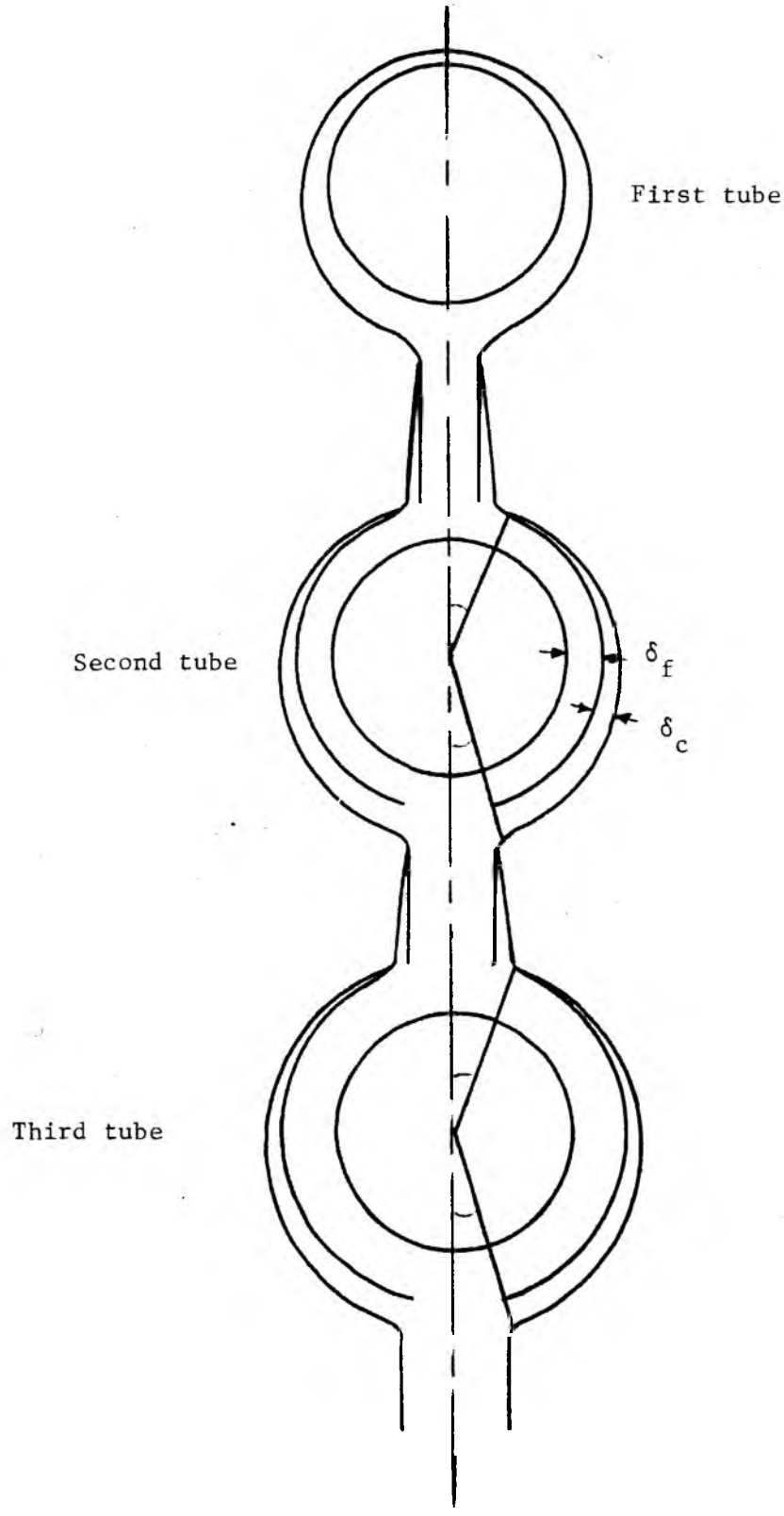

Figure 6.2.2. Physical model for condensation on multiple tubes.

well as the Jakob number and Prandtl number and Reynolds number of the condensate sheet.

6.3. Results and Discussion

Examination of the governing differential equations indicates that for values of ϕ approaching ϕ_o, simple expressions could be obtained for the coefficients of δ_1, δ_2 and δ_c indicated in Equation 6.2.16. They are:

$$\left.\begin{aligned} & a_1 \left[\frac{36\bar{R}}{Pr_f \sin\phi_o \bar{\delta}_f}\right]^{1/3} \\ & a_2 \left[\frac{24\bar{R}}{Pr_f \sin\phi_o \bar{\delta}_f^2}\right]^{1/2} \\ & a_3 \left[-\frac{1}{4} a_2 + \frac{1}{2}\sqrt{\frac{1}{4} a_2 + \frac{16}{3^{2/3}} \frac{Ja}{Re_f^{2/3}} \frac{R}{Pr_f \sin^{1/3}\phi_o}}\right] \end{aligned}\right\} \quad 6.3.1$$

Thus for small values of $\phi - \phi_o$

$$\begin{aligned} \bar{\delta}_1 &= a_1(\phi - \phi_o)^{1/3} + \ldots \\ \bar{\delta}_2 &= a_2(\phi - \phi_o)^{1/2} + \ldots \\ \bar{\delta}_3 &= a_3(\phi - \phi_o)^{1/2} + \ldots \end{aligned} \quad 6.3.2$$

Using these functions for starting values the governing equations were solved numerically using a standard Runga-Kutta algorithm on a Hewlett-Packard 3000 minicomputer. The average heat transfer coefficient was then determined as indicated in Equations 6.2.31-6.2.33.

After solving the governing equations the solutions were applied to the solution of the multiple tube problem as indicated previously. Calculations made in this paper correspond to the experimental work

of Young (33). In these experiments the wall temperature was kept constant, the tube pitch was two diameters and the outside tube diameter was 0.375 inches, ~ 95 mm. For these conditions Figure 6.3.1 shows the ratio of the presently determined average heat transfer coefficient to that reported by Nusselt (22) for $0.04 \leq Ja \leq 0.20$. It is clear that Nusselt's solution is in increasing error as the number of tubes in a vertical row increases. Further there is a weak dependence on Ja with the error increasing as Ja increases. The results shown in Figure 6.3.1 are well correlated by the expression,

$$\frac{\bar{h}_n}{\bar{h}_{nun}} = [1 + 0.103\ Ja^{0,212}(n - 1)^{1/2}] \ . \qquad 6.3.3$$

Figures 6.3.2-6.3.5 show the comparison of the present model with the experimental results of Young (33). In addition, the results of Chen's (31) analysis are also shown. Although the present analysis shows a definite improvement over that of Chen the experimental data are generally higher than we predict. The relatively close tube spacing can lead to high vapor velocities as has been pointed out by Fujii et al. (35). For close tube spacing they note that it is unlikely that the falling condensate sheets will accelerate to the degree that considerable splashing will occur as has been argued by some investigators. However, surface waves and partially "drop-wise" condensation as well as appreciable vapor velocity could induce higher heat transfer rates. They argue that the latter is the primary reason why the heat transfer is higher than would be predicted by a model such as developed herein.

If the tube pitch is large the falling condensate sheet between

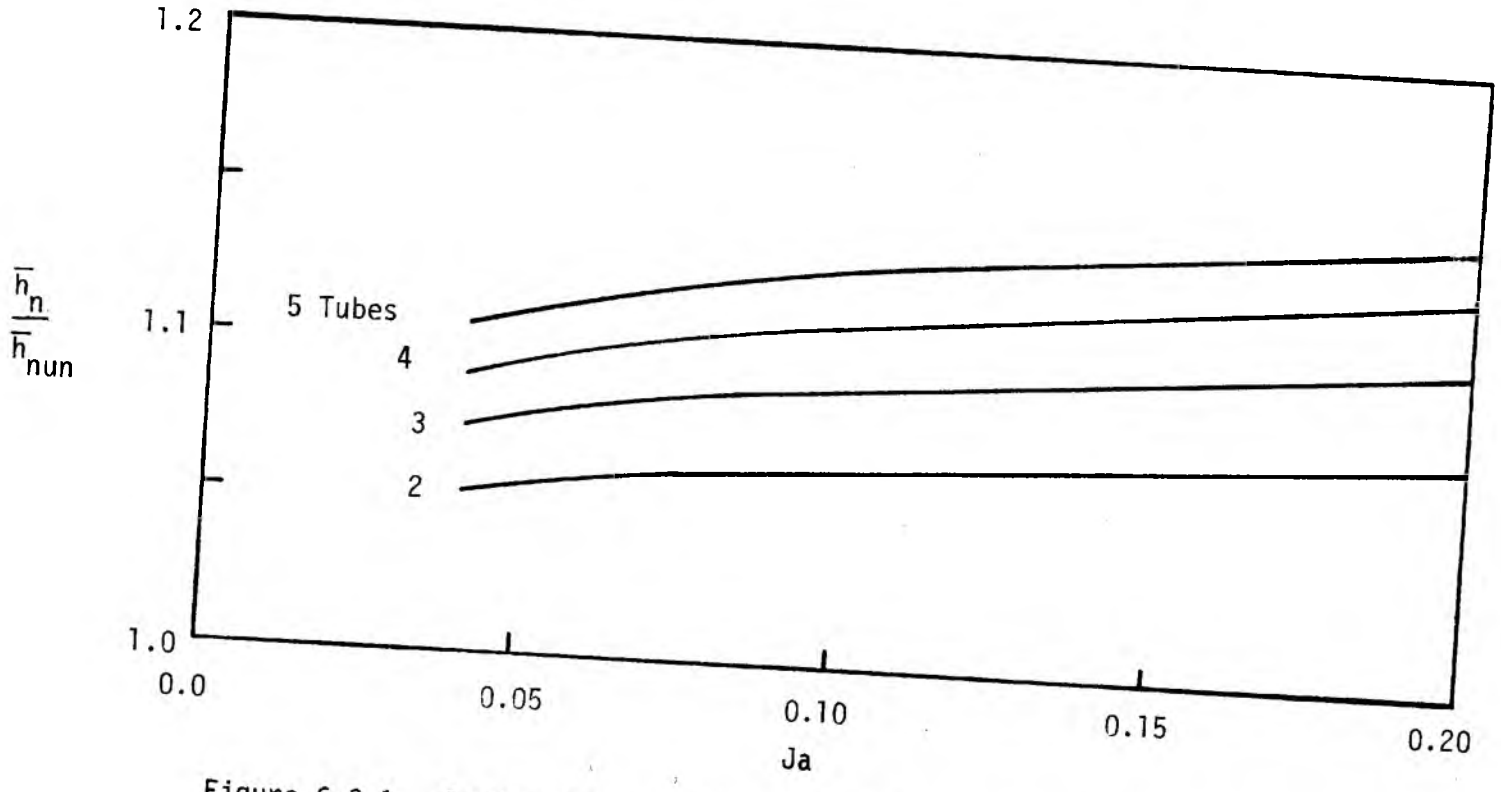

Figure 6.3.1. Ratio of average heat transfer coefficient over n tubes to that obtained from Nusselt's analysis as a function of Jakob number.

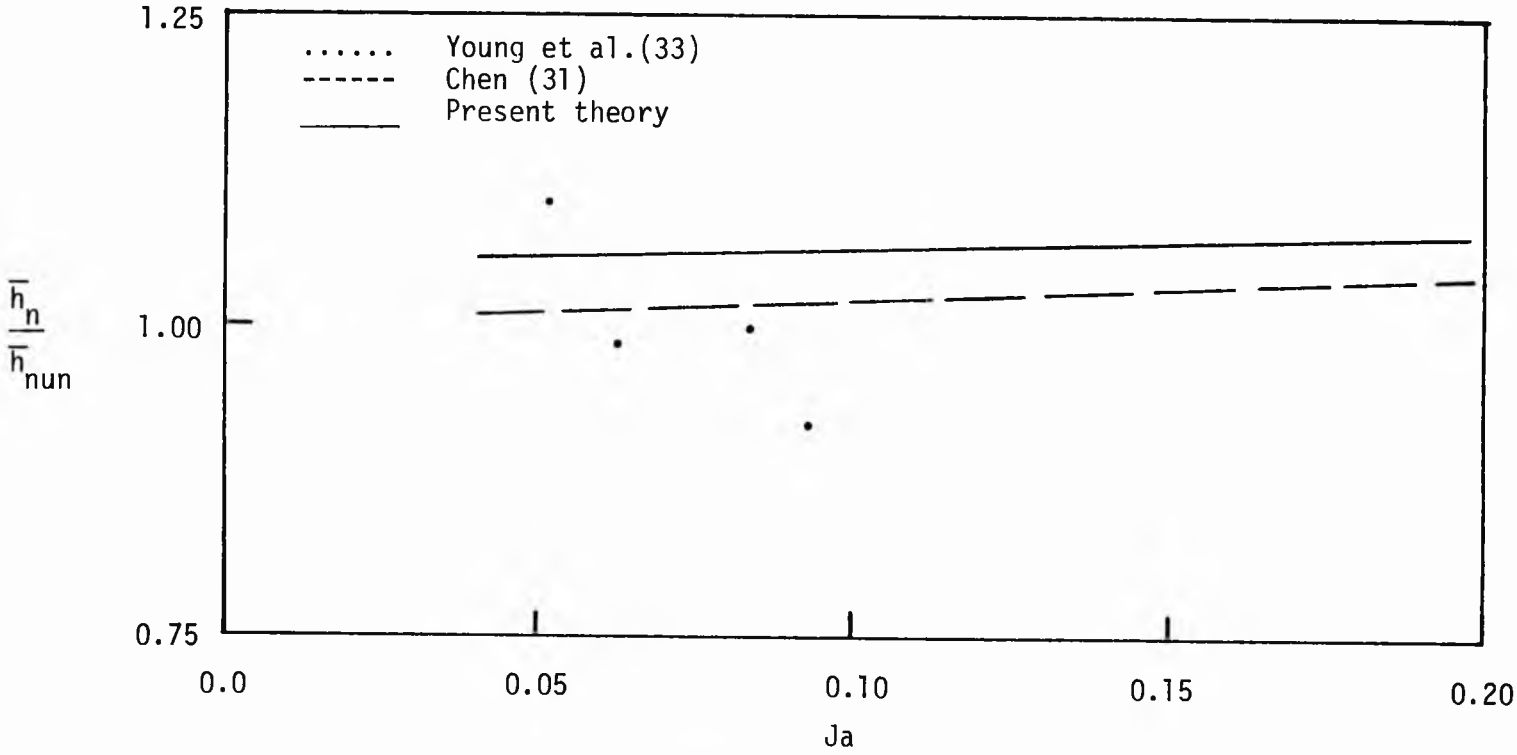

Figure 6.3.2. Ratio of average heat transfer coefficient over two tubes to that obtained from Nusselt's analysis as a function of Jakob number.

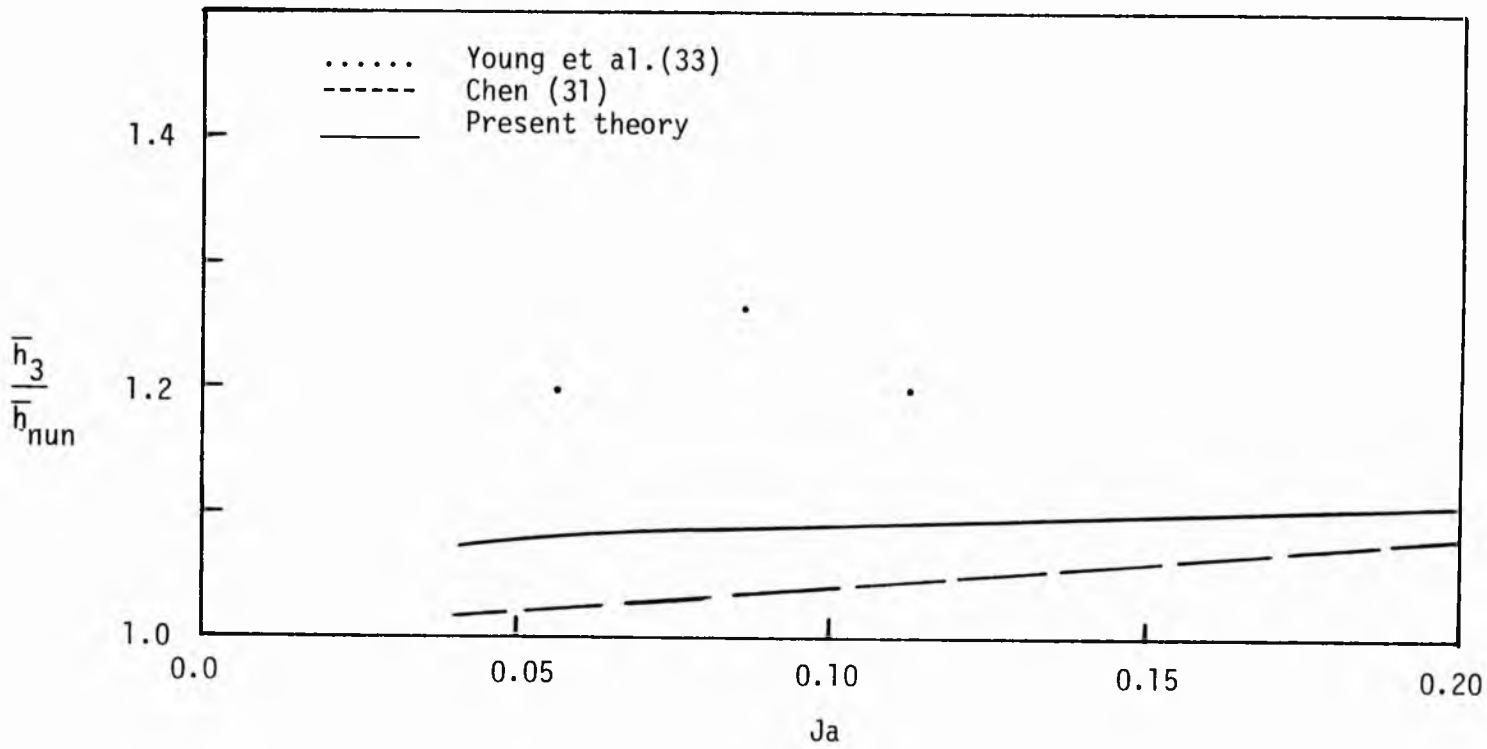

Figure 6.3.3. Ratio of average heat transfer coefficient over three tubes to that obtained from Nusselt's analysis as a function of Jakob number.

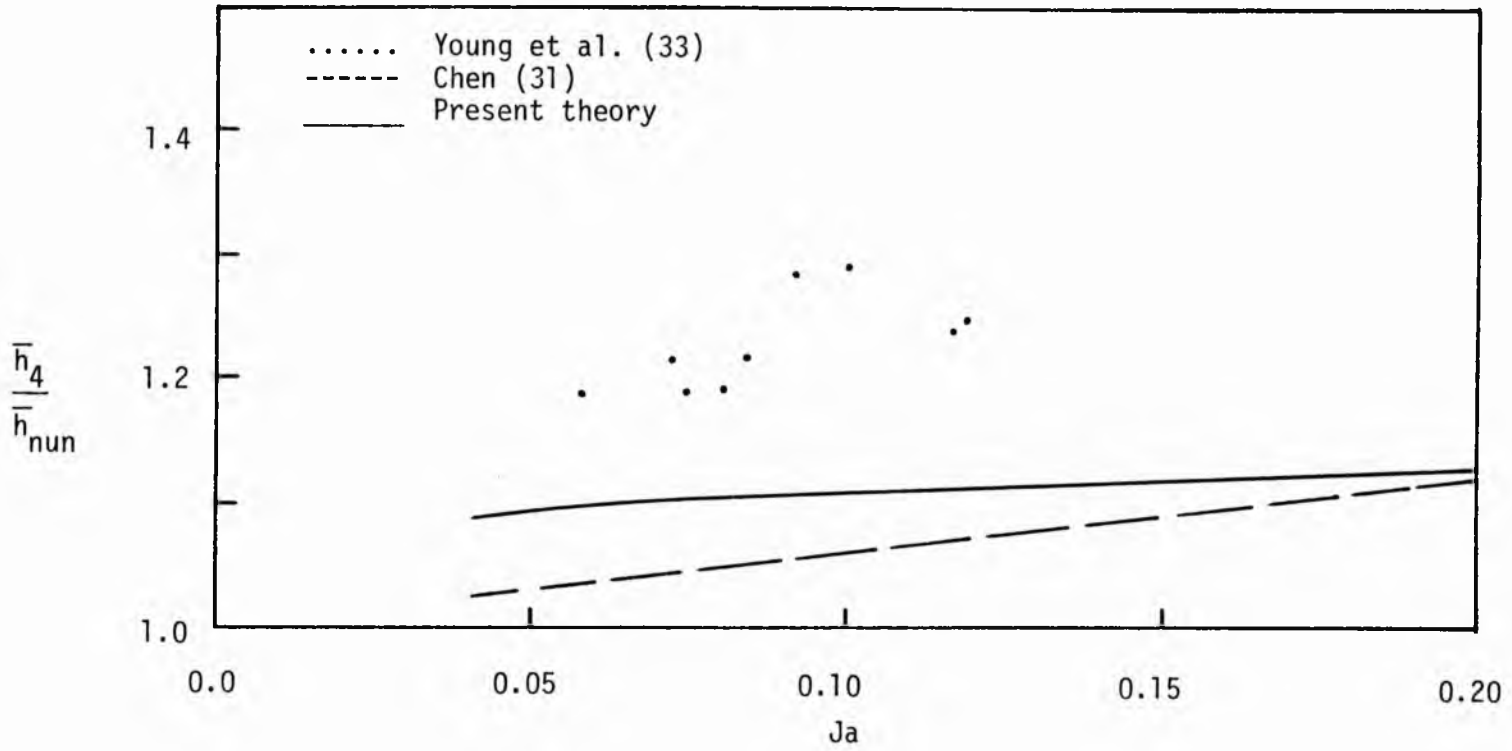

Figure 6.3.4. Ratio of average heat transfer coefficient over four tubes to that obtained from Nusselt's analysis as a function of Jakob number.

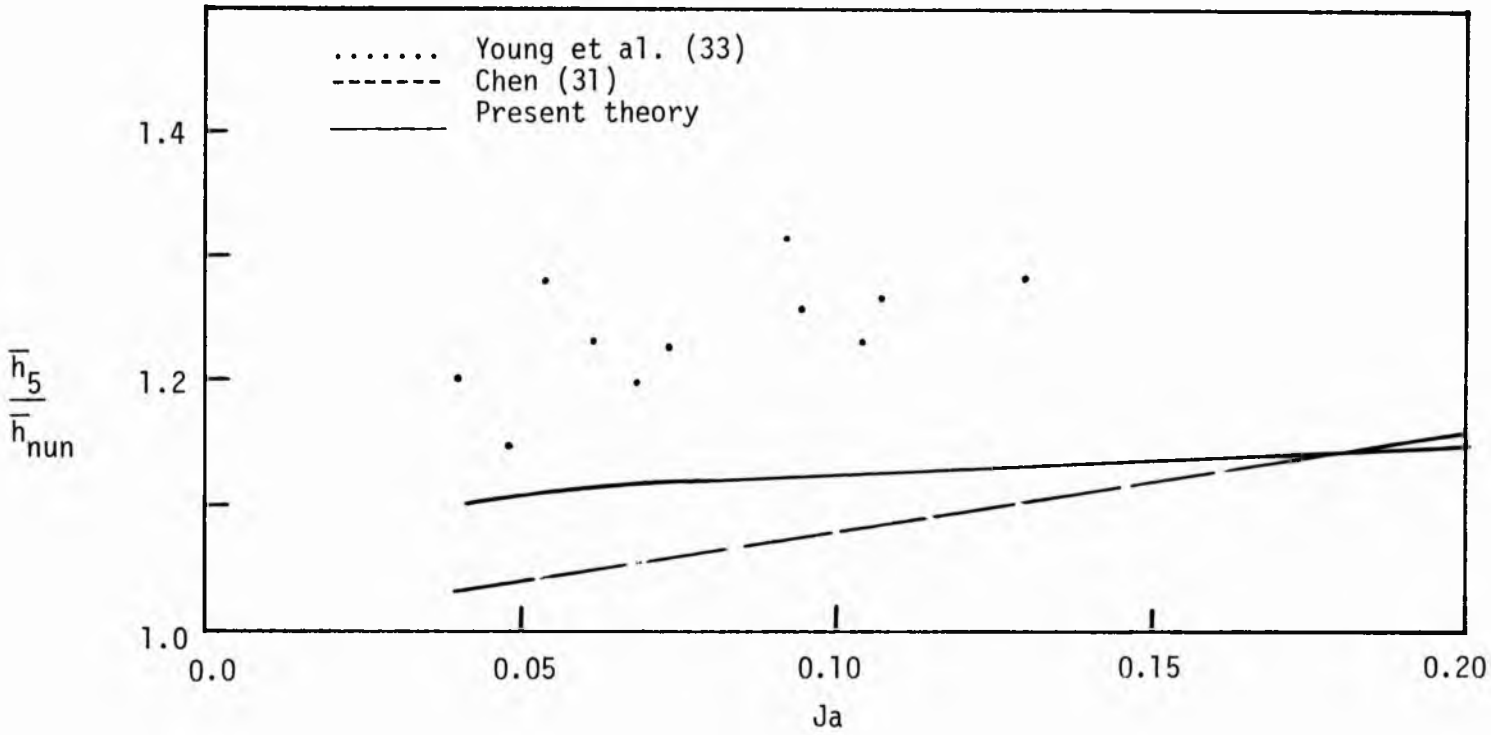

Figure 6.3.5. Ratio of average heat transfer coefficient over five tubes to that obtained from Nusselt's analysis as a function of Jakob number.

tubes will accelerate to a high velocity and the condensate sheet will become thinner. Both of these effects will make T_o approach T_{sat}. Thus, Chen's solution should become applicable. However, Chen neglects the distance needed to establish the thermal boundary layer moving outward from the wall. He requires the same temperature profile as for condensation on a single tube. A high velocity in the film will, of course, make it thinner and increase the heat transfer coefficient, yet the established temperature profile reduces it. These effects together make his heat transfer increase at a faster rate than ours as Jakob number increases when applied to a pitch ratio of two. However, at low values of Jakob number Chen's analysis yields significantly lower values of h_n.

REFERENCES

1. Rai, V.C., and Pinder, K.L., "Direct Contact Condensation of Steam in a Packed Column with Immiscible Heat Transfer Agents," Canadian Journal of Chemical Engineering, Vol. 2, 1974, pp. 170-174.

2. Bokay, A. and Jaszay, T., "High Performance Jet Condensers for Steam Turbines," Proceedings of the Sixth International Heat Transfer Conference, Vol. 2, August 1978, pp. 61-65.

3. Joseph, K., Source Book on the Production of Electricity from Geothermal Energy, U.S. Department of Energy Publication, March 1980, pp. 413-417.

4. Jacobs, H.R. and Fanner, H., "Direct Contact Condensers - - A Literature Survery," Energy Development Administration, Report No. DEE/1523-3, February 1977.

5. Kudo, A.E. and Equsa, T.T.,"Basic Studies of Vapor Suppression," Proceedings of the Fifth International Heat Transfer Conference, Vol. 3, September 1974, pp. 221-225.

6. Minkowycz, W.J. and Sparrow, E.M., "Condensation Heat Transfer in the Presence of Noncondensibles, Interfacial Resistance, Super heating, variable Properties and Diffusion," International Journal of Heat and Mass Transfer, Vol. 9, 1966, pp. 1125-1144.

7. Jacobs, H.R. and Bogart, J.A., "Condensation on Immiscible Falling Films," Paper No. 80-HT-110, ASME National Heat Transfer Conference, Orlando, Florida, July 1980.

8. Jacobs, H.R. and Nadig, R., "Condensation on an Immiscible Falling Film in the Presence of a Noncondensible Gas," Heat Exchangers for Two-Phase Application, HTD - Vol 27, pp. 99-106, ASME National Heat Transfer Conference, Seattle, Washington, July 1983.

9. Nadig, R., Condensation on an Immiscible Falling Film in the Presence of a Noncondensible Gas, Master's Thesis, University of Utah, Salt Lake City, Utah, March 1983.

10. Hausbrand, E., Evaporating, Condensing and Coolant Apparatus, D. Van Nostrand Co., 5th ed., New York, 1933.

11. How, H., "How to Design Barometric Condensers," Chemical Engineering, pp. 174-182, February 1956.

12. Oliker, I., "On Calculation of Heat and Mass Transfer in Jet Type Direct Contact Heaters," Paper No. 76-HT-21, ASME National Heat Transfer Conference, St. Louis, Missouri, August 1976.

13. Kutateladze, S.S., Heat Transfer in Condensing and Boiling, Chapter 7, Moscow, 1952. English Translation by U.S. Atomic Energy Commission, AEC-TR-3770, 2nd Edition.

14. Hasson, D., Luss, D. and Peck, R., "Theoretical Analyses of Vapor Condensation on Laminar Jets," International Journal of Heat and Mass Transfer, Vol. 7, pp. 969-981, 1964.

15. Hasson, D., Luss, D., and Navon, V., "An Experimental Study of Steam Condensing on a Laminar Water Sheet," International Journal of Heat and Mass Transfer, Vol. 7, pp. 983-1001, 1964.

16. Jacobs, H.R., and Bogart, J.A., and Pensel, R.W., "Condensation on a Thin Film Flowing Over an Adiabatic Sphere," Proceedings of the Seventh International Heat Transfer Conference, Vol. 5, pp. 89-94, Munich, 1982.

17. Sparrow, E.M. and Lin, S.H., "Condensation Heat Transfer in the Presence of a Noncondensible Gas," ASME Journal of Heat Transfer, August 1964, pp. 430-436.

18. Sparrow, E.M., Minkowycz, W.J. and Saddy, M., "Forced Convection Condensation in the Presence of a Noncondensibles and Interfacial Resistance," International Journal of Heat and Mass Transfer, Vol. 10, 1967, pp. 1829-1845.

19. Rose, J.W., "Condensation of a Vapor in the Presence of a Noncondensing Gas," International Journal of Heat and Mass Transfer, Vol. 12, 1969, pp. 233-237.

20. Taitel, Y. and Tamir, A., "Condensation in the Presence of a Noncondensible Gas in Direct Contact," International Journal of Heat and Mass Transfer, Vol. 12, 1969, pp. 1157-1169.

21. Jacobs, H.R. and Nadig, R.,"Condensation on Coolant Jets and Sheet," ASME Paper 84-HT-28, National Heat Transfer Summer Conference Niagara Falls, New York, August 1984.

22. Nusselt, W., "Die Oberflachen Kondensation des Wasserdaujes," Zeitschrijt des Vereines Deutscher Ingenieure, Vol. 60, 1916, pp. 541-569.

23. Roshnow, W.M., "Heat Transfer and Temperature Distribution in Laminar Film Condensation," Transactions of ASME, Vol. 78, 1956, pp. 1645-1648.

24. Sparrow, E.M. and Gregg, J.L., "A Boundary-Layer Treatment of Laminar Film Condensation," Journal of Heat Transfer, Transactions of ASME, Series C, Vol. 81, 1959, pp. 13-18.

25. Chen, M.M., "An Analytical Study of Laminar Film Condensation: Part 1 - Flat Plates," Journal of Heat Transfer, Transactions of ASME, February 1961, pp. 48-54.

26. Murty, N.S., and Sastri, V.M.K., "Condensation on a Falling Liquid Film," Heat Transfer 1974, Proceedings of the 5th International Heat Transfer Conference, Vol. III, September 3-7, 1974, pp. 231-235.

27. Eckert, E.R.G. and Drake, R.M., Heat and Mass Transfer, Second Edition, McGraw-Hill Book Company, 1959, pp. 338.

28. Al-Diwany, H.K., Rose, J.W., "Free Convection Film Condensation of Steam in the Presence of Non-condensing Gases," International Journal of Heat and Mass Transfer, 1973, Vol. 16, pp. 1359-1369.

29. More, J.J., Garbow, B.S. and Hillstrom, K.E., User Guide for Minpack - 1, Argonne National Laboratory, Illinois, August 1980.

30. Sparrow, E.M. and Gregg, J.L., "Laminar Condensation Heat Transfer on a Horizontal Cylinder," Journal of Heat Transfer, Transactions of ASME, Series C, Vol. 81, 1959, pp. 291-296.

31. Chen, M.M., "An Analytical Study of Laminar Film Condensation: Part 2 - Single and Multiple Horizontal Tubes," Journal of Heat Transfer, Transaction of ASME, February 1961, pp. 55-60.

32. Koh, J.C.Y., "An Integral Treatment of Two Phase Boundary Layer in Film Condensation," Journal of Heat Transfer, August 1961, pp. 359-362.

33. Young, F.L., and Wohlenberg, W.J., "Condensation of Saturated Freon - 12 on a Bank of Horizontal Tubes," Transaction of ASME, Vol. 64, 1942, pp. 787-794.

34. Katz, D.L., and Geist, J.M., "Condensation on a Six Finned Tubes in a Vertical Row," Transaction of ASME, Vol. 70, 1948, pp. 907-914.

35. Fujii, T., Behara, U., Hirata, K., Oda, K., "Heat Transfer and Flow Resistance in Condenation of Low Pressure Steam Flowing Through Tube Banks," International Journal of Heat and Mass Transfer, Vol. 15, No-2, February 1972, pp. 247-261.